2019

LINKING HISTORICAL, FIELD, AND SATELLITE DATA TO DETERMINE THE RELATIONSHIP BETWEEN GAS EMISSIONS AND VEGETATION CHANGE IN THE PUHIMAU GEOTHERMAL AREA EAST RIFT ZONE KILAUEA, HAWAII

Christie Torres Rosa
Michigan Technological University, cetorres@mtu.edu

LINKING HISTORICAL, FIELD, AND SATELLITE DATA TO DETERMINE THE RELATIONSHIP BETWEEN GAS EMISSIONS AND VEGETATION CHANGE IN THE PUHIMAU GEOTHERMAL AREA EAST RIFT ZONE KILAUEA, HAWAII

By

Christie Eileen Torres Rosa

A THESIS

Submitted in partial fulfillment of the requirements for the degree of

MASTER OF SCIENCE

In Geology

MICHIGAN TECHNOLOGICAL UNIVERSITY

2019

This thesis has been approved in partial fulfillment of the requirements for the Degree of MASTER OF SCIENCE in Geology.

Department of Geological and Mining Engineering and Sciences

Thesis Advisor: *Chad D. Deering*

Committee Member: *Curtis Edson*

Committee Member: *Snehamoy Chatterjee*

Department Chair: *John S. Gierke*

Table of Contents

List of Figures

List of Tables

Acknowledgments

I would like to thank my advisor Dr. Chad Deering for giving me the opportunity to participate in such a wonderful experience as this research was. Since my first internship under your guidance, I was able to learn, research and visit amazing places in the world. You always gave the motivation and tools to always go beyond and for that I am grateful. Dr. Curtis Edson, for teaching me the amazing world of remote sensing and always keep me motivated saying I could do it. Dr. Snehamoy Chatterjee for always being available to answer the million questions I had about geostatistics, thank you for all your patience. I would also like to thank NASA (grant # NNX15AR97G), the King Chavez Program (KCP), and department of GMES at Michigan Tech for providing me support and the Digital Globe Foundation for providing all the imagery that was used for this research. Amol Paithankar for always being available to help me with all the software I didn't know how to use, you are truly the best!

This work is dedicated to my family and friends because without their support I wouldn't be able to be the person that I am today. Mom, dad, Frances, and Orvil you guys gave me the support I never knew I deserved, there are no words to describe how grateful I am and how proud I am to have you as my family, no matter the distance you are always there rooting for me. To Ricardo and Amahia, because you both deserve a world where you can accomplish everything you dream. Last but not least to Melissa, and Sam I feel like the luckiest girl having you both as more than friends, family. I was able to complete this journey because you both were the biggest cheer team I have ever dreamed of, thanks for all the encouragement and love you gave me all these years.

List of Abbreviations

ERZ	East Rift Zone
SGeMS	Stanford Geostatistical Modeling Software
HyspIRI	Hyperspectral Infrared Image
SGS	Sequential Gaussian Simulation
NIR	Near Infrared
SWIR	Short Wave Infrared
PAR	Photosynthetically Active Radiation
CO_2	Carbon Dioxide
H_2S	Hydrogen sulfide
SO_2	Sulfur Dioxide

Abstract

The Puhimau geothermal area, located near the summit of the Kilauea volcano, Hawaii, has been suggested to represent a 'window' into the East Rift Zone. The quantification of CO_2 and H_2S soil gas emissions improves our understanding of its gas emission mode- including total emission and spatial distribution and contribute to a more accurate estimation of total CO_2 and H_2S in the thermal area – and how these gas emissions relate to observed vegetation health from satellite data. The total emission of CO_2 and H_2S was interpolated by the sequential Gaussian simulation method (SGS) using Stanford Geostatistical Modeling Software (SGeMS). Ranges for total flux emissions for CO_2 are 14.09 to 14.21 t d^{-1} and 0.0759 to 0.0764 t d^{-1} for H_2S. Results show that faults or fractures covered by sinter are very likely to exist at Puhimau, based on the similarity between the correlation of high flux areas and the trend of the regional faults. An analysis of images derived from satellite remote sensing data was also utilized to track changes in vegetation health in the Puhimau geothermal area through time. These results indicate changes in vegetation health occur that correlate with specific volcanic events. However, the precise source of these changes in vegetation health remain inconclusive and could be the result of changes in soil gas emissions, soil temperature, or both.

1 Introduction

Volcanoes around the world can affect communities in several ways, negatively impacting human and animal health, and vegetation (Oppenheimer, 2002; Longo et al., 2005; Longo and Yang, 2008; Selinus, 2013; van Manen, 2014). Historically, monitoring efforts have been focused on active vents that emit large enough gas contents that they can be measured using spectral imaging tools. In contrast, potentially active areas with anomalous, but diffuse soil gas emissions are rarely monitored. However, persistent diffuse degassing of CO_2 and H_2S can be used to trace the existence of cryptic structural features which can potentially be the source of a new fissure or emerging vent due to magma migration. Some studies have shown that monitoring changes in this type of gas emission can help to locate new emerging eruptive vents and/or fissures and, therefore, predict future eruptions (Giammanco, et al., 1998; McGee et al 2006). High emissions of CO_2, H_2S, and/or an increase in soil temperature can also lead to stressed and/or killed vegetation in the areas that can potentially become vent openings. Therefore, remotely measuring vegetation health that is affected by diffuse soil gas emissions using satellite imagery has the potential to be used as an effective new volcano monitoring technique.

Shifts in vent and fissure locations at the Kilauea volcano Hawaii have been documented throughout the years, but predicting the precise location that they will emerge along the East Rift Zone, in particular, has been challenging. In 1960, the Kapoho eruption (40 km away from the Kilauea summit) occurred within only hours of the recorded seismic activity. From 1983 to 1986 eruptions occurred along two different fissure vents at Napau and Pu'u'O'o only 5 km apart with cessation and vent shifting from one fissure to another

on the order of days to weeks. Subsequently, from 1986 to 1992 the activity moved 3 km to Kupaianaha and eventually back to Pu'u'O'o. Prior to each of these events, the activity was only recognized within a couple of hours before it began (USGS, 1998). The short period of seismic activity that preceded these eruptions highlights the need for monitoring techniques that provide the community with an earlier warning prior to the eruptions. Importantly, all of the aforementioned areas were covered by dense vegetation of the Ohia forest. Links between gas emissions and vegetation have been previously studied, for example, experiments by Rouse in 2010 showed that high levels of CO_2 concentrations in vegetation lead to a degradation response in leaves that can be seen for up to one month (Rouse, 2010). Similar results have been also documented for H_2S, vegetation exposed to gas lead to leaf necrosis (Li, 2013). Pre-eruptive degassing monitoring of vegetated areas would have had provided a longer timeframe of days to months to predict the event zones (Giammanco, et al., 1998; McGee et al 2006; Rouse, 2010).

The Puhimau geothermal area in the Hawaii Volcanoes National Park is a thermally active area with stressed vegetation along the rims of the feature which will provide a useful inside of the interactions between gas emissions and vegetation health extend. It was first studied by Jaggar (1938) and later on by McGee et al. (1996-1998), described as a thermally active zone and a potential window into the East Rift Zone (Jaggar, 1938; McGee et al., 2006). The geothermal area has a potential to be a window into the East Rift Zone where, if a correlation between soil gas emissions and vegetation can be established, changes in the thermal zone can be indicative of future eruptive events in the East Rift Zone with longer time frames.

A soil gas emission measurement field campaign was coordinated with the NASA HyspIRI remote sensing experiments at the Puhimau geothermal area from February 13 to March 6, 2017. We utilized an accumulation chamber etc. to measure soil gas emissions and temperature. Subsequently to the fieldwork campaign and to complement NASA HyspIRI work, normalized difference vegetation index, supervised classification and the image difference tool on ArcGIS will help to establish a better picture on the understanding of the behavior of the Puhimau geothermal feature and its degassing style with eruptive activity from the East Rift Zone on the Kilauea volcano. The objective of the study was to 1) quantify the total emission of CO_2 and H_2S at diffuse soil; 2) identify spatial distribution of the gas emissions and ground temperature; and 3) explore the potential spatiotemporal relationship between volcanic activity in the East Rift Zone and changes in vegetation health in Puhimau geothermal area using remote sensing products.

2 Geological Setting

The Kilauea volcano is located on the Pacific Plate, which is the largest tectonic plate with an approximate area of 103 million km^2. Kilauea and the Hawaii - Emperor seamount chain of volcanoes have formed as the result of the Pacific Plate moving over the Hawaii hotspot (Morgan, 1972). The Hawaii hotspot has remained largely stationary since the Cenozoic Era and it's being fed by a mantle plume as deep as the core mantle boundary (Morgan, 1972). The ascent of this mantle plume and impingement on the Pacific plate has resulted in the near continuous production of magma and a highly active volcanic region (Morgan, 1972).

3 Eruptive History of the Kilauea Volcano and the East Rift Zone

Kilauea volcano is one of the most thoroughly studied and continually monitored volcanoes in the world. However, understanding its eruptive history has been challenging due to the lack of exposed rock given the frequency of new lava flows (Figure 1) (USGS, 2016). The oldest rocks collected at the submarine slopes of the volcanoes indicate that it has been in its shield building stage in the last 155,000 years ago (USGS, 2016). For the past 2,500 years, Kilauea has transitioned between explosive (tephra dominated) and effusive (lava-flow dominated) activity, depending on the quantity of magma that supplies the volcanic activity (USGS, 2016). Historically, the volcano has been dominated by effusive activity for the past 200 years (USGS, 2016).

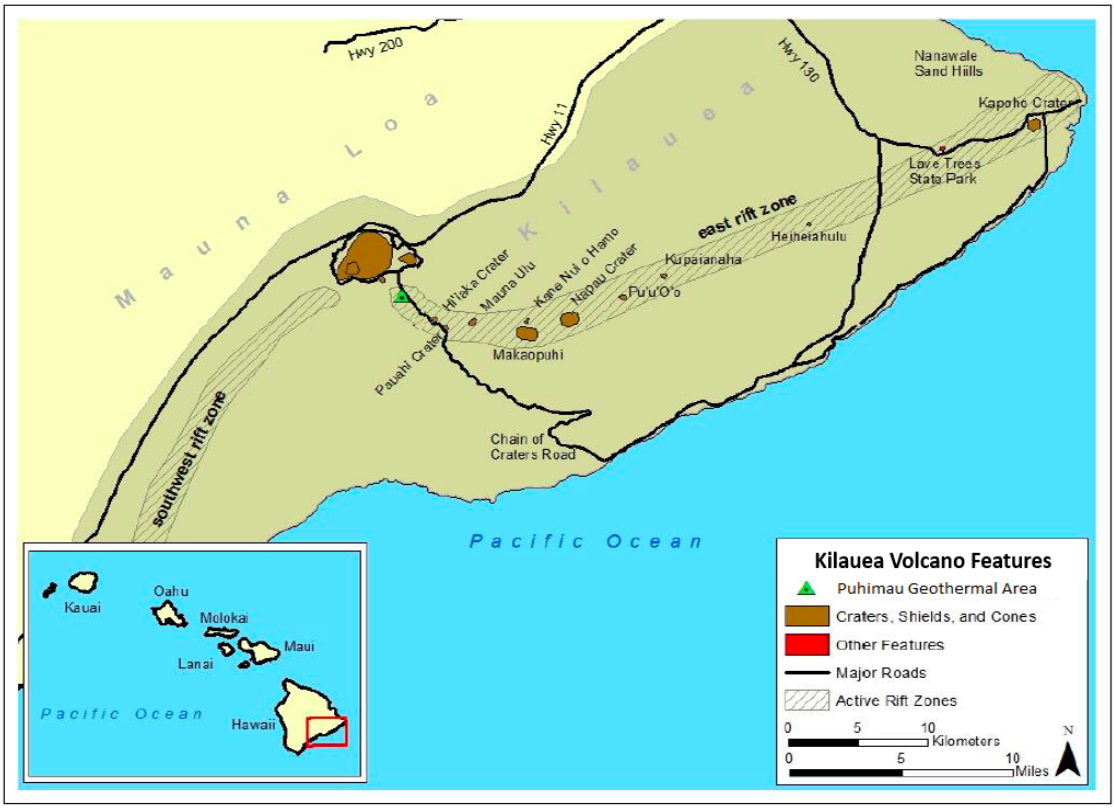

Figure 1. Location of the Kilauea volcano, its craters, shields, and cones that are documented thought its eruptive history. Eruptive history from the craters is: from 1924 Halema‘uma‘u crater (biggest crater on the

figure), 1955 events at lower Puna, 1960 the Kapoho crater, 1969 to 1974 Mauna Ulu, and from 1983 to present Pu'u'O'o in the East Rift Zone. Represented as a green triangle is the Puhimau geothermal area, study site.

The documentation of previous eruptive activity of Kilauea traces back to May 1924 where an explosive eruption occurred at the Halema'uma'u crater with more than 50 episodes in a 2.5-week timespan (USGS, 2018). The activity was preceded by a draining of the lava lake and high seismic activity during the previous months (USGS, 2018). Residents described it as the most powerful Kilauea explosion, due to the size of blocks being thrown from the crater weighing up to 14 tons (USGS, 2018). This episode changed the geomorphology of the crater by doubling its diameter and increasing the depth to 400 meters. This change in the crater morphology coincided with the lava lake disappearing until 2008 (USGS, 2018).

In 1955, the first activity since 1840 was documented in the East Rift Zone. This event lasted for 88 days and included 24 vent openings (USGS, 2018). This also represented a shift in activity from the summit and covered nine miles in the Puna district (USGS, 2018). The event started with an increase in seismic activity at the Kilauea caldera and the Pahoa area (lower East Rift Zone) as many as 700 earthquakes were recorded days before the first vent opening. Fountains as high as 500 feet were observed and extensive lava flows reached the sea (USGS, 2018). This event was characterized by vent shifting during the 88 days and activity ceased in the active zones as soon as new vent openings developed (USGS, 2018).

Similar events continued to occur in subsequent years at the Kilauea caldera and the East Rift Zone. For example, in 1959 the Kilauea Iki eruption occurred and was characterized by lava fountains (up to 580 meters high), and the formation of a lava lake,

and construction of a cinder cone; representing a shift from East Rift zone activity the summit of the volcano (USGS, 2017). This event was followed by the 1960 Kapoho eruption, which shifted the locus of eruptive activity to the east coast at Kapoho village just 47 km from the summit (USGS, 2018). This eruption began with lava fountaining, followed by Aa lava flows that lasted for a month (USGS, 2018). By 1969 activity had moved to the west side of the East Rift Zone at Mauna Ulu, south of the summit at the Chain of Craters road, and lasted five years, with a hiatus of 3.5 months in late 1971 (USGS, 2017). This activity was characterized by three initially brief and small eruptions, followed by a larger single eruption that had lava fountains and flows that reached the shoreline (USGS, 2017).

In 1983 the Pu'u'O'o eruptive event began and continues today representing and the largest volume of magma released to the surface from Kilauea and the East Rift zone in 500 years. (USGS, 2019). Pu'u'O'o eruptions are divided in 61 events covering an area of 144 km^2 and have added 179 hectares of material to the surface of the Big Island (USGS, 2019).

4 Description of field locality

The Puhimau geothermal area is an irregular feature with an area of 200 by 400 meters located in the Upper East Rift Zone, 2.5 km south of the Kilauea volcano summit (Figure 2). The geothermal feature formed in 1936 when a plug of magma rose beneath the Ohia forest and increased ground temperatures to 85°C, killing vegetation within in an area approximately 200 meters in diameter (Hinkle, 1978; Jagger, 1938; Zablocki, 1978). The area has remained active since, releasing steam through focused at fumaroles and fractures,

but also as diffuse gas emissions through the soil. Previous research suggests that the shape of the feature is governed by the geometry and pathways of magma intrusion beneath the Ohia forest (Jagger, 1938; Zablocki, 1978; Dunn and Hardee, 1985).

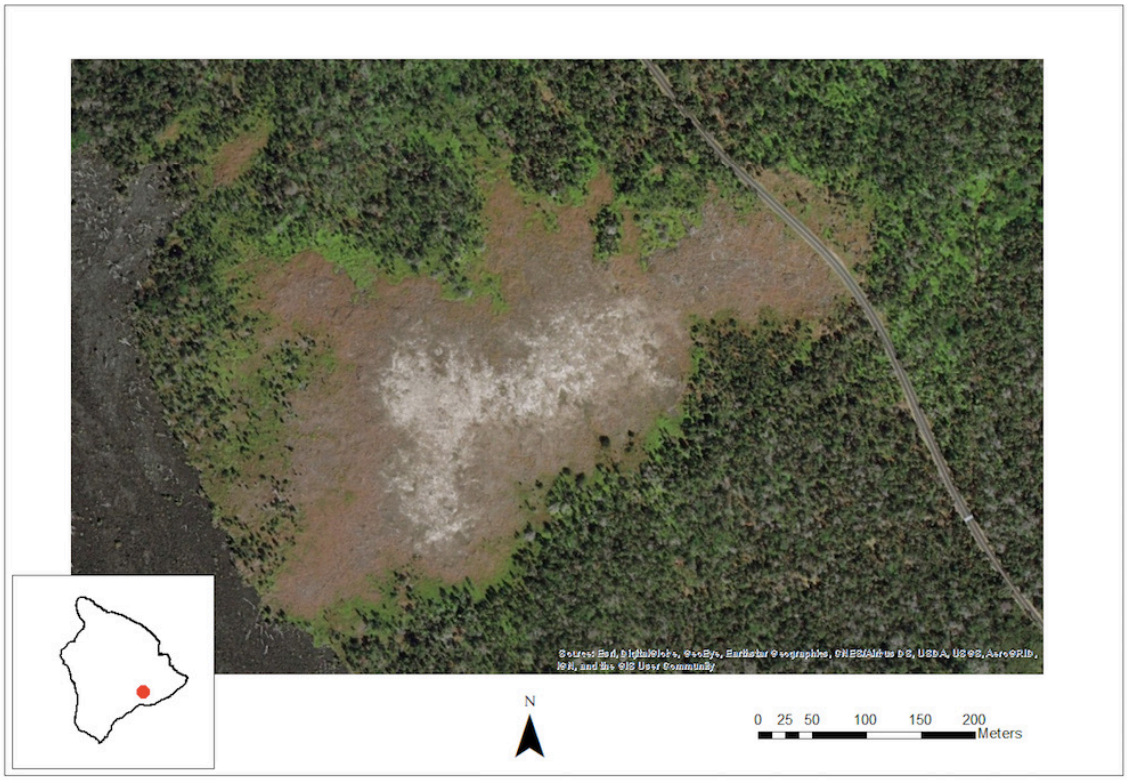

Figure 2. *Puhimau geothermal area, at the East Rift Zone of Kilauea, Hawaii. Area of study for the field campaign and data collection. Imagery from ArcGIS online database.*

The surface and center of the Puhimau geothermal area are characterized by barren ground formed by clay as a result of the alteration of lapilli and ash from the 1970 A.D. Keanakaoko'I eruption (Casadevall and Hazlett et al., 1983; McPhie, 1990, McGee et al. 2006). The outer regions of the feature are covered mostly by lichen, moss and short dry grasses leading into the native tall grasses, ferns, and trees that show little sign of being affected by elevated ground temperatures or soil gas emissions (McGee et al. 2006). The

west and south-west region of the thermal feature are surrounded by an Aa lava flow emplaced in 1974 (McGee et al. 2006).

Previous research suggests that the Puhimau geothermal area is emitting gases such as CO_2, sulfur, mercury, and helium (Gerlach and Taylor, 1990; Hinkle, 1978; McGee et al. 2006). Based on McGee et al. (2006) soil gas surveys from 1996 the total amount of CO_2 emissions was 27 ± 3 t d^{-1} and 17 ± 2 t d^{-1} for 1998 (McGee et al. 2006). Research by Hinkle (1978) quantified sulfur being released from the geothermal area up to 100 ppb, but the chemical form was not identified. From 1987-1989 Barnard et al. (1990) conducted research using neutron activation/gamma-ray spectroscopy to measure sulfur emissions, but they did not exceed the detection limit (10 ppm) (Barnard et al.,1990; Hinkle, 1978). Values of mercury have been estimated at 10 ppm, which are 100 times higher than surrounding areas of the feature (Hinkle, 1978). The source of mercury has been attributed to hot groundwater dissolving mercury in host rocks and being released as vapor through fractures (Davies and Notcutt, 1996). Helium was quantified as 1.5 ppm above ambient values at the center of the feature (Hinkle, 1978).

The Puhimau geothermal area is unique because it is one of the few places in the East Rift Zone that has well-developed soils that can allow gas to be emitted, making it an area where evidence of magma migration can be recorded (Decker, 1987). During the last two of the five intrusive events in 1980 changes in the Puhimau geothermal area were recorded as precursory events. In the first event, an increase in SO_2 was briefly detected prior to the beginning of the intrusive activity (Decker, 1987). Additionally, an increase in gas emissions was recorded by a chemical sensor that monitors H_2, SO_2, and H_2S prior to the east rift eruption that began in 1983 and still continues today (McGee et al., 2006).

5 Methodology

5.1 Field campaign (February 13 to March 6, 2017)

We made measurements of diffuse soil gas emissions, soil temperature and GPS coordinate information for each sample location. Other information such as air temperature, real humidity, and wind speed were collected three times a day; morning, noon and afternoon. Data collection was planned to be done for 22 days, but only 10 days had the optimal conditions. All measurements were taken during dry soil days, and over similar times during the day to maintain consistency in the sampling conditions. Data was collected using a systematic random sampling method that extended from the center of the geothermal feature to approximately the beginning of the tree line in vegetated areas resulting in 280 initial measurements; referred to hereafter as Phase 1 sampling. The spacing between measurements ranged between 20 meters and 40 meters. An additional 120 measurements were collected as part of Phase 2 sampling. The optimal locations were determined using data from Phase 1 to create a variogram and locate new measurement points were variation in soil gas emissions was high or near areas with no data that were inside the geothermal feature. Phase 2 of the measurement campaign was based on descriptions on adaptive sampling strategies using kriging variance as described by Delmelle (2014). From those 400 measurements, only 280 have soil temperature data due to a breakage in the thermometer probes (Figure 3).

The same sampling technique was used at each point of measurement, which consisted of placing the accumulation chamber on the ground creating a seal to avoid external factors such as contamination from other gases. The handheld computer was used to start each measurement that lasted from 70 to 160 seconds; length of measurement

interval varied depending on how stable the concentration curves were and the rate of gas emission (Figure 4).

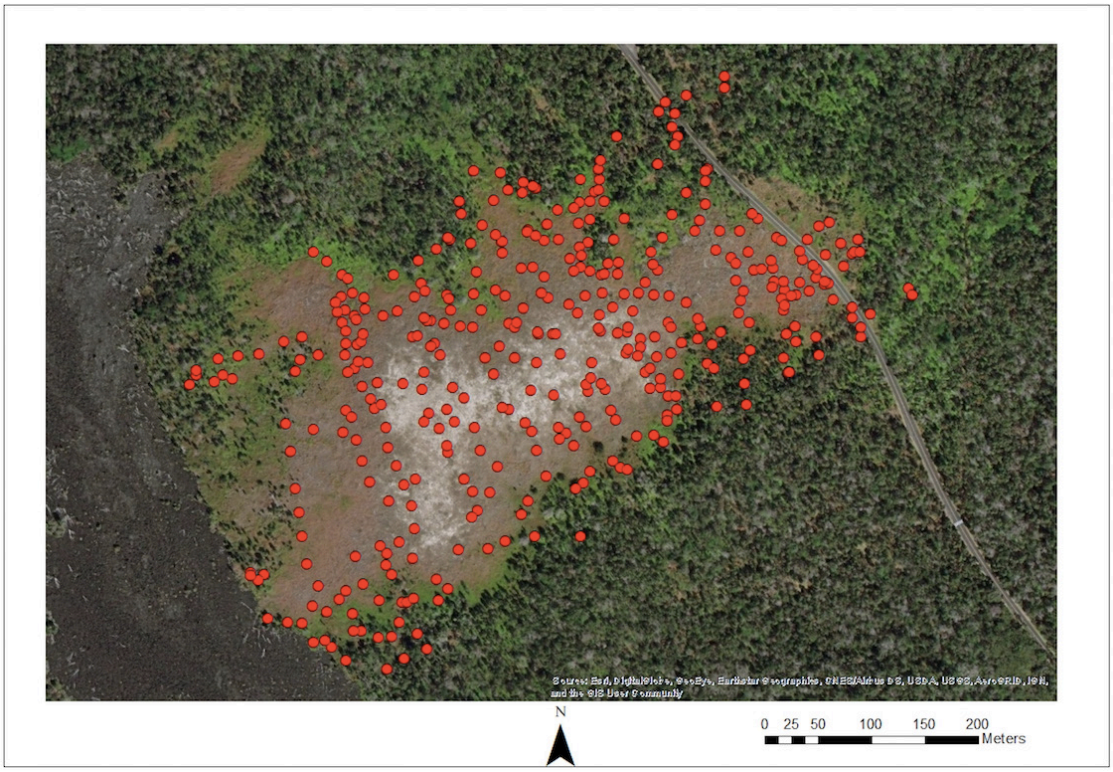

Figure 3. *Location of the 400 sample locations at the Puhimau geothermal area during the February-March 2017 field campaign. Imagery from ArcGIS online database.*

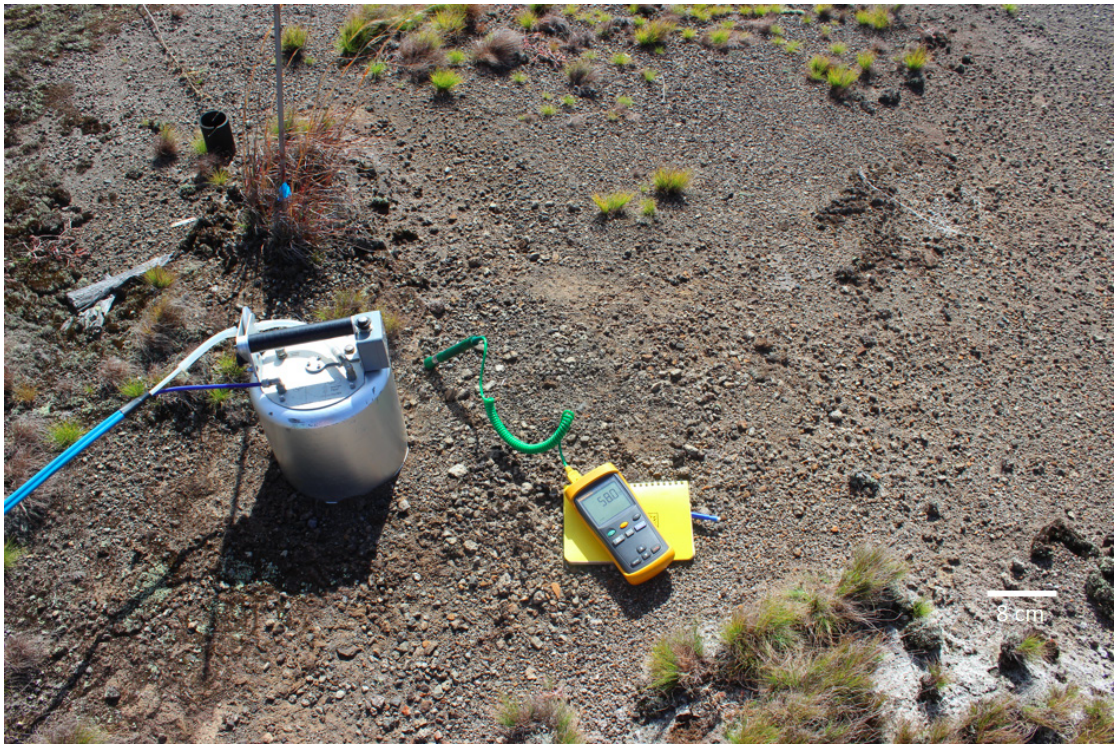

Figure 4. *Example of how the equipment was set up for each measurement showing the accumulation chamber and the soil thermometer.*

5.2 Diffuse Soil Degassing Data Analysis

Units were converted for both CO_2 and H_2S from ppm s^{-1} to g m^{-2} d^{-1} to change the values of concentration to a flux for further data processing. The following equations were used:

$$F\ g = F\ ppm * K * mCO_2$$

$$F\ g = F\ ppm * K * mH_2S$$

Where F g represents the flux value in g m^{-2} d^{-1}, F ppm is the concentration value in ppm s^{-1}, mCO_2 and mH_2S are the molecular weight of both gases and K means:

$$K = \frac{86400 * P}{10^6 * Tk * R} * \frac{V}{A}$$

Where P is barometric pressure in hectopascal (HPa), Tk is temperature in Kelvin (K), R is a gas constant value of $8.314 * 10^{-2}$bar∗L/K/mol, V represents the volume of the chamber in m^3, and A is the area of the chamber in m^2. Values under the limit of detection (LOD) were replaced by $\frac{LOD}{\sqrt{2}}$ for H_2S to eliminate zeros in the dataset; Croghan and Egeghy (2003) and Verbovsek (2011) argued that this is the best substitution method for values that fall under the LOD.

A stochastic simulation algorithm was used to calculate the total CO_2 and H_2S flux that was being released from the geothermal area. Sequential Gaussian Simulation (SGS) allows for the analysis of the spatial correlation of the data using a near neighbor approach to estimate unknown values in the area. The SGeMS software was used to process the SGS using 1,000 simulations for both CO_2 and H_2S flux. The SGS simulation needs a semi-variogram model to be able to estimate unknown points inside the grid, which is critical to produce accurate maps and to estimate the total flux in the feature (Figure 5 and 6). After the simulations are done, a total flux can be calculated by multiplying each simulated gas cell by the cell size and then adding the results of each multiplication within the grid.

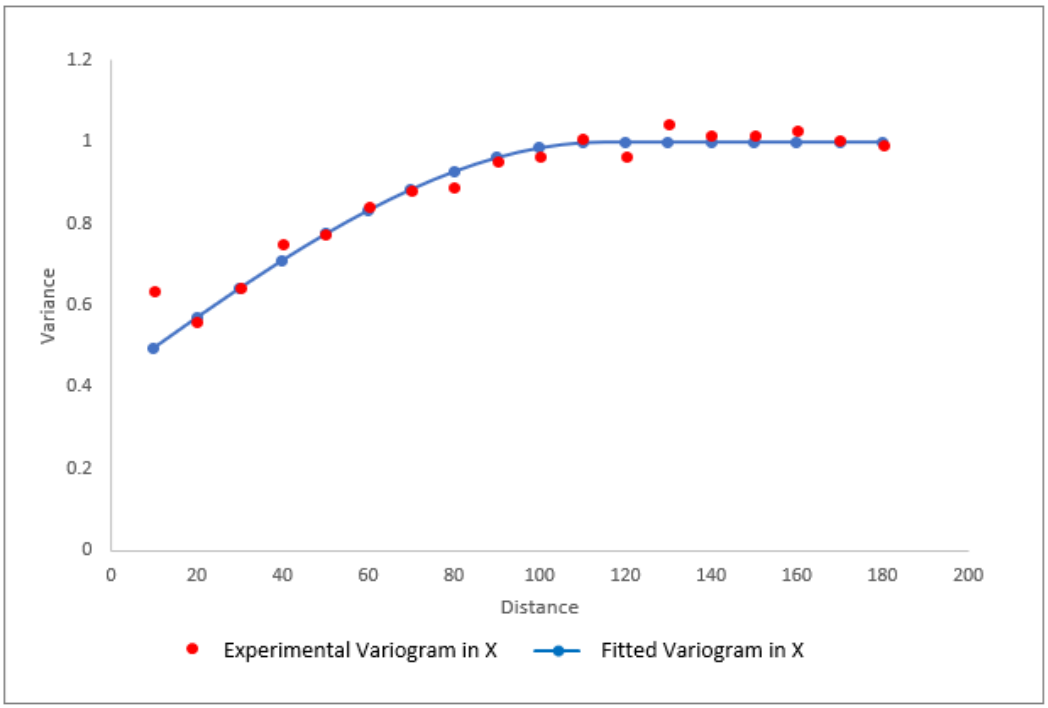

Figure 5. *Omnidirectional variogram model for the 1,000 simulations of CO_2. In red the experimental variogram and in blue the fitted variogram.*

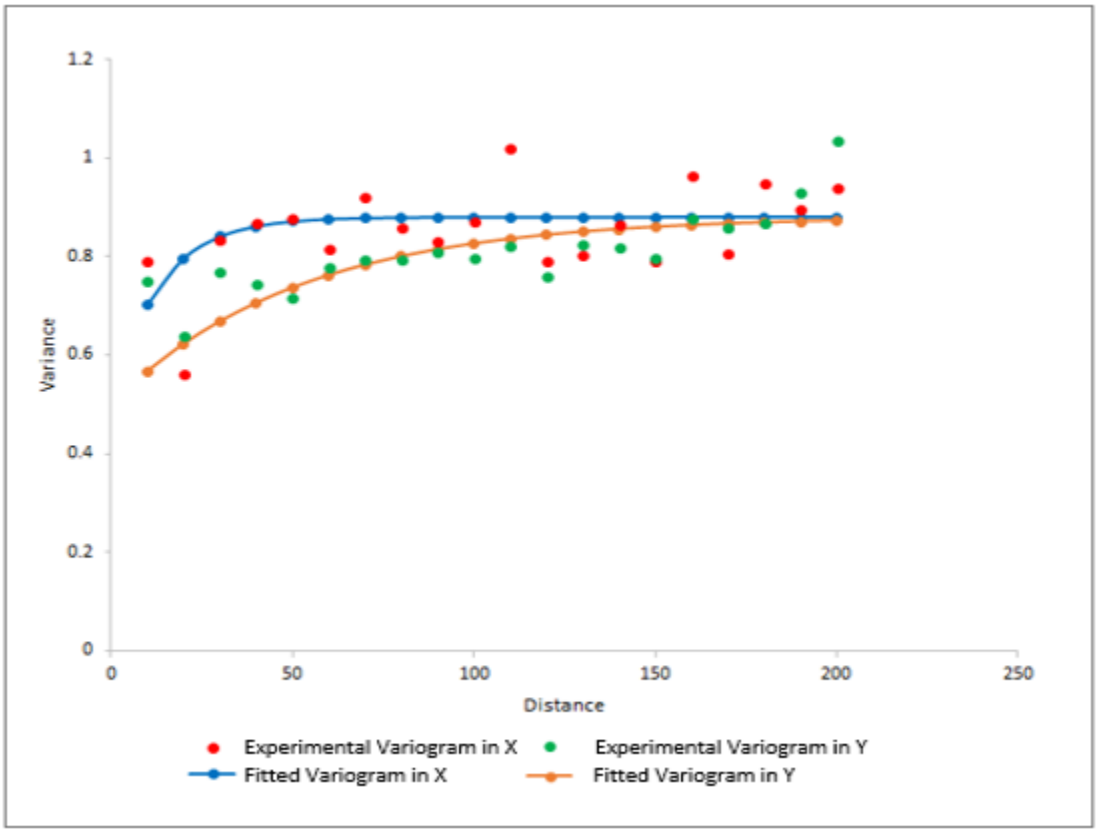

Figure 6. *Two direction (X and Y) variogram model for the 1,000 simulations of H_2S. In red the experimental variogram in the x direction and in blue the fitted variogram. In green the experimental variogram in the Y direction and in orange the fitted variogram.*

5.3 Remote Sensing Applications to Volcanic Environments

In this study, high-resolution multispectral imagery provided by the Digital Globe Foundation was used to establish a spatiotemporal correlation between vegetation and volcanic activity through time. There were two main goals for this component of the study: 1) Characterize the behavior of the Puhimau geothermal area gas emission distribution and the relationship to the surrounding vegetation; and 2) Determine if there is a correlation between changes in the distribution and/or size of the geothermal feature and periodic increases in eruption activity along the East Rift Zone. To achieve this, two distinct analyses were made and compared: 1) Normalized Difference Vegetation Index, and 2)

Land Cover changes using supervised classification. Following the methodology of Aburas et. al. (2015), NDVI was used as an indicator of Land Cover changes and to quantify changes in the size of the feature through time. NDVI can also be used as an indicator of vegetation health using vegetation reflectance values. These changes in vegetation health, can potentially be linked to volcanic activity in the East Rift Zone to understand how the feature behaves when changes occur prior to, during, and after eruptive events.

A total of nine high-resolution images from four different satellites are described in Table 1.

Year	**Satellite**	**Spatial Resolution**	**Spectral Resolution**	**Spectral Range**
2002 *2007*	QuickBird4	2.62 m	Visible & NIR	450-900 nm
2010 *2011*	GeoEye1	1.84 m		450-920 nm
2012 *2013*	WorldView2	1.84 m	Visible, NIR, Coastal, Yellow, Red edge, & NIR 2	400-900 nm
2014 *2016* *2017*	WorldView3	1.24 m		400 to 1040 nm

Table 1. *Resolution information about the imagery used in the analysis obtained from the Satellite Imaging Corporation website (https://www.satimagingcorp.com/satellite-sensors/).*

The images were processed using ERDAS Imagine 2016 and ArcGIS 10.14 version software. On the other hand, down-sampling using ArcGIS was made so all the imagery

had the ground sample distance (cell size) of 2.62 meters. The purpose of this step is to have consistency between the images and to make accurate calculations of the area size of classes that the analysis will have. Images were masked using ERDAS Imagine to the same extent, focusing on the Puhimau geothermal feature.

5.4 Normalized Difference Vegetation Index (NDVI)

Using ERDAS Imagine software a Normalized Difference Vegetation Index was calculated using the equation:

$$NDVI = \frac{NIR - Red}{NIR + Red}$$

This calculation allows for the creation of a graphical representation of land surface characterization from healthy (green) vegetated areas to those with bare soil that range from 1 to -1, respectively. Numerical values of the results were changed to descriptive land cover classes typical of those ranges, based on spectral signature values and ground knowledge. This was done to have a better interpretation of what type of vegetation is being stressed more in relation to the proximity of the highly active flux areas (Figure 7).

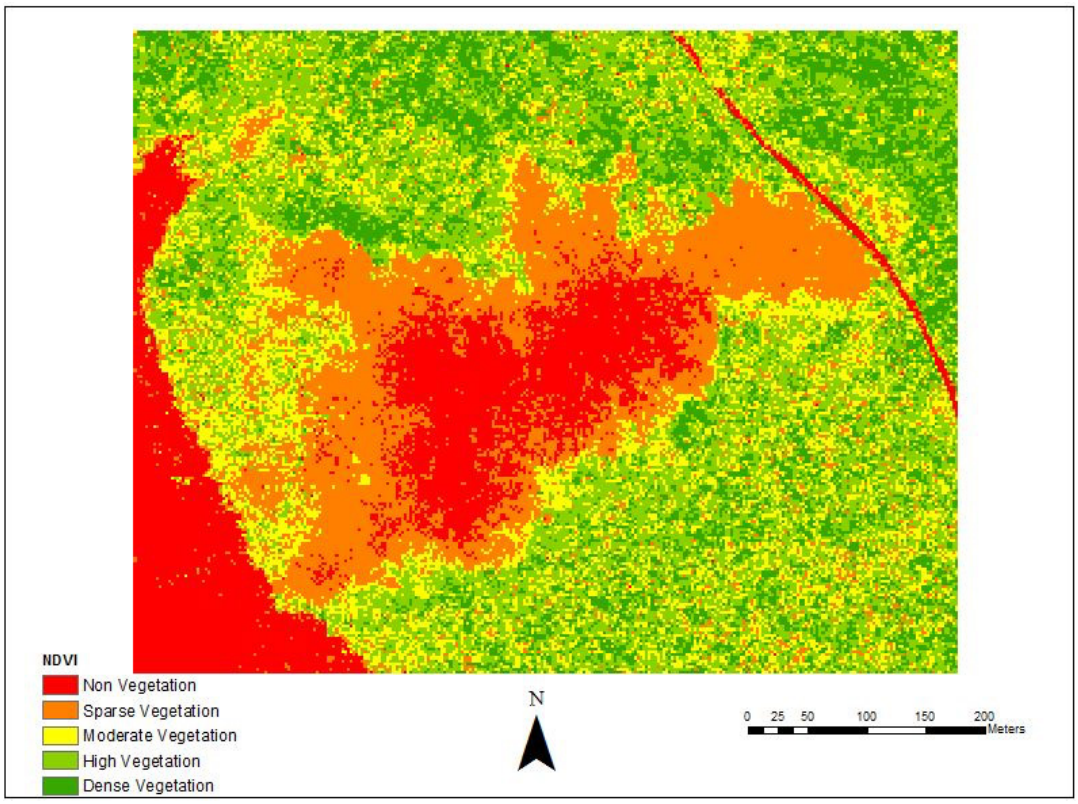

Figure 7. *NDVI classification for the Puhimau geothermal area for 2017.*

5.5 Supervised Classification and Difference

Using ERDAS Imagine, a supervised classification of the same imagery was done including 15 classes with 30 training samples per class. The training samples were selected from known location points based on field observations. These 15 classes were merged into 5 classes matching the same characteristics as the descriptive classes of the NDVI classification. Also, it allows one to establish a change detection for each class through the years. Change detection is used to quantify the area change through time. In this study, it is used as a proxy to understand how the Puhimau geothermal site is behaving through time in terms of its vegetation. Lastly, using the supervised classification images the Difference tool in Image Analysis from ArcGIS was used to highlight the areas of change through

time. This tool was used to generate a visual representation of how much a specific area in the feature changed and how it compares to patterns in fluxes over time with volcanic activity in nearby regions.

6 Results

6.1 Diffuse soil gas fluxes and soil temperature

During the field campaign at the Puhimau geothermal area, 400 measurements for CO_2 and H_2S were made ranging from 4.4 to 2,473.1 g m^{-2} d^{-1} and 0.006 to 2.510 g m^{-2} d^{-1}, respectively (Figure 8, 9 and Table 2). Average flux values are 88.18 g m^{-2} d^{-1} for CO_2 and 0.46 g m^{-2} d^{-1} for H_2S. In addition, 280 soil temperature measurements were collected ranging from 18.3°C to 93.9°C with an average of 52.8°C (Figure 10 and Table 2). Correlation plots between gas fluxes and soil temperature indicate that there is no correlation between them (Figure 11, 12, and 13).

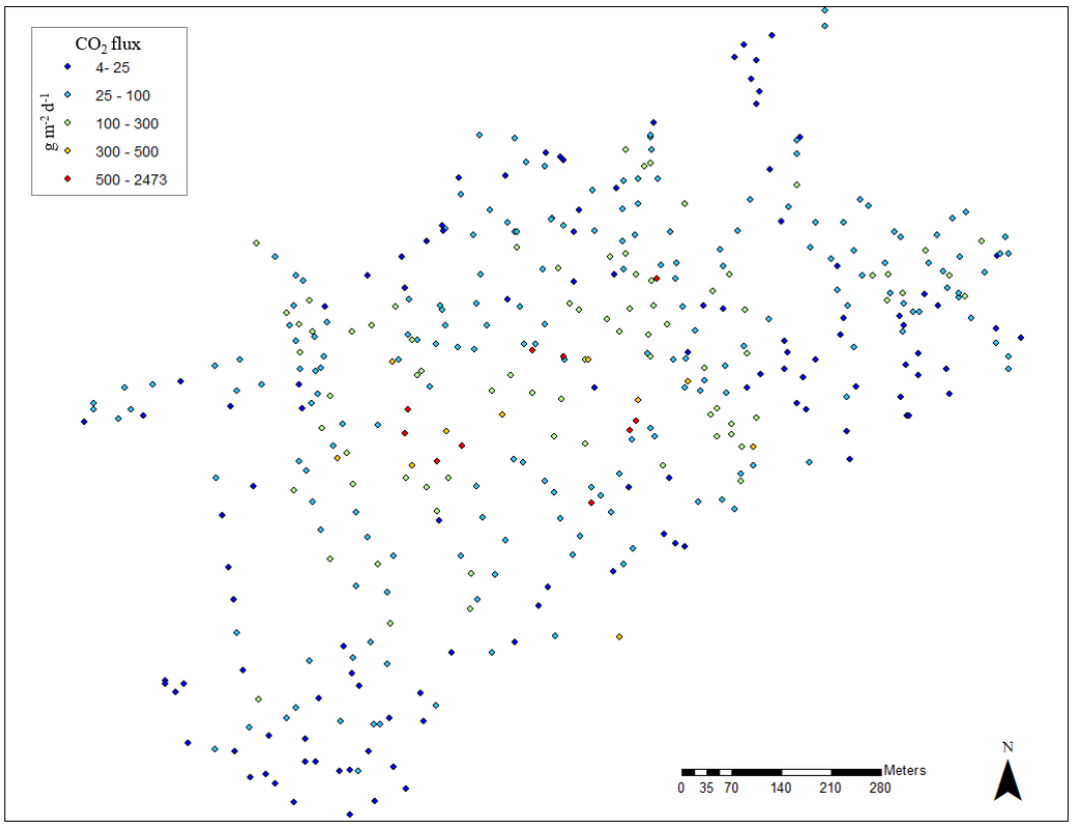

Figure 8. *Data distribution for CO_2 gas emissions at the Puhimau geothermal area values are in g m^{-2} d^{-1}.*

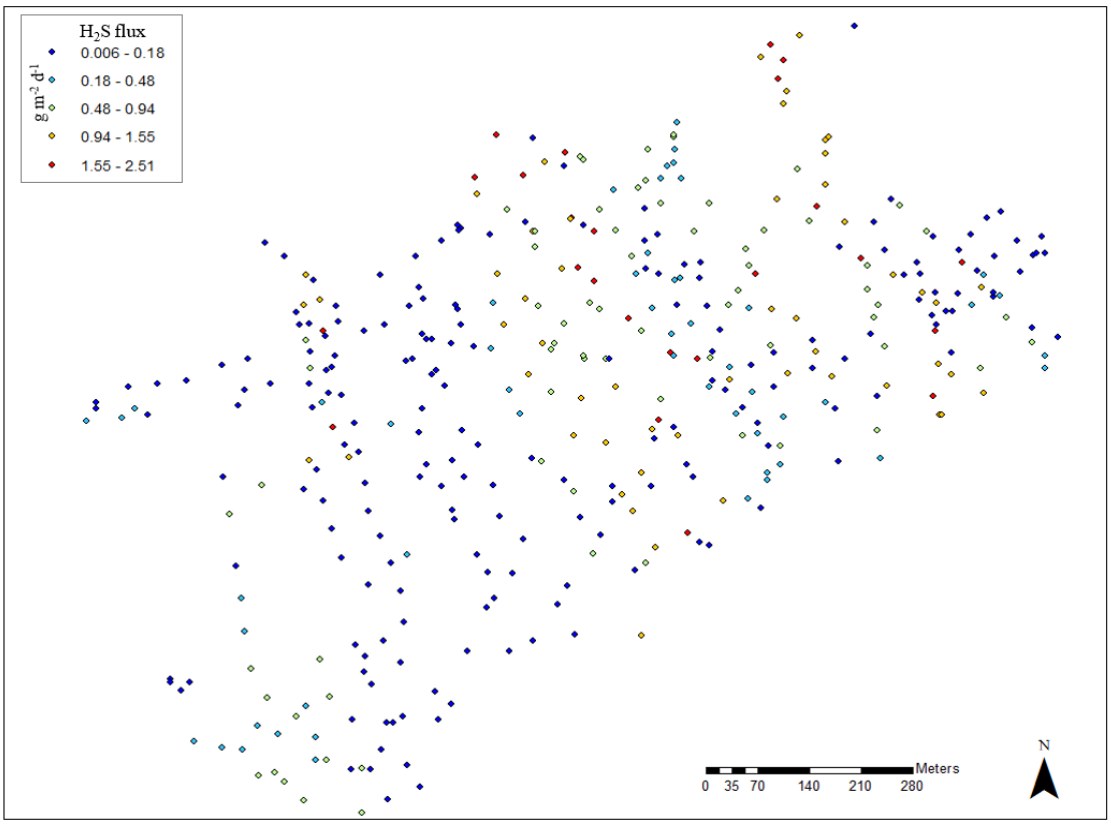

Figure 9. *Data distribution for H_2S gas* emissions at the Puhimau geothermal area values are in g m^{-2} d^{-1}.

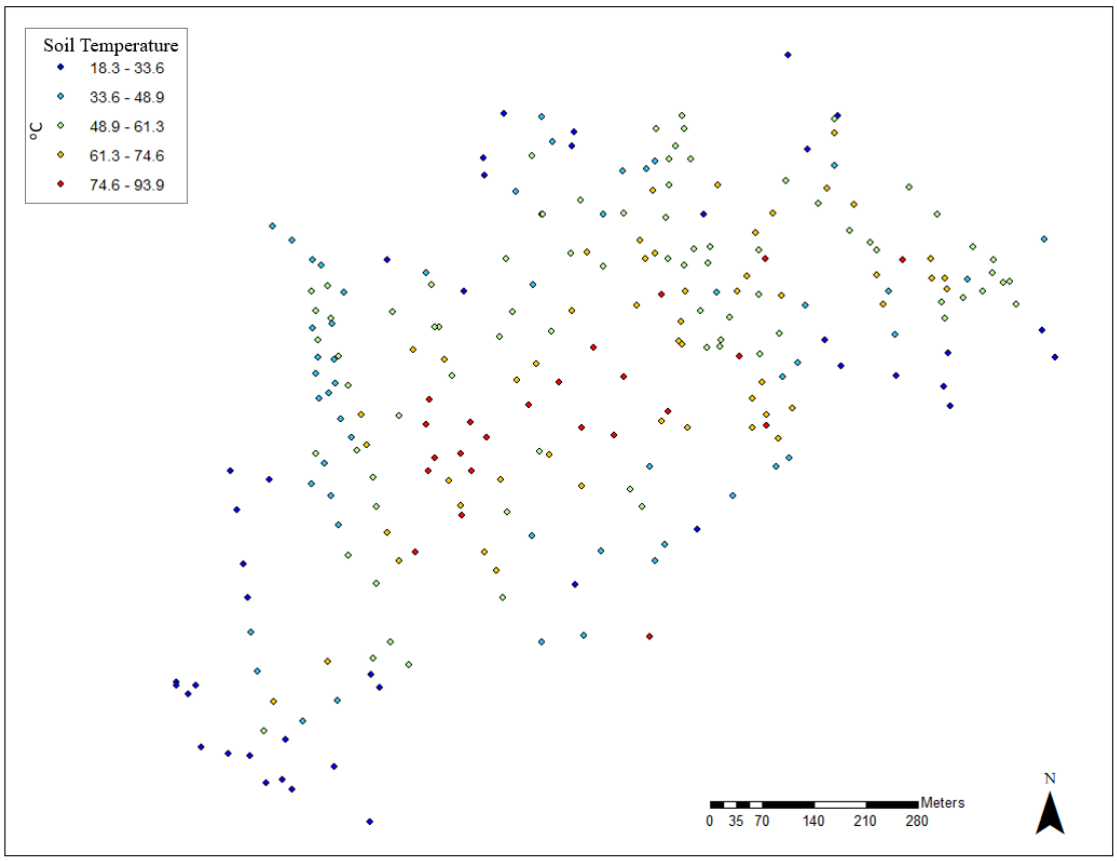

Figure 10. *Data distribution for ground temperature (~15cm) for the Puhimau geothermal area. Soil temperature values are in °C.*

	Minimum	Maximum	Average	Standard deviation	Variance
CO_2 ($g\ m^{-2}\ d^{-1}$)	4.4	2,473.1	88.18	170.22	28974.67
H_2S ($g\ m^{-2}\ d^{-1}$)	0.006	2.510	0.46	0.56	0.32
Soil Temperature (°C)	18.3°	93.9°	52.8°	17.35°	301.04°

Table 2. *Data statistics for CO_2, H_2S, and soil temperature at the Puhimau geothermal area collected during the 2017 field campaign.*

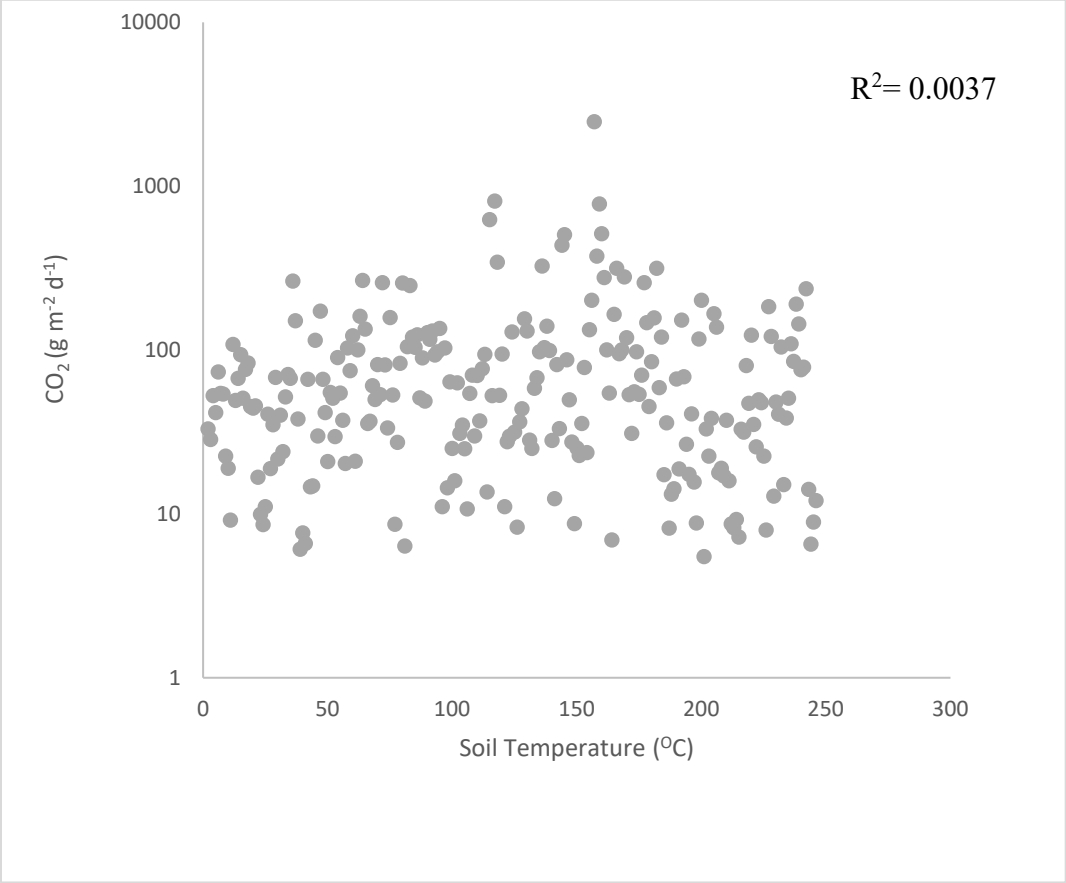

Figure 11. *Scatter plot showing a lack of correlation between CO_2 and soil temperature. Depth of soil temperature measurements: ~15cm.*

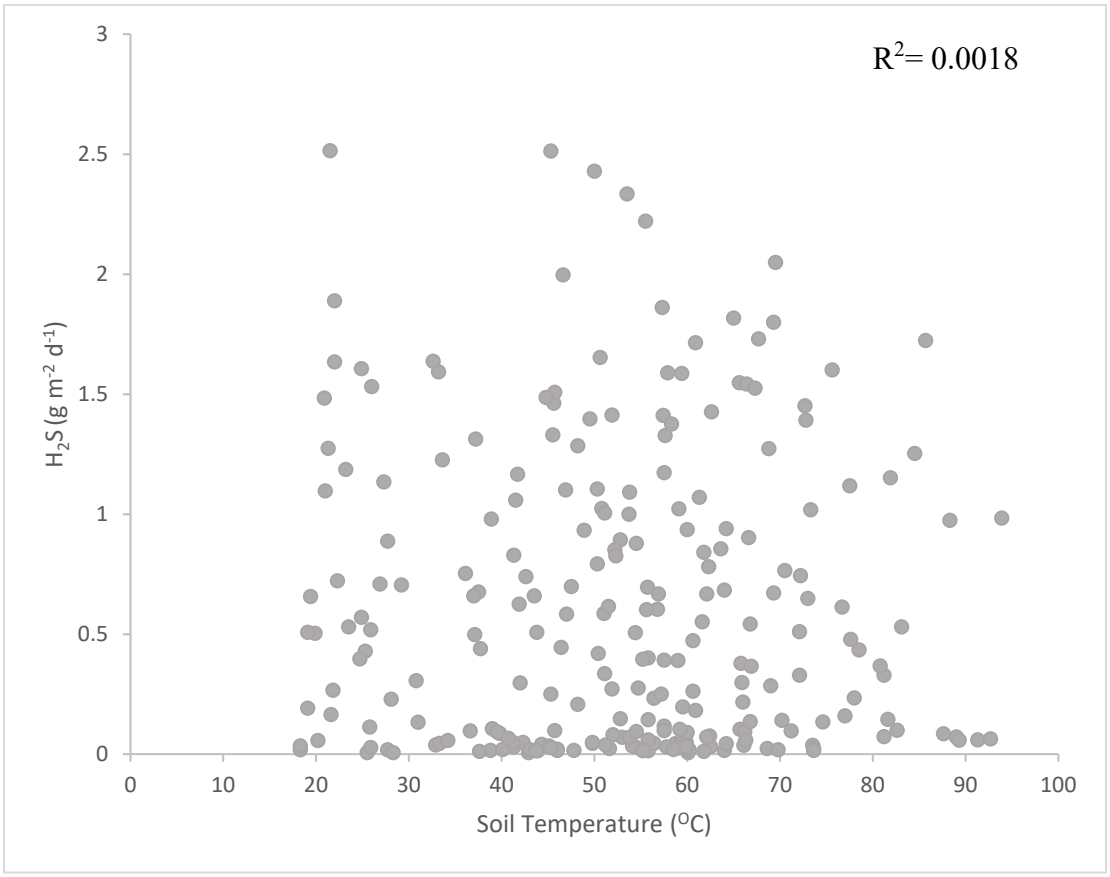

Figure 12. *Scatter plot showing a lack of correlation between H_2S and soil temperature. Depth of soil temperature measurements: ~15cm.*

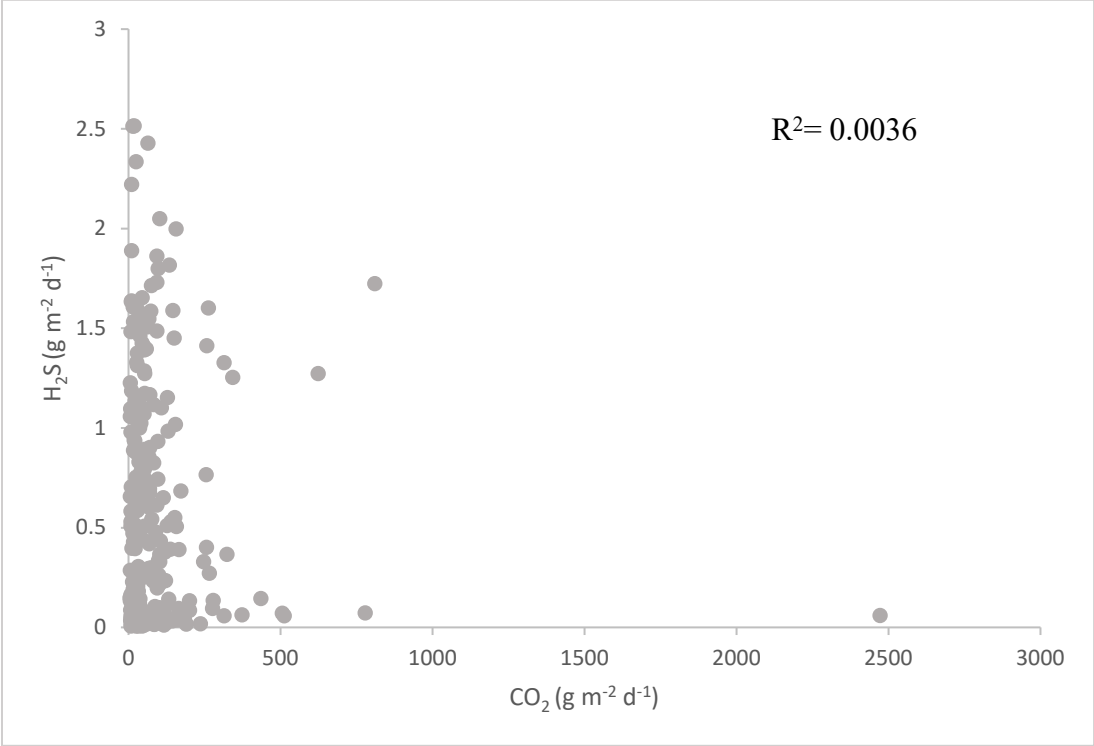

Figure 13. *Scatter plot showing a lack of correlation between CO_2 and H_2S.*

6.2 Sequential gaussian simulation

6.2.1 CO_2 Flux

Using SGeMS software, a sequential Gaussian simulation (SGS) was performed for CO_2 with a total of 1,000 realizations. The SGS derived flux map for CO_2 showed the center of the geothermal feature has the highest flux (Figure 14). In this area, we also observed fumaroles and other steam activity (Figure 15) and the ground was either completely bare or contained little or no vegetation (Figure 16). The center of the feature was also where the highest soil temperatures were recorded. The calculated total emission rate for the feature with 99% confidence is 80.82 to 81.50 g m^{-2} d^{-1}.

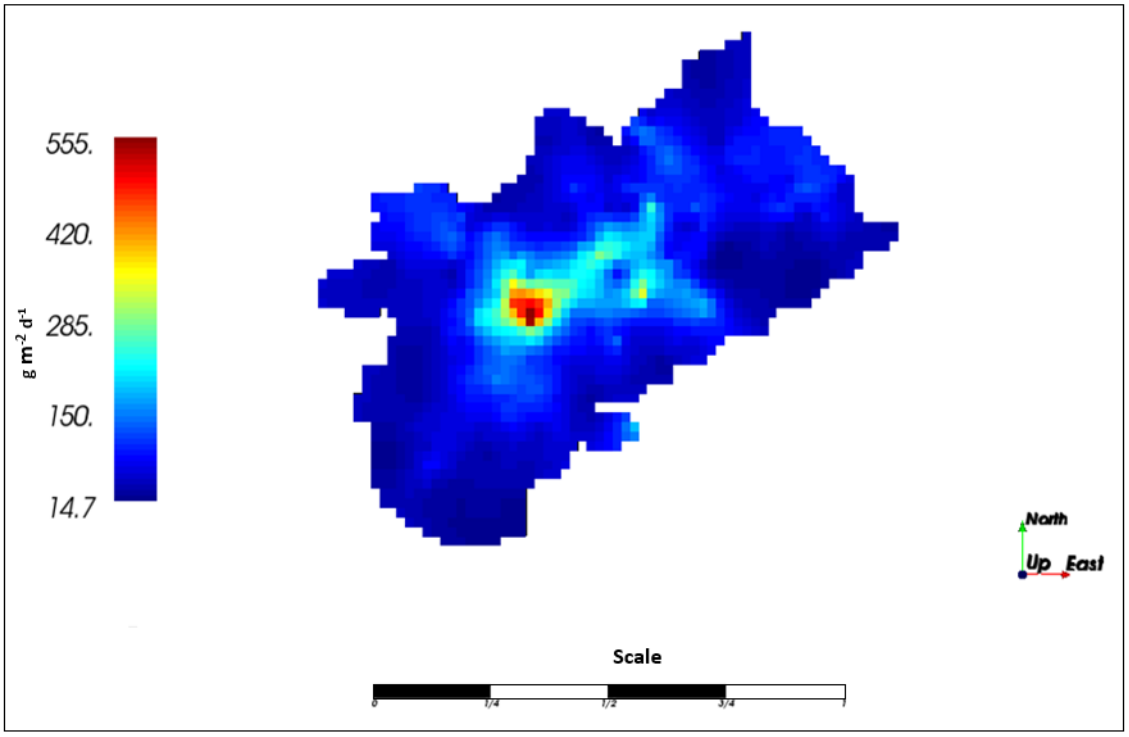

Figure 14. *Map of the SGS average results for CO_2 flux modeled for the Puhimau geothermal area. CO_2 flux values are in g m^{-2} d^{-1}.*

Figure 15. *Example of a fumarole with steam activity at the center of the Puhimau geothermal feature, an area that shows a high CO_2 flux value based on the SGS model.*

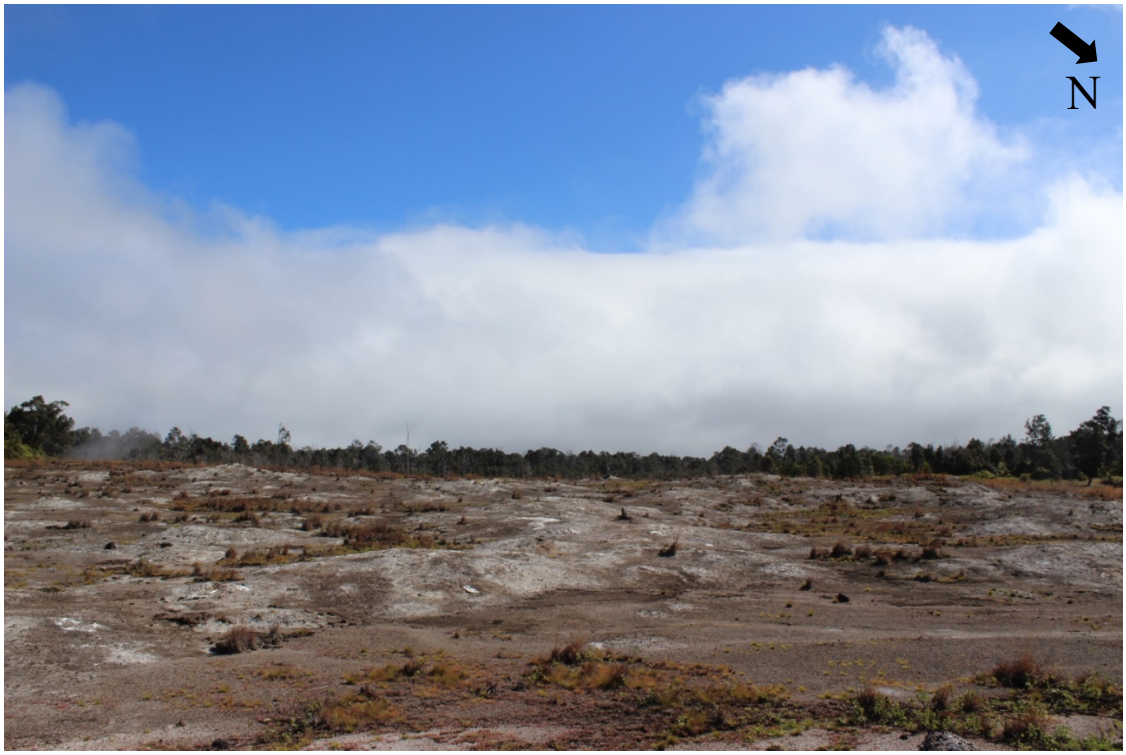

Figure 16. *Center of the Puhimau geothermal area showing lack of vegetation, bare soil, and fumaroles with steam activity. This area was identified as the highest CO_2 flux emissions based on SGS model results.*

6.2.2 H_2S Flux

After performing the same methodology for CO_2, 1,000 realizations were made using SGS for H_2S, the flux map generated showed that areas in the northeast corner of the feature have the highest flux (Figure 17). With a 99% confidence interval, the total flux of H_2S for the Puhimau geothermal feature ranges from 0.435 to 0.438 g m^{-2} d^{-1}. Based on field observations these areas were mostly covered in vegetation and not part of the active center with a high flux of CO_2 (Figure 18). However, active fumaroles were present in areas with elevated H_2S emissions. These fumaroles appeared much larger and to have more steam being released than those at the center of the feature in the northeast region that had elevated CO_2 emissions (Figure 19). The soil temperature for the northeast region of the geothermal feature had values in the low to mid ranges.

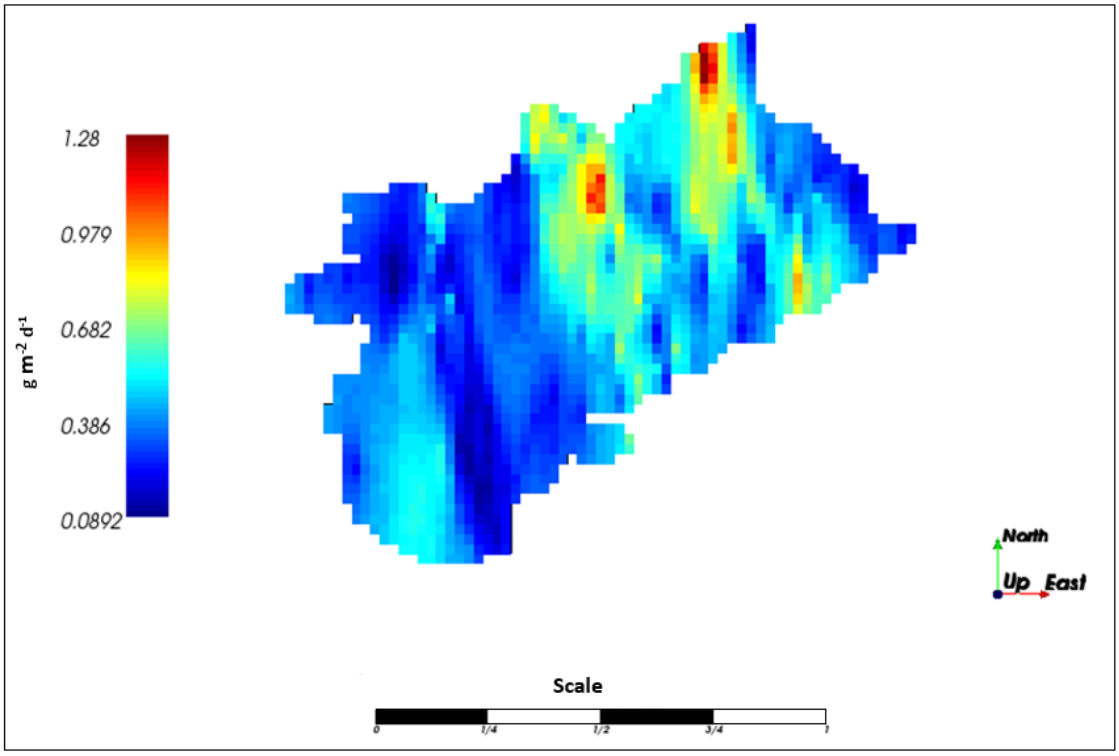

Figure 17. *Map of the SGS average results for H_2S flux modeled for the Puhimau geothermal area. H_2S flux values are in g m^{-2} d^{-1}.*

Figure 18. *Fumarole with steam activity at the northeast region of the Puhimau geothermal feature, an area with high flux H_2S based on the modeled flux map of H_2S.*

Figure 19. *Fumarole with steam activity at a high H_2S flux area at the northeast region of the Puhimau geothermal feature.*

6.3 Normalized difference vegetation index (NDVI)

In order to quantify the spatiotemporal behavior of the feature, an NDVI analysis through time was done to establish if changes in the feature can be correlated with changes in volcanic activity. Nine different images from 2002, 2007, 2010, 2011, 2012, 2013, 2014, 2016, and 2017 were selected. The selected time slices are based on 1) images that were close to previous study dates, 2) important volcanic activity or events in the surrounding areas particularly in the East Rift Zone, and 3) limited cloud coverage/interference.

An NDVI analysis was performed using ERDAS Imagine, and as a post-processing step the results were classified into five different classes: (1) non-vegetation, (2) sparse vegetation, (3) moderate vegetation, (4) high vegetation, and (5) dense vegetation (Appendix III and Figure 7). Classes were defined based on field observations and the vegetation present in distinct areas of the feature. Non-vegetation is characterized as barren, mostly loose soil, and lava fields. Sparse vegetation was described as low grasses and moderate vegetation as tall grasses. High vegetation was characterized as mostly ferns and shrubs. Lastly, dense vegetation was described as trees.

Results show that from the 37.75 hectares of land area, the most significant land coverage is moderate, high, and dense vegetation through the studied years (Figure 20). Small changes occurred from 2002 to 2009; however, from 2010 to 2017 the area showed high variability in vegetation types. From 2002 to 2011 non-vegetation and sparse vegetation declined from 6.7 to 0 and 7.0 to 5.4 hectares, respectively. In contrast, moderate, high, and dense vegetation increased from 5.2 to 8.7, 8.2 to 11.6, and 10.7 to 12 hectares, respectively, through time. The opposite trend can be seen in 2013 were areas

with non-vegetation and sparse vegetation increased in area from 0 to 6, and from 5.4 to 7.7 hectares. In 2014 a decline for non-vegetation and sparse vegetation can also be noted whereas from 2016 to 2017 the area increased. Alternatively, the most significant change was on dense vegetation where the area declined from 8.2 to 5.7 hectares (Figure 21).

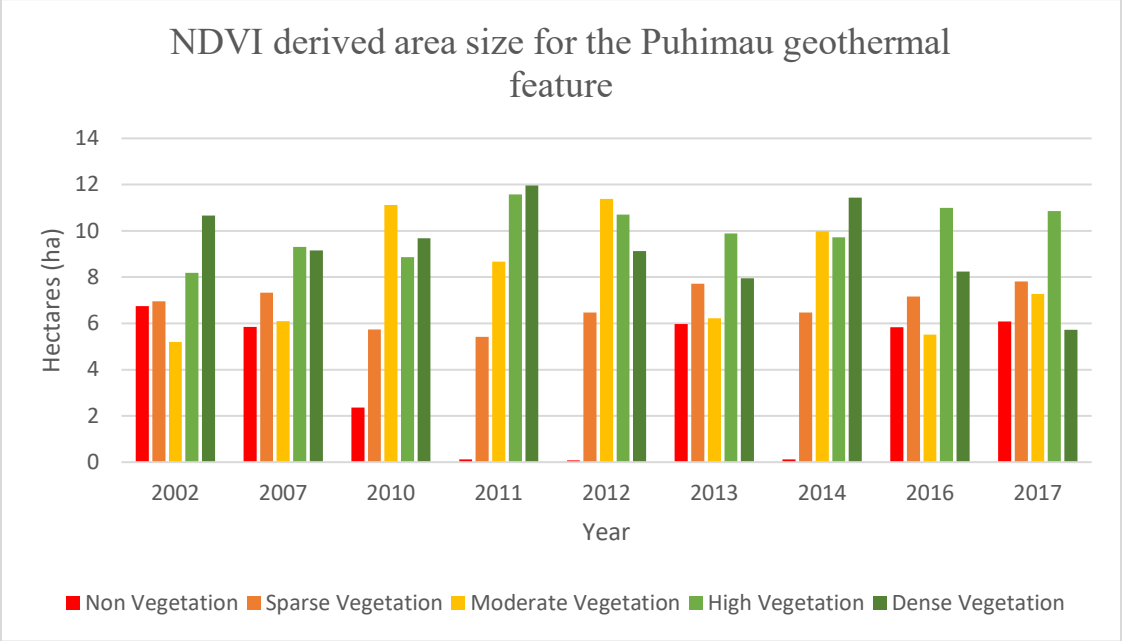

Figure 20. *NDVI derived area of classes in hectares from 2002 to 2017 for the Puhimau geothermal feature.*

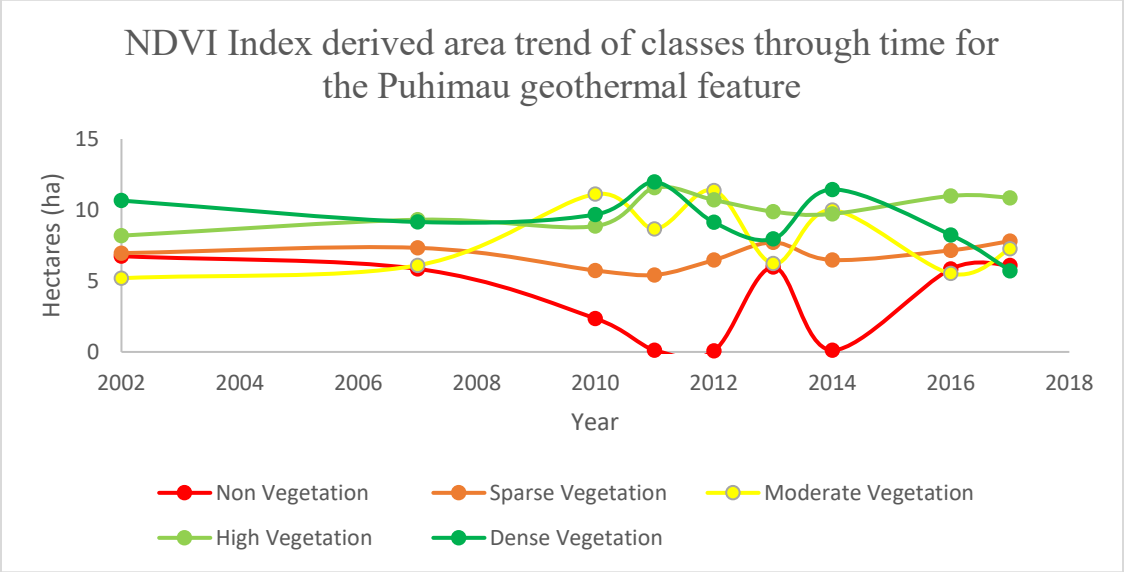

Figure 21. *NDVI derived area of classes trends in hectares from 2002 to 2017 for the Puhimau geothermal feature.*

6.4 Supervised classification and Difference

Using the same imagery from the NDVI analysis, a supervised classification was performed to understand how vegetation at the Puhimau geothermal feature changed from 2002 to 2017. The same classes from the NDVI analysis were used: (1) non-vegetation, (2) sparse vegetation, (3) moderate vegetation, (4) high vegetation, and (5) dense vegetation (Appendix IV). For every class, 30 training samples were drawn from known location based on ground observations to establish spectral signature clusters. Next, using the 'Difference from the Image Analysis' tool in ArcGIS, the classified images were compared to quantify the changes in the total area of vegetation types.

The 'Difference' tool allows selecting two images at a time and highlight areas where pixels show variance from its initial classification. In this study, the comparison was from non-vegetation to dense vegetation and from dense vegetation to non-vegetation. The classified images that were selected for comparison were based on the NDVI trend analysis

results that showed the biggest change in vegetation types through time (Figure 21). Since there was no significant change between 2002 and 2007 the analysis started after that period.

- 2007 to 2010: Increased vegetation at the center of the feature. Northside rim of the feature lost vegetation (Figure 22).
- 2010 to 2011: The northeastern part of the showed an increase in vegetation (Figure 23).
- 2011 to 2013: The center of the feature grew in size making the area less vegetated. South corners of the area also lost vegetation. (Figure 24).
- 2013 to 2014: The northern rim of the area showed a decrease in vegetation (Figure 25).
- 2014 to 2017: The feature showed an increase in vegetation in most areas, especially the northwest section of the entire feature. The southeast area showed scatter variability in vegetation (Figure 26).

Lastly, a comparison from 2007 and 2017 show that the biggest changes in the Puhimau geothermal area occurred at the north and northeastern zones of the feature where non-vegetated areas grew with time and the south and southeast zones that increased in vegetation (Figure 27).

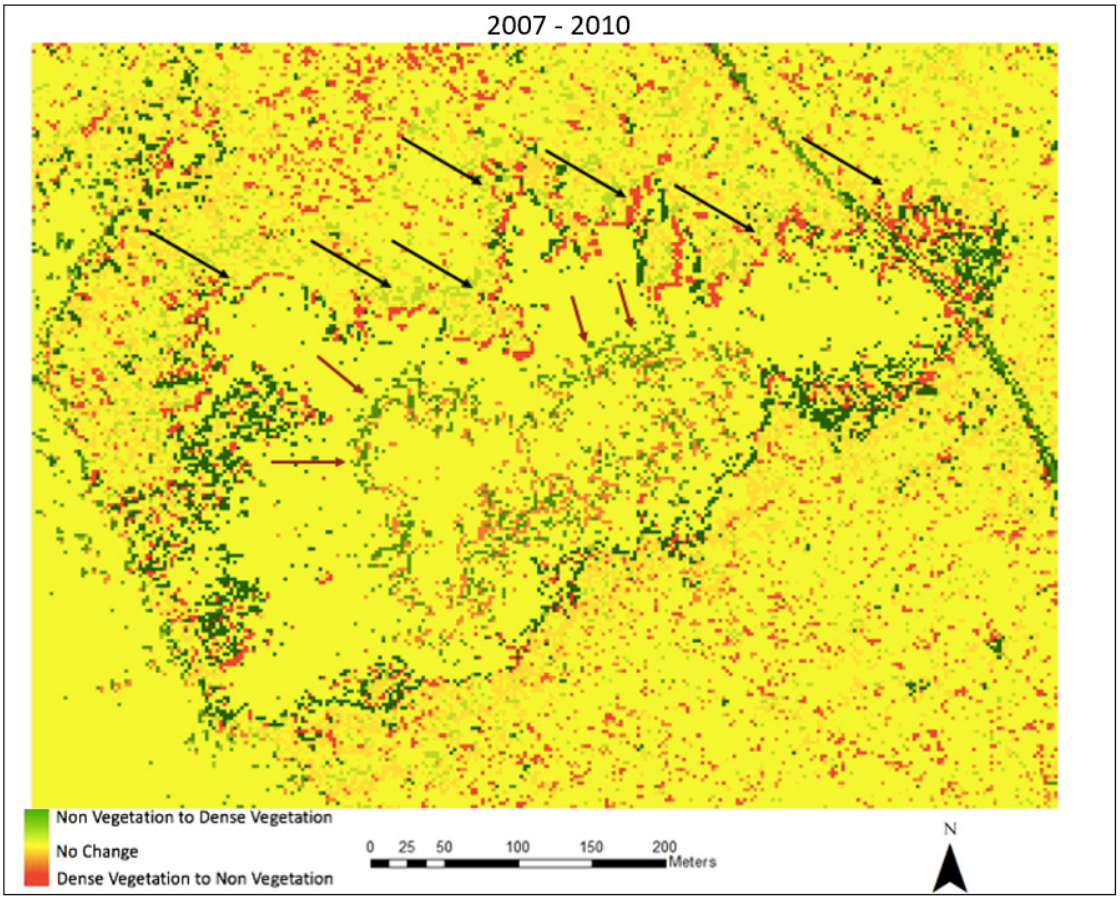

Figure 22. *Map of vegetation change from 2007 to 2010 indicating changes in the outer part of the center of the Puhimau geothermal feature from no vegetation to denser vegetation (brown arrows) and a loss of vegetation at the north side rim (black arrows).*

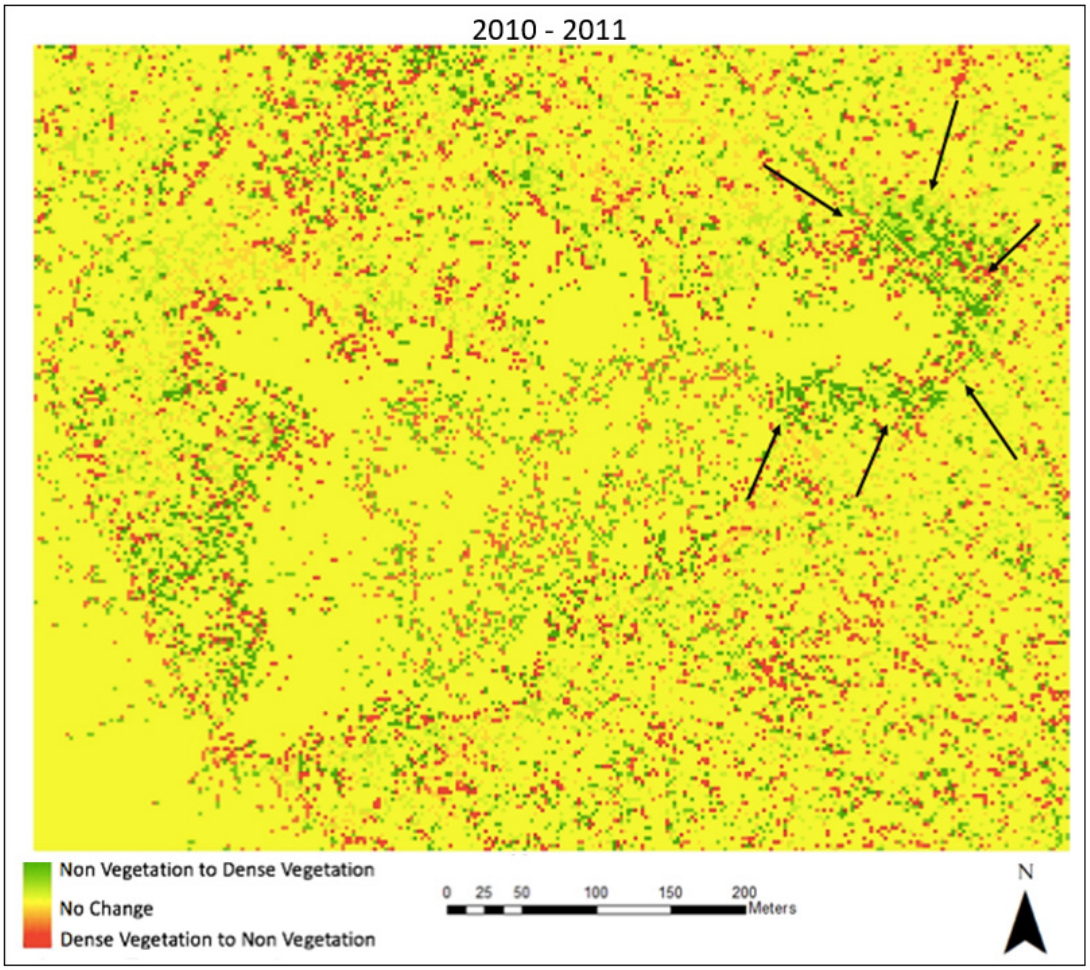

Figure 23. *Map of vegetation change from 2010 to 2011 showing changes in the eastern part of the center of the Puhimau geothermal feature from no vegetation to denser vegetation (black arrows).*

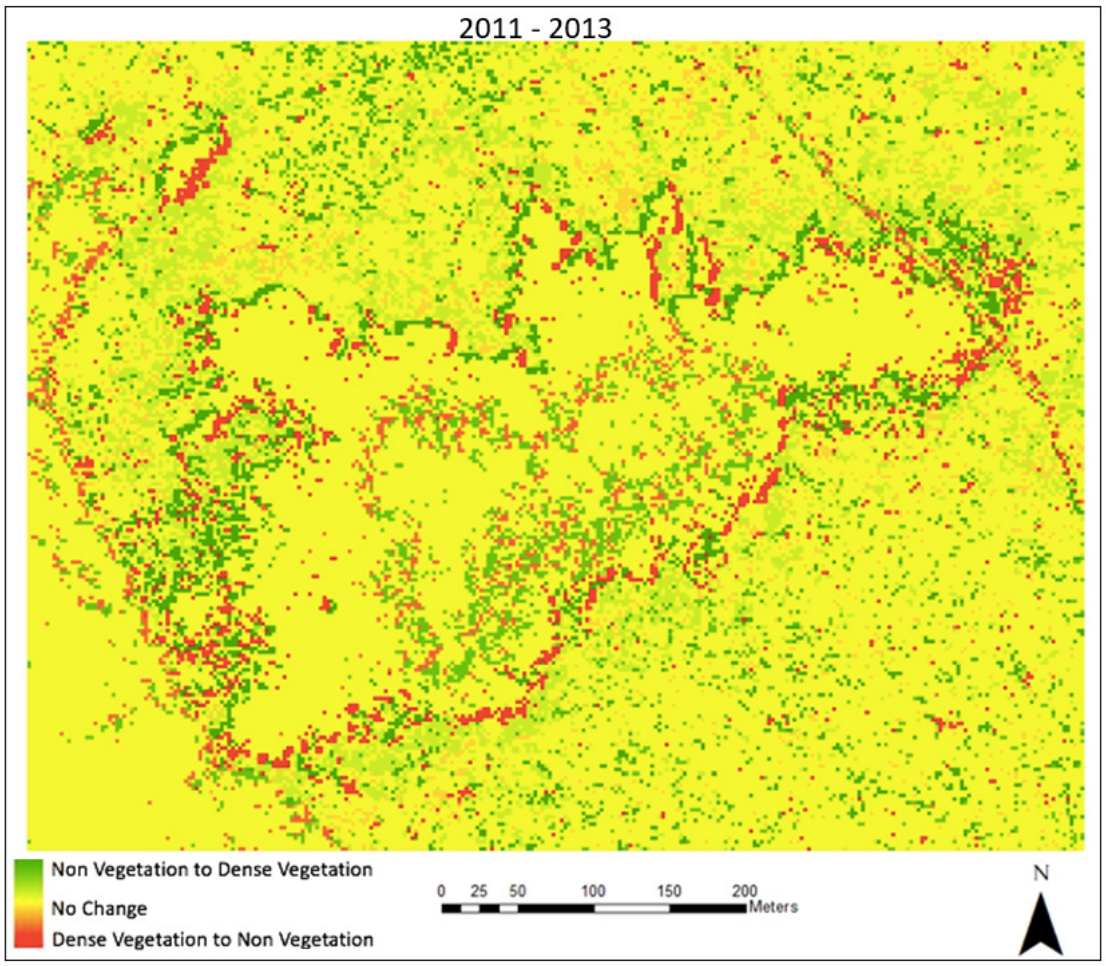

Figure 24. *Map of vegetation change from 2011 to 2013 highlighting changes in the center and rims of the Puhimau geothermal feature from denser vegetation to no vegetation.*

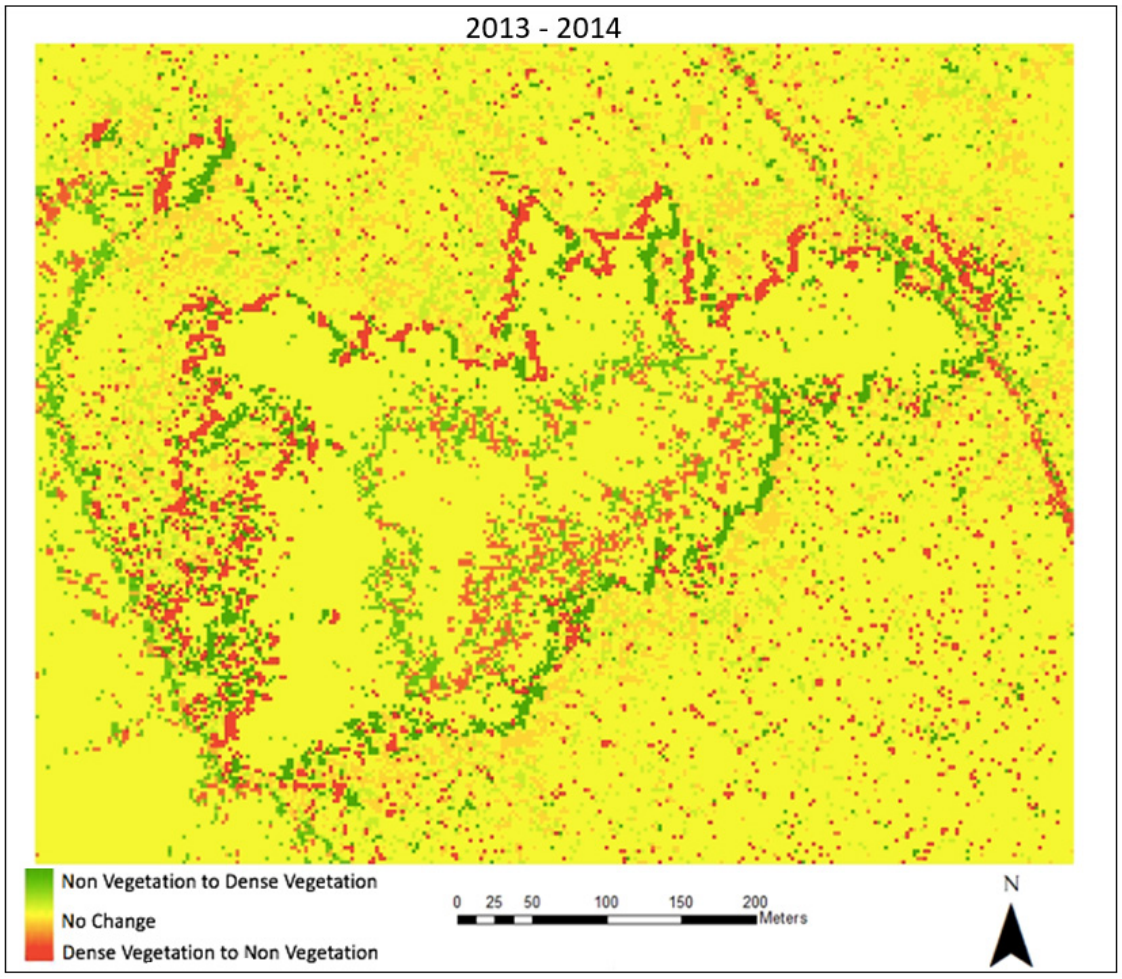

Figure 25. *Map of vegetation change from 2013 to 2014 indicating changes in the northern outer part of the Puhimau geothermal feature from denser vegetation to no vegetation.*

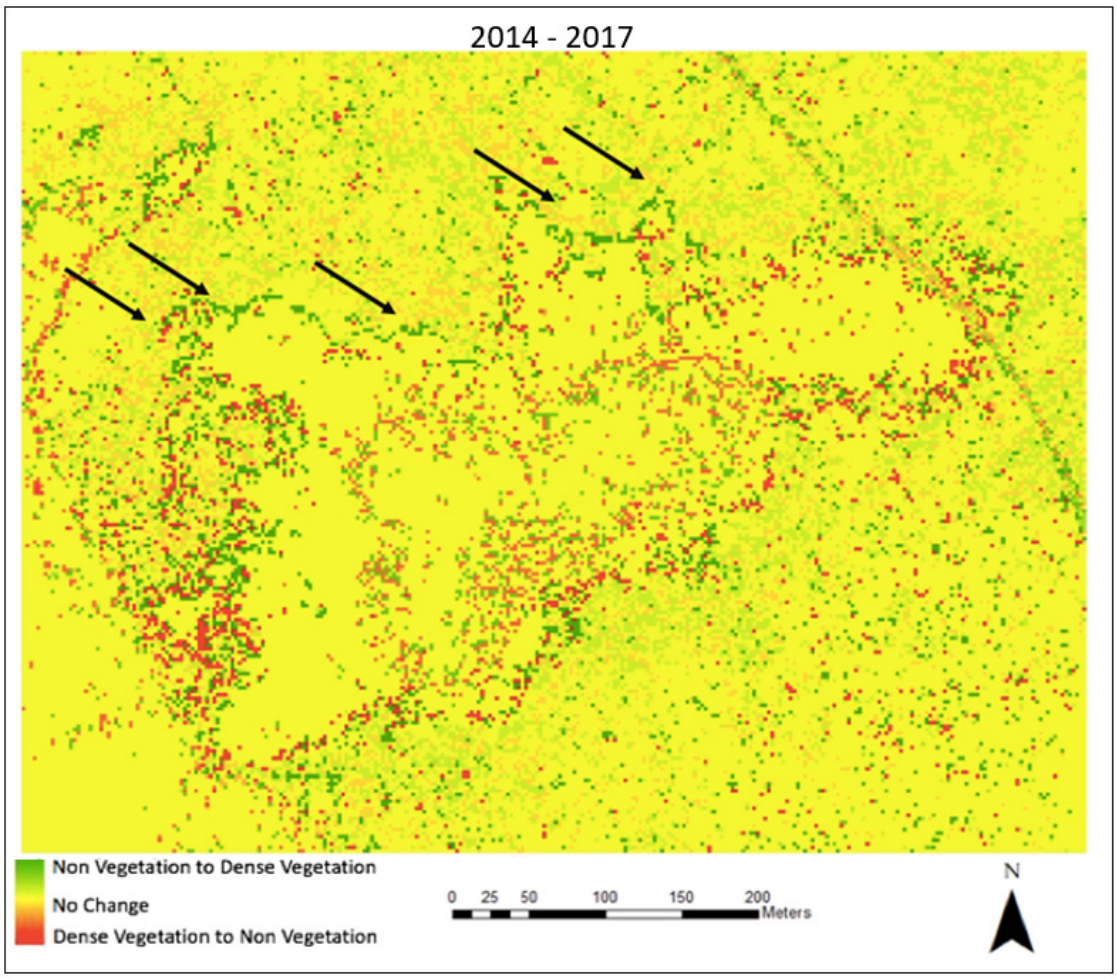

Figure 26. *Map of vegetation change from 2014 to 2017 indicating changes in the northern outer part of the Puhimau geothermal feature from no vegetation to denser vegetation (black arrows).*

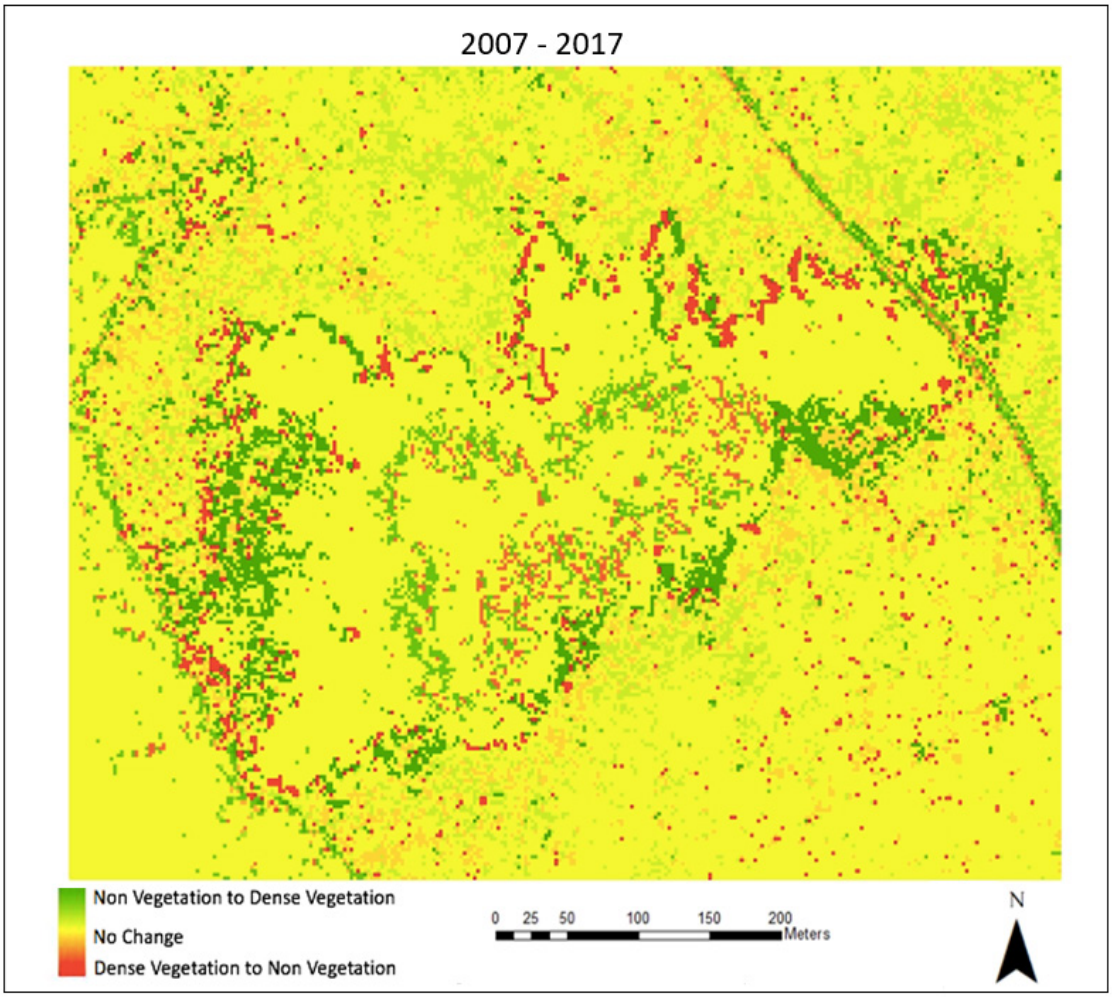

Figure 27. *Map of vegetation change from 2007 to 2017 for the Puhimau geothermal feature.*

7. Discussion

7.1 Diffuse CO_2 flux

The total output of soil gas CO_2 emissions for the Puhimau geothermal area ranged from 14.09 to 14.21 t d^{-1} with a 99% confidence interval and is considered to be almost exclusively magmatic in origin. Although geochemical isotope data was not collected during the field campaign, based on previous research it is well established that the CO_2 being released from the Puhimau geothermal area is of magmatic origin; mirroring the same composition of gas from the summit magma chamber of Kilauea (Friedman et al, 1987; Gerlach and Taylor, 1990). Based on the quantification of the diffuse degassing at the Puhimau geothermal area it can be established that the feature is not a major contributor of the total CO_2 budget of the Kilauea volcano as measurements at the summit indicate an emission rate of 8,500 t d^{-1} (Gerlach et al, 1998). In addition, Pu'u'O'o, which is located along the East Rift Zone, has also shown comparatively low emission rates of 240 to 300 t d^{-1}, but an order of magnitude greater than the Puhimau geothermal feature. This disparity is due to the fact that 94 to 97% of the CO_2 is emitted into the atmosphere from the summit reservoir (Gerlach and Graeber, 1985; Greenland et al, 1985).

The total flux emissions for Puhimau of 14.09 to 14.21 t d^{-1} in comparison to previous surveys from 1996 and 1998 are lower; in 1996 the area had an emission rate of 27 ± 3 t d^{-1} and 17 ± 2 t d^{-1} for 1998 (McGee et al, 2006). These changes in flux emission rates can be attributed to temporal variations in meteorological forces, changes in groundwater flow, shallow faulting, and volcanic activity (Gerlach et al, 2001; McGee and Gerlach, 1998; Rogie et al, 2001). Also, in both of the previous surveys, areas with the highest soil

temperatures corresponded with higher CO_2 emissions (McGee et al, 2006). In our survey, even though there is not a clear statistical correlation between CO_2 and soil temperature the center of the feature is the area with higher values for both parameters. Therefore, we suggest the hypothesis of one hidden fault that goes from the south-west to the north-east direction of the feature is likely to exist at the Puhimau geothermal area (Figure 28).

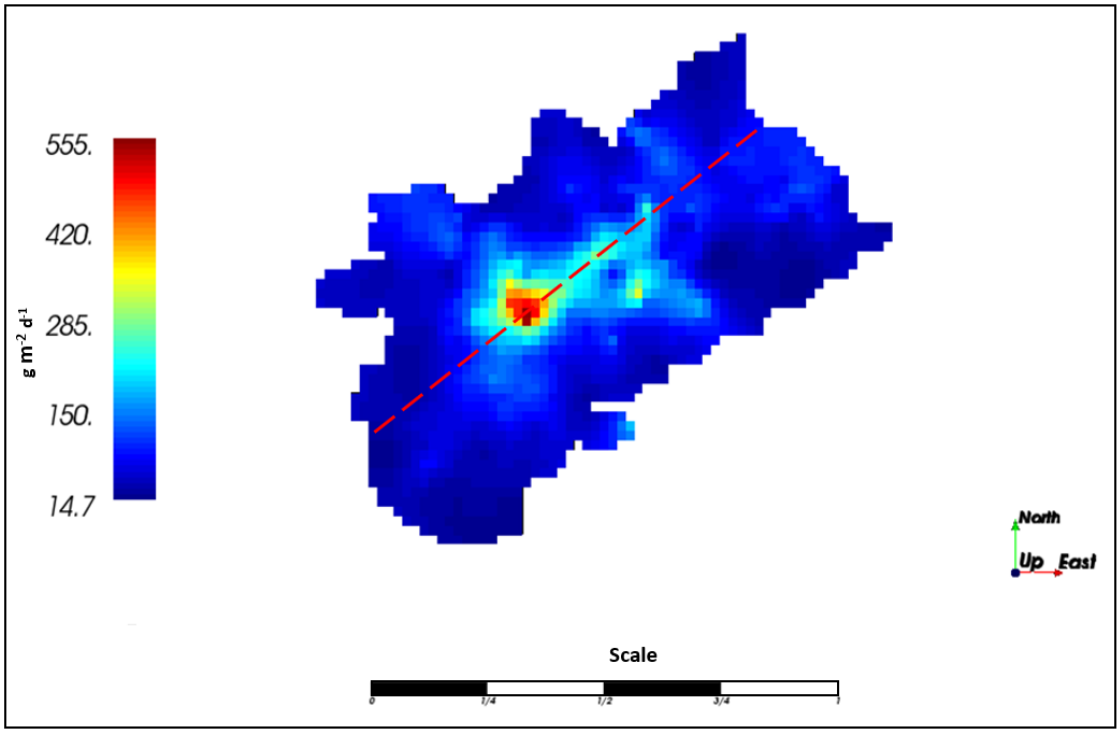

Figure 28. *Hypothesized fault based on the relationship between high CO_2 flux and topography at the Puhimau geothermal area.*

7.2 Diffuse H_2S flux

The emission of SO_2 from the Pu‘u ‘O‘o vent, East Rift Zone and the summit of Kilauea was quantified in 1995 by McGee and Gerlach (1998) estimating 2,160 t d^{-1} at the vent and in 1998 Gerlach et al. (1998) estimating 210 t d^{-1} at the summit (McGee and Gerlach,

1998; Gerlach et al, 1998). Based on the previous estimations of gas emissions it can be established that the magma injected into the East Rift Zone retains most of its volatiles and it's rich in SO_2 after the loss of most of its CO_2 (McGee et al, 2006; Gerlach et al, 1998 Sutton et al., 2001). During previous surveys at the Puhimau geothermal area and the Upper East Rift Zone, there was no apparent evidence of Sulphur emissions (McGee et al, 2006). In contrast, during our 2017 survey flux emissions of H_2S above detection limits were found and quantified.

The total flux emissions of H_2S at the Puhimau geothermal feature were determined to be from 0.0759 to 0.0764 t d^{-1}. The emission of a SO_2 rich gas at the surface suggests magma underneath the geothermal feature at a shallow depth. High solubility of SO_2 in basalts exsolve at very low pressures requires that magma that passes underneath the Puhimau Geothermal must be shallow enough to release SO_2 over part of the area. The change in SO_2 to H_2S may be attributed to the scrubbing of the sulfur in the at shallow depths (0.5 to 2km) in the system (Ingebritsen and Scholl, 1993; Kauahikaua, 1993; Tilling and Jones, 1991). Based on previous self-potential studies, dikes in the East Rift Zone constrained and impounded water resulting in a shallow water table at the Upper East Rift Zone (Jackson and Kauahikaua, 1987). Therefore, it is likely that SO_2 undergoes hydrolysis due to the fact that the main magma conduit resides below the water table in the Upper East Rift Zone (Symonds et al., 2001).

7.3 Origin of soil gas emission distribution

The underlying structures (faults and fractures) can be revealed in the Puhimau geothermal area based on the distribution of the gas flux emissions. Previous research shows that areas with high CO_2 emissions are localized along eruptive fissures, a system of faults, fractures, craters, fumaroles, and collapsed rims (Giammanco et al., 1998; Lewicki and Brantley, 2000; Chiodini et al. 2001; Cardellini et al., 2003; Frondini et al., 2004; Giammanco et al., 2006; Padrón et al., 2008; Ranaldi, 2008; Melián et al., 2014; Harvey and Harvey, 2015). Based on the results of the SGS average map for CO_2 flux at the Puhimau geothermal area the highest emissions had a southeast to northwest orientation (Figure 28). Surveys from 1996 and 1998 also showed a southeast to northwest alignment of areas with high CO_2 emissions (McGee et al, 2006). In contrast, the distribution of high H_2S flux also shows evidence of an orientation, but is roughly orthogonal to the orientation of the high CO_2 flux distribution.

The difference in solubility between CO_2 and SO_2 and the suggestion that there are likely two distinct magma reservoirs underneath the surface of the geothermal area may explain the difference in gas structures and areas with high flux emissions of H_2S and CO_2 at the Puhimau geothermal area. Previous research shows that CO_2 is less soluble in magma than SO_2, and is, therefore, released at high pressures estimated to be at the base of the magma reservoir (7km; Dixon et al., 1995; Gerlach et al., 2002; Hager et al., 2008). In contrast, the higher solubility of sulfur in magma indicates storage at much shallower depths (Wallace and Charmichael, 1992). Magma with higher concentrations of CO_2 appear to move in an east-west direction below the surface of the Puhimau geothermal area,

while magma with depleted CO_2 and rich in SO_2 appears to rise to shallower depths moving north-south towards the East Rift Zone.

Based on the orientation of the high gas emissions it appears that there are likely three subvertical hidden faults/fractures beneath the Puhimau geothermal area (Figure 29). Two faults/fractures are oriented sub-parallel to each other corresponding to high H_2S emissions whereas a perpendicular fault/fracture corresponds to high CO_2 emissions. The orientation of high H_2S emissions are in line with the Sulfur banks steam fissure feature in the north area of the Kilauea summit, just 5 km north from the Puhimau geothermal area (Figure 30). Whereas the east-west orientation of the CO_2 emissions at Puhimau are similar in orientation to the high CO_2 emissions that dominate the Steam vent geothermal feature in a similar orientation just north of the Kilauea crater based on recent measurements of soil gas in that area (Deering, C.D. pers comm).

Fault system maps generated from seismic activity at the Kilauea volcano (University of Hawaii database, 2007) don't show evidence of faults intersecting the geothermal area, suggesting that these hidden faults/fractures are aseismic, possibly because they are filled by magma (Figure 31). The location of the fault/fracture intersection at the Puhimau geothermal area can explain the orientation of the anomalous gas emission fluxes (Curewitz and Karson, 1997; Rowland; Sibson, 2004 and Egbert et al., 2014). Previous research at other geothermal areas such as the Brady's geothermal system in the Basin-and-Range Province show that areas with degassing anomalies coincide with uplflow zones from deep reservoirs reaching permeable fault zones and fault intersections (Egbert et al., 2014). A higher permeability in fault intersection zones allow gases to reach the surface (Curewitz and Karson, 1997; Rowland and Sibson, 2004).

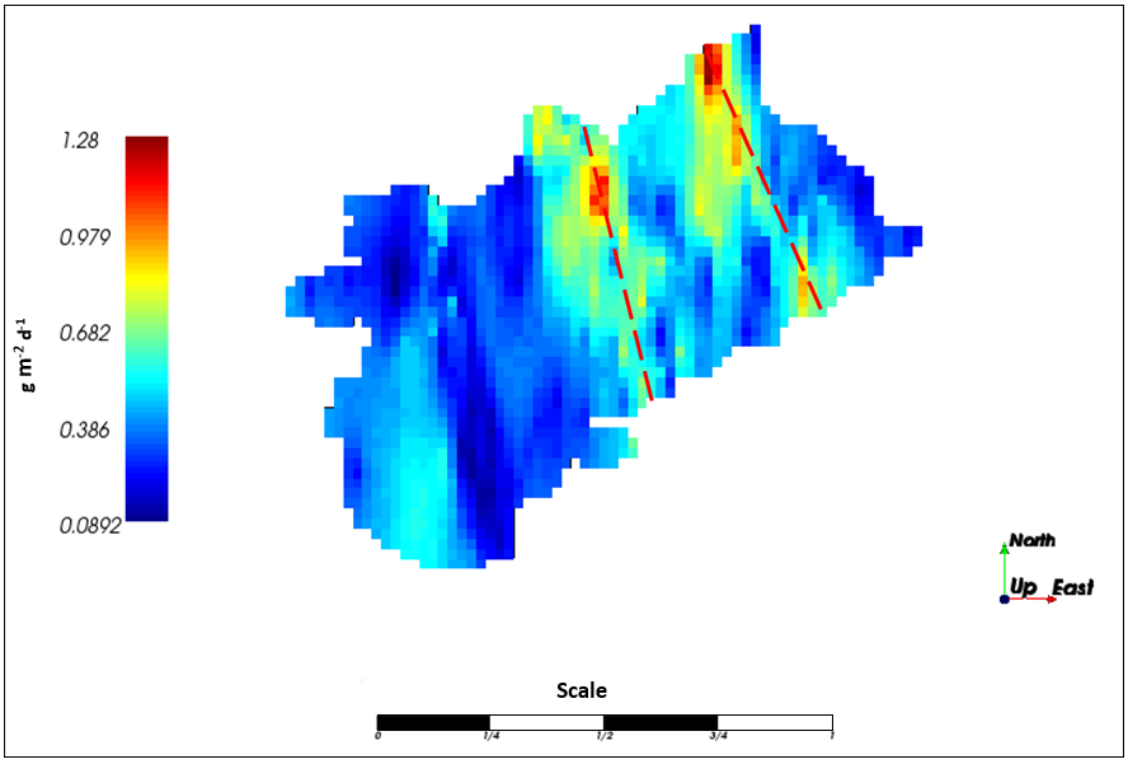

Figure 29. *Hypothesized faults/fractures based on the relationship between high H_2S flux and topography at the Puhimau geothermal area.*

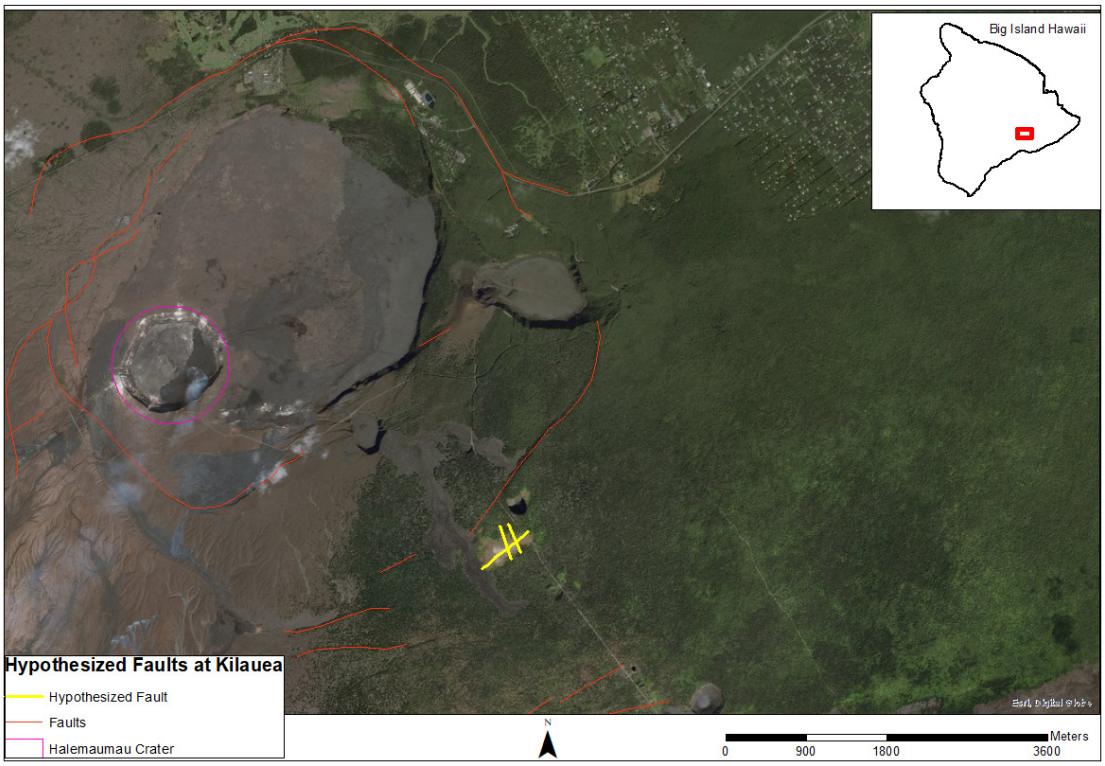

Figure 30. *Hypothesized faults/fractures at the Puhimau geothermal area and fault system at the Kilauea volcano. Fault data downloaded from:* https://catalog.data.gov/dataset/hawaii-faults-9f554

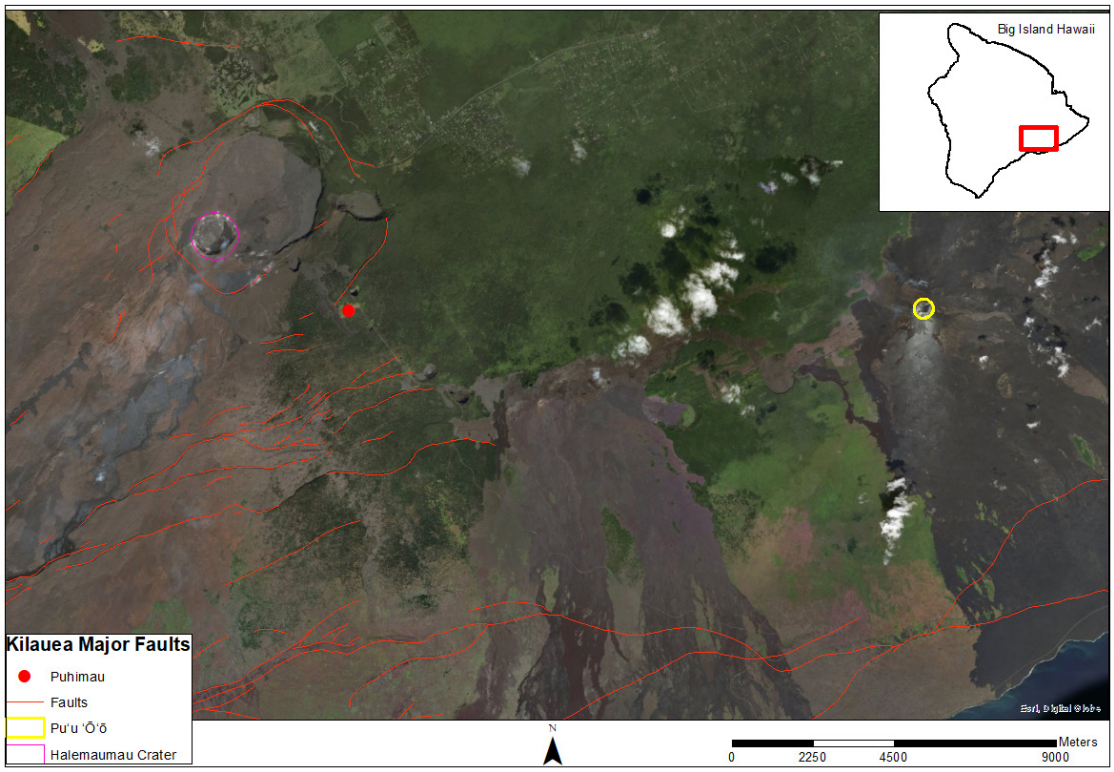

Figure 31. *Major faults at the Kilauea volcano summit and part of the East Rift Zone. No faults are identified at the Puhimau geothermal area. Fault data downloaded from: https://catalog.data.gov/dataset/hawaii-faults-9f554*

The geometry of the conduits below the Puhimau geothermal area was described by previous studies, (e.g. Klein et al. in 1987) and reported that the Upper East Rift Zone has a multi-tiered complex of conduits that reflect a honeycomb feature just 3 km below the surface that is 2-3 km wide (Klein et al., 1987). A three-dimensional velocity structure study by Dawson et al. (1999) suggested that there are two high V_p/V_s zones indicating that there are two distinct magma reservoirs below the surface of the geothermal area that form a V-shape pathway just at 1-4 km depth (Dawson et al., 1999). The results of this study are consistent with those of this study suggesting that there are two distinct magma reservoirs at the Kilauea volcano.

7.4 Spatiotemporal changes in vegetation health and/or extent

Results of spatiotemporal changes in vegetation health and/or extent are based on the use of multispectral imagery. Even though multispectral imagery does not have the necessary band information to offer details regarding which of the two possible phenomena can be occurring or its causes. However, hyperspectral imagery, on the other hand, can provide the necessary information to understand the phenomena affecting vegetation at the geothermal feature. Major effects of CO_2 on plants can be detected on leaf nitrogen content, with an increase in CO_2, nitrogen decreases causing lower photosynthetically active radiation (PAR) absorption, increased leaf thickness, and lower stomatal conductance, leading to plant necrosis (Gutshick, 2007; Rouse, 2010). A waveband that can detect these changes in nitrogen is centered at 550 nm because of the low reflectance and strong absorption of nitrogen in SWIR bands (Thenkabail et al., 2011). Another waveband that can highlight the CO_2 and vegetation interactions is centered at 970 or 1245 nm because it detects plant moisture fluctuations related to plant stress (Thenkabail et al., 2011). Alternatively, the effects of H_2S on vegetation are considered to be a harmful phytotoxin, reducing/limiting plant growth and development, defoliation, and leaf lesions (Li, 2013). These interactions between H_2S and vegetation can be detected best at a wavelength centered at 515 nm (Thenkabail et al., 2011). Multispectral imagery in comparison to hyperspectral imagery provides general information between the interactions of vegetation and gas emissions.

Volcanic activity in 2007 at the Kilauea volcano was described as the start of a new period at the summit, where it had remained quiet for 25 years until late that year. This increase in magmatic activity was marked by an increase in SO_2 emissions and seismic activity that led to the formation of a new crater in 2008 (USGS, 2017). In 2011 a magma intrusion event occurred in the Upper East Rift Zone that increased the continuous activity at the Puʻu ʻŌʻō vent; while at the summit a lava lake was forming (USGS, 2017). Meanwhile in the Puhimau geothermal area changes in vegetation where noticed along the north and north-east rims of the feature where areas previously vegetated became bare soil. In contrast, the center of the feature identified as the area with high CO_2 emissions showed an increase in vegetation; i.e. grasses grew or became healthier.

For the period from 2011 to 2013, volcanic activity showed that in Puʻu ʻŌʻō lava began filling the crater reflecting an increase in pressure within the magma plumbing system in the East Rift Zone (USGS, 2017; USGS, 2019). At the same time, the lava lake at the summit showed periods of "gas pistoning" where gases intermittently accumulated and were released ultimately leading to a rise in the lava lake (USGS, 2019). Vegetation at the Puhimau geothermal area showed that the center of the feature "grew" and the south rims lost vegetation (Figure 24).

Later on, in 2014, Puʻu ʻŌʻō activity appeared to remain relatively constant until 2017. At the summit, the lava lake continued to increase until 2017 where activity appears to remain constant (USGS, 2017; USGS, 2019). At the Puhimau geothermal feature, vegetation increased in most of its areas with scattering variability but no major changes (Figure 26).

Based on the image analysis difference results, spatiotemporal changes in the Puhimau geothermal area showed there is correlation between volcanic activity and vegetation changes. If constant volcanic activity is disturbed in either the Kilauea summit or Pu‘u ‘Ō‘ō the geothermal feature also have changes in its vegetation health/extent. These changes in volcanic activity can be a difference in degassing or eruptive frequency. The information remains inconclusive to establish what areas in the feature are prone or more susceptible to experience changes and which parameter between gas and temperatures appear to be affecting the vegetation. On the other hand, if the eruptive activity remains constant at the summit and the Pu‘u ‘Ō‘ō vent the vegetation at the Puhimau geothermal remains relatively unchanged with scattered variations that don’t fallow any pattern relative to those observed for both gases. To make a more conclusive analysis and correlation there is a need of more detailed data of the eruptive activity from both the Kilauea summit and Pu‘u ‘Ō‘ō. This detailed data would need to include information from prior, during and after any eruptive activity. Also, diffuse degassing data from various years is needed to quantify the total flux emissions and correlate it with vegetation changes. Lastly, hyperspectral imagery is also needed to establish which gas is causing the damages in vegetation and how long these changes in vegetation health can be traced before an eruption happens.

8. Conclusion

In the field campaign from February to March 2017 we measured soil gas emissions for the Puhimau geothermal area using the accumulation chamber method. The results of this study indicate that the total flux of CO_2 is 14.09 to 14.21 t d^{-1} and for H_2S is 0.0759 to 0.0764 t d^{-1}. Based on the distribution of gas emissions determined by our kriging model

there appears to be an alignment of CO_2 and H_2S. The structure of the emissions for these two gases vary and are likely the result of differences in the solubility of the two gases (SO_2 has a relatively higher solubility in silicate magmas compared to CO_2). Cryptic structural features can be traced as one fault/fracture that is oriented in an east-west direction that is deep and emits almost exclusively CO_2 and two other faults/fractures that are approximately subparallel in a north-south direction that reach shallower depths and are dominated by emission of H_2S gas. Multispectral imagery was used to establish spatiotemporal relationships between vegetation health and extent and volcanic activity at Kilauea volcano. We have shown that the vegetation health and extent in and around the Puhimau geothermal area decreases, recording distinct changes in volcanic activity at the Kilauea summit and Pu‘u ‘Ō‘ō vent in the East Rift Zone. Results remain inconclusive to establish the precise relationship between soil gas emissions and/or ground temperature that trigger vegetation changes.

References

Aburas, M. M., et al., 2015. Measuring land cover change in Seremban, Malaysia using NDVI index. Procedia Environmental Sciences, 30, 238–243.

Barnard, W.M., Halbig, J.B., and Fountain, J.C., 1990. Geochemical study of fumarolic condensates from Kilauea Volcano, Hawaii, Pacific Science 44, 197–206.

Cardellini, C., Chiodini, G., Frondini, F., 2003a. Application of stochastic simulation to Co2 flux from soil: Mapping and quantification of gas release. J. Geophys. Res. 108, 1–13. doi:10.1029/2002JB002165.

Casadevall, T.J. and Hazlett, R.W., 1983. Thermal areas on Kilauea and Mauna Loa volcanoes,Hawaii, J. Volcanol. Geotherm. Res. 16, 173–188.

Chiodini, G., Cioni, R., Guidi, M., Raco, B., Marini, L., 1998. Soil CO2 flux measurements in volcanic and geothermal areas. Appl. Geochemistry 13, 543–552. doi:10.1016/S0883-2927(97) 00076-0

Chiodini, G., Frondini, F., Cardellini, C., Granieri, D., Marini, L., Ventura, G. (2001). CO2 degassing and energy release at Solfatara volcano, Campi Flegrei, Italy. J. Geophys. Res. 106, 16,213–16,221.

Croghan, C.W. and Egeghy, P.E., 2003. Methods of dealing with values below the limit of detection using SAS. US-EPA, editor.

Curewitz, D., Karson, J.A., 1997. Structural settings of hydrothermal outflow: Fracture permeability maintained by fault propagation and interaction. Journal of Volcanology and Geothermal Research, 79, 149 – 68.

Davies, F. and Notcutt, G., 1996. Biomonitoring of atmospheric mercury in the vicinity of Kilauea, Hawaii, Water, Air and Soil Pollution 86, 275–281.

Dawson, P.B., Chouet, B.A., Okubo, P.G., Villasenor, A., and Benz, H.M., 1999. Three-dimensional velocity structure of the Kilauea caldera, Hawaii, Geophys. Res. Lett. 26, 2805–2808.

Decker, R.W., 1987. Dynamics of Hawaiian volcanoes: An overview. In Volcanism in Hawaii (Decker, R.,Wright, T., and Stauffer, P. eds.), U.S. Geological Survey Professional Paper 1350, pp. 997–1018.

Delmelle E.M., 2014. Spatial Sampling. In: Fischer M., Nijkamp P. (eds) Handbook of Regional Science. Springer, Berlin, Heidelberg

Dixon, J.E., Stolper, E.M., Holloway, J.R.,1995. An experimental study ofwater and carbon dioxide solubilities in mid-ocean ridge basaltic liquids, part I, calibration and solubility models. Journal of Petrolology 36, 1607–1631

Dunn, J.C. and Hardee, H.C., 1985. Surface heat flow measurements at the Puhimau hot spot, Geophysics 50, 1108–1112.

Jolie E, Klinkmueller M, Moeck I, Bruhn D., 2016. Linking gas fluxes at Earth's surface with fracture zones in an active geothermal field. Geology, G37412-1

Friedman, I., Gleason, J., and Jackson, T., 1987. Variation of d13C in fumarolic gases from Kilauea volcano. In Volcanism in Hawaii (Decker, R., Wright, T., and Stauffer, P. eds.), U.S. Geological Survey Professional Paper 1350, pp. 805–807.

Frondini, F., Chiodini, G., Caliro, S., Cardellini, C., Granieri, D., & Ventura, G., 2004. Diffuse CO_2 degassing at Vesuvio, Italy. Bulletin of volcanology, 66(7), 642-651.

Gerlach, T.M. and Graeber, E.J., 1985. Volatile budget of Kilauea Volcano, Nature 313, 273–277.

Gerlach, T.M. and Taylor, B.E., 1990. Carbon isotope constraints on degassing of carbon dioxide from Kilauea Volcano, Geochim. Cosmochim. Acta 54, 2051–2058.

Gerlach, T.M., McGee, K.A., Sutton, A.J., and Elias, T., 1998. Rates of volcanic CO2 degassing from airborne determinations of SO2 emission rates and plume CO2/SO2: Test study at Pu‘u ‘O‘o cone, Kilauea volcano, Hawaii, Geophys. Res. Lett. 25, 2675–2678.

Gerlach, T.M., Doukas, M.P.,McGee, K.A., and Kessler, R., 2001. Soil efflux and total emission rates of magmatic CO2 at the Horseshoe Lake tree kill, Mammoth Mountain, California, 1995–1999, Chem. Geol. 177, 101–116.

Gerlach, T.M., McGee, K.A., Elias, T., Sutton, A.J., Doukas, M.P., 2002. Carbon dioxide emission rate of Kilauea Volcano: implications for primary magma and the summit reservoir. Journal of Geophysical Research-Solid Earth 107 (B9) art. no.-2189.

Giammanco, S., Gurrieri, S., & Valenza, M., 1998. Anomalous soil CO_2 degassing in relation to faults and eruptive fissures on Mount Etna (Sicily, Italy). Bulletin of Volcanology, 60(4), 252- 259.

Giammanco, S., Gurrieri, S., & Valenza, M., 2006. Fault-controlled soil CO_2 degassing and shallow magma bodies: summit and lower east rift of Kilauea volcano (Hawaii), 1997. pure and applied geophysics, 163(4), 853-867.

Greenland, L.P., Rose, W.I., and Stokes, J.B., 1985. An estimate of gas emissions and magmatic gas content from Kilauea volcano, Geochim. Cosmochim. Acta 49, 125–129.

Gutshick V.P, 2007. Plant acclimation to elevated CO2 – from simple regularities to biogeographic chaos. Ecological Modelling, 200,433-451.

Hager, S. A., T. M. Gerlach, and P. J. Wallace., 2008, Summit CO2 emission rates by the CO2/SO2 ratio method at Kilauea Volcano Hawai'i, during a period of sustained inflation, J. Volcanol. Geotherm. Res., 177, 875–882, doi:10.1016/j.jvolgeores.2008.06.033.

Harvey, M. C., & Harvey, C. C., 2015. Soil CO2 flux surveys: A review of the techniques in geothermal exploration. In Proceedings World Geothermal Congress 2015, Melbourne, Australia, 19-25 April 2015 (paper accepted).

Hinkle, M., 1978, Helium, mercury, sulfur compounds, and carbon dioxide in soil gases of the Puhimau Thermal Area, Hawaii Volcanoes National Park, Hawaii., United States Department of the Interior Geological Survey., Open-File Report 78-246.

Jackson, D.B. and Kauahikaua, J., 1987. Regional self-potential anomalies at Kilauea volcano. In Volcanism in Hawaii (eds. Decker, R., Wright, T., and Stauffer, P.), U.S. Geological Survey Professional Paper 1350, pp. 947–959.

Jagger, T. A., Jr., 1938, Chain-of-crater crisis: Volcano Lett., 459, 2-4.

McGee, K. A., Sutton, A. J., Elias, T., Doukas, M. P., & Gerlach, T. M. 2006. Puhimau Thermal Area: A Window into the Upper East Rift Zone of Volcano, Hawaii? pure and applied geophysics, 163(4), 837-851.

Klein, F.W., Koyanagi, R.Y., Nakata, J.S., and Tanigawa, W.R. (1987), The seismicity of Kilauea's magma system. In Volcanism in Hawaii (eds. Decker, R., Wright, T., and Stauffer, P.), U.S. Geological Survey Professional Paper 1350, pp. 821–825.

Lewicki, J. L., & Brantley, S. L., 2000. CO2 degassing along the San Andreas fault, Parkfield, California. Geophys. Res. Lett, 27(1), 5-8.

Li Z.G., 2013. Hydrogen Sulfide: A multifunctional gaseous molecule of plants. Russian Journal of Plant Physiology, 60, no. 6, 733-740.

McGee, K.A. and Gerlach, T.M., 1998, Airborne volcanic plume measurements using a FTIR spectrometer, Kilauea volcano, Hawaii, Geophys. Res. Lett. 25, 615–618.

McPhie, J., Walker, G.P.L., and Christiansen, R.L., 1990. Phreatomagmatic and phreatic fall and surge deposits from explosions at Kilauea volcano, Hawaii, 1790 A.D.: Keanakakoi ash member, Bull. Volcanol. 52, 334–354.

Melián, G., Hernández, P. a, Padrón, E., Pérez, N.M., Barrancos, J., Padilla, G., Dionis, S., Rodríguez, F., Calvo, D., Nolasco, D., 2014. Spatial and temporal variations of diffuse CO2 degassing at El Hierro volcanic system: Relation to the 2011-2012 submarine eruption. J. Geophys. Res. 119, 6976–6991. doi:10.1002/2014JB011013.Received

Morgan, W.J., 1972, Plate motion and deep mantle convection, in Shangam, R., et al., eds., Studies in Earthe and space sciences: A volume in honor of Harry Hammond Hess: Boulder, Colorado, Geological Society of Amareica Memoir 132, p.7-22

Padrón, E., Hernández, P. a., Toulkeridis, T., Pérez, N.M., Marrero, R., Melián, G., Virgili, G., Notsu, K., 2008. Diffuse CO2 emission rate from Pululahua and the lake-filled Cuicocha calderas, Ecuador. J. Volcanol. Geotherm. Res. 176, 163–169. doi:10.1016/j.jvolgeores.2007.11.023.

Ranaldi, M., 2008. Studio delle emissioni di gas in aree vulcaniche e geotermiche: implicazioni strutturali, geotermiche e di pericolosità.

Rogie, J.D., Kerrick, D.M., Sorey, M.L., Chiodini, G., and Galloway, D.L., 2001. Dynamics of carbon dioxide emission at Mammoth Mountain, California, Earth and Planet. Sci. Lett. 188, 535–541

Rouse J.H., Shaw J.A., Lawrence R.L., Lewicki J.L., Dobeck L.M., Repasky K.S., SpanglerL.H., 2010. Multi-spectral imaging of vegetation for detecting CO2 leaking from underground. Environ Earth Sci (2010) 60:313–323 DOI 10.1007/s12665-010-0483-9

Rowland, J. V. and Sibson, R. H., 2004. Structural controls on hydrothermal flow in a segmented rift system, Taupo Volcanic Zone, New Zealand. Geofluids, 4: 259-283.

Sutton, A.J., Elias, T., Gerlach, T.M., and Stokes, J.B., 2001. Implications for eruptive processes as indicated by sulfur dioxide emissions from Kilauea Volcano, Hawaii, 1979—1997, J. Volcanol. Geotherm. Res. 108, 283–302.

Symonds, R.B., Gerlach, T.M., and REED, M.H., 2001. Magmatic gas scrubbing: Implications for volcano monitoring, J. Volcanol. Geotherm. Res. 108, 303–341.

Thenkabail, P.S., Lyon, G.J., and Huete, A. 2011. Advances in hyperspectral remote sensing of vegetation and agricultural crops. Chapter 1. Pp. 3-29. In Thenkabail, P.S., Lyon, G.J., and Huete, A. 2011. Book entitled: “Hyperspectral Remote Sensing of Vegetation”. CRC Press-Taylor and Francis group, Boca Raton, London, New York. Pp. 781.

University of Hawaii., 2015. Hawaii Faults [data set]. Retrieved from http://gdr.openei.org/submissions/532.

U.S. Geological Survey., 1998. Eruption History of Kilauea Volcano, Hawai`i. Retrieved January 20, 2019, from http://hvo.wr.uSGS.gov/kilauea/history/

U.S. Geological Survey., 2016. Kīlauea Volcano Erupts in Explosive and Effusive Cycles. Retrieved January 20, 2019, from https://volcanoes.uSGS.gov/volcanoes/kilauea/geo_hist_summary.html

U.S. Geological Survey., 2017. 1959 Kilauea Iki Eruption. Retrieved January 20, 2019, from https://volcanoes.uSGS.gov/volcanoes/kilauea/geo_hist_kilauea_iki.html

U.S. Geological Survey., 2017. 1969-1974 Mauna Ulu Eruption. Retrieved January 20, 2019, from https://volcanoes.uSGS.gov/volcanoes/kilauea/geo_hist_mauna_ulu.html

U.S. Geological Survey., 2018. The May 1924 Explosive Eruption of Kīlauea. Retrieved January 20, 2019, from https://volcanoes.uSGS.gov/volcanoes/kilauea/geo_hist_1924_halemaumau.html

U.S. Geological Survey., 2018. Kīlauea 1955 Lower East Rift Zone Eruption in Lower Puna. Retrieved January 20, 2019, from https://volcanoes.uSGS.gov/volcanoes/kilauea/geo_hist_1955.html

U.S. Geological Survey., 2018. 1960 Kapoho Eruption Provided Lesson In Kilauea Behavior. Retrieved January 20, 2019, from https://volcanoes.uSGS.gov/volcanoes/kilauea/geo_hist_kapoho.html

U.S. Geological Survey., 2019. The Pu‘u ‘Ō‘ō Eruption Lasted 35 Years. Retrieved January 21, 2019, from https://volcanoes.uSGS.gov/volcanoes/kilauea/geo_hist_1983.html

Verbovzek, T., 2011. A comparison of parameters below the limit of detection in geochemical analyses by substitution methods. RMZ Materials and Geoenvironment., 58(4) 393-404.

Wallace, P.J., Carmichael, I.S.E., 1992. Sulfur in basaltic magmas. Geochimica et Cosmochimica Acta 56, 1863–1874.

Zablocki, C.J., 1978. Applications of the VLF induction method for studying the volcanic process of Kilauea Volcano, Hawaii: J. Volcanology and Geothermal Res., 3, 155-195.

Appendix I

Accumulation chamber technique principles

To quantify the total amount of diffuse soil gas (CO_2 and H_2S) emitted within the Puhimau geothermal area we employed the accumulation chamber technique, which has been proven as an effective method (Giammaco et al., 1998, 2006; Chondini et al., 1998, 2001; Frondini et al., 2004;). The accumulation chamber method was applied in the Puhimau geothermal area using a portable diffuse flux-meter by West System (S.r.L.) (Figure 32). The instrument assemblage consisted of a type B accumulation chamber with a volume of $6.231*10^{-3}$ m^3 and a base area of $3.140*10^{-2}$ m^2, a LICOR LI-820 CO_2 gas analyzer, a TOX05 H_2S gas analyzer, and a Trimble portable handheld computer. Instruments such as a Garmin GPS, and a Fluke 51-2T thermometer with a 12in. probe were also used as part of data collection. The detection limits for the West system portable flux-meter are 0.001 g m^{-2} d^{-1} to 300 g m^{-2} d^{-1} for CO_2 and 0.00025 g m^{-2} d^{-1} to 0.5 g m^{-2} d^{-1} for H_2S (values obtained from personal communication with Davide Continanza from West Systems S.r.L).

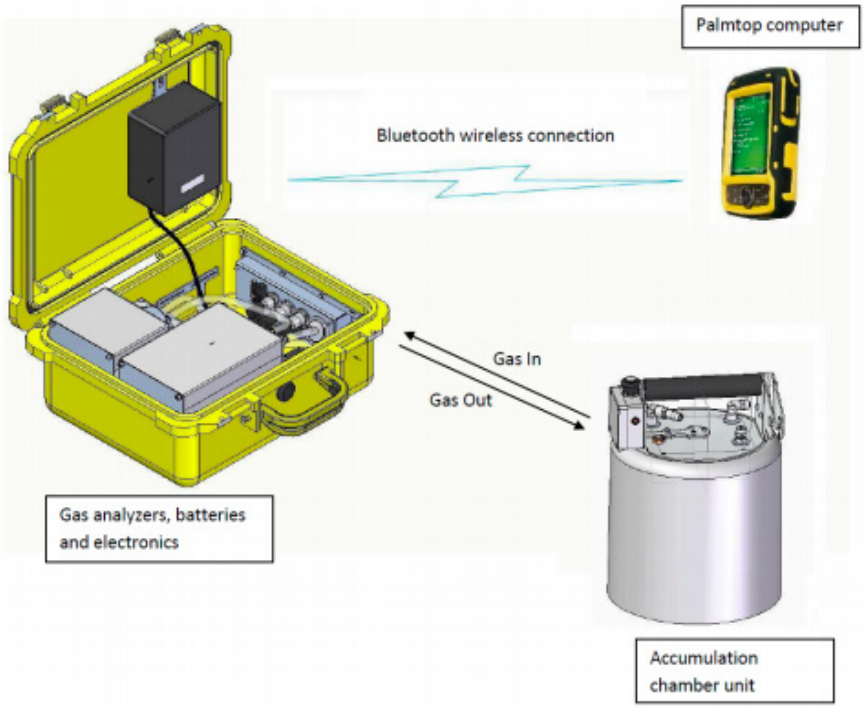

Figure 32. *Sketch of the West System portable flux-meter instrument including: accumulation chamber (type B), handheld computer, and a hard case that included a battery, gas analyzer, and gas tubes that were connected to the accumulation chamber. Modified from WestSystem S.r.l. Handbook*.

Appendix II

Sequential Gaussian simulation validation models

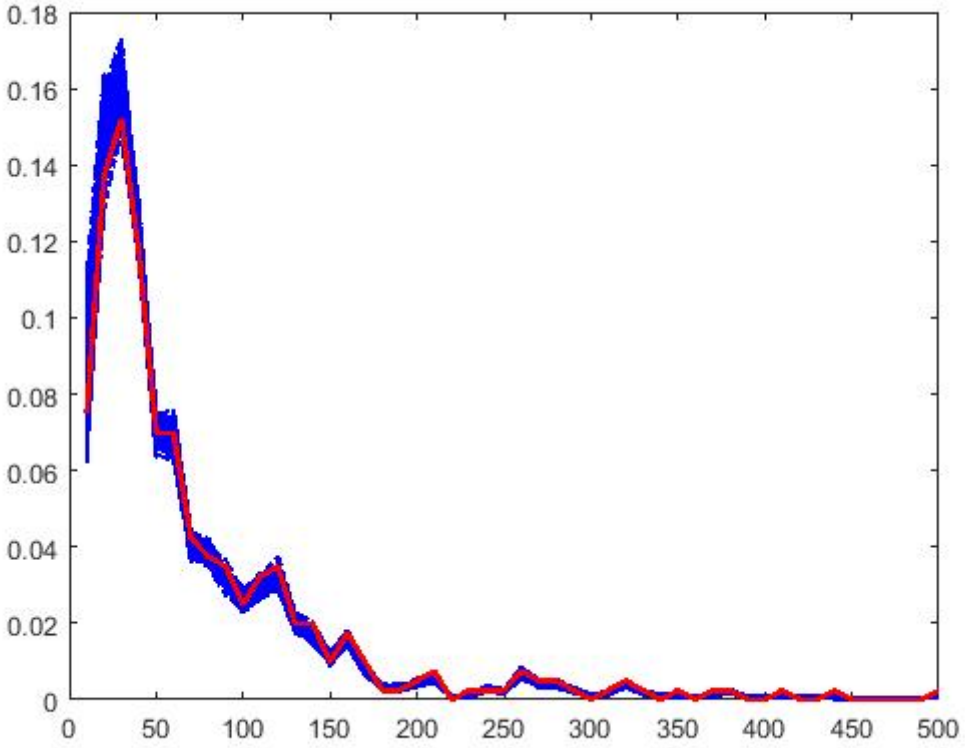

Figure 33. *Histogram validation of the CO2 model*

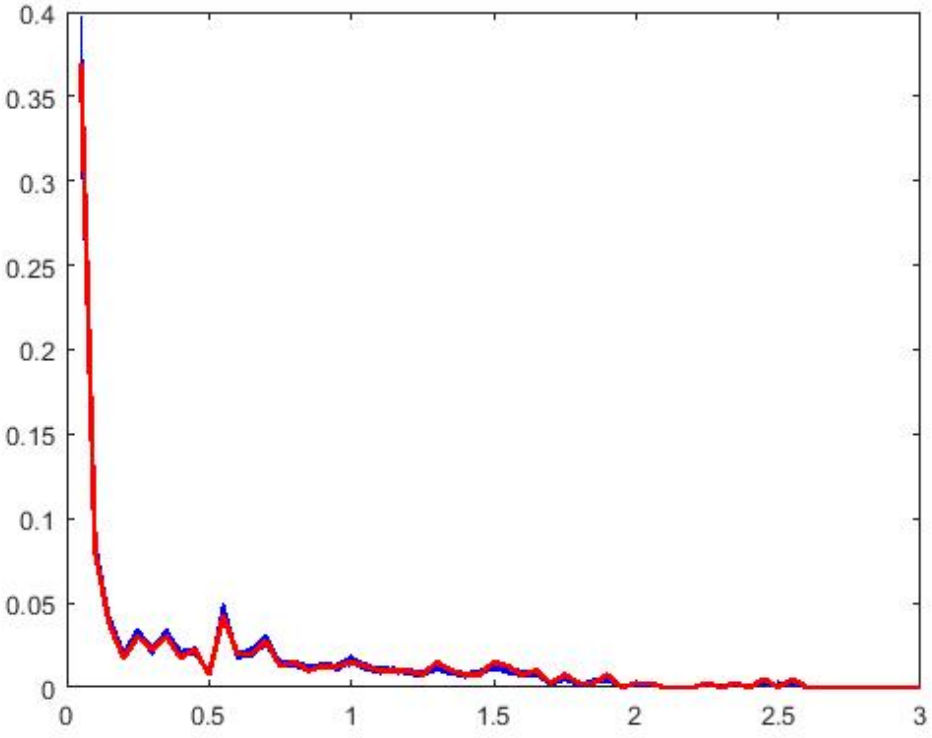

Figure 34. *Histogram validation model of H_2S*

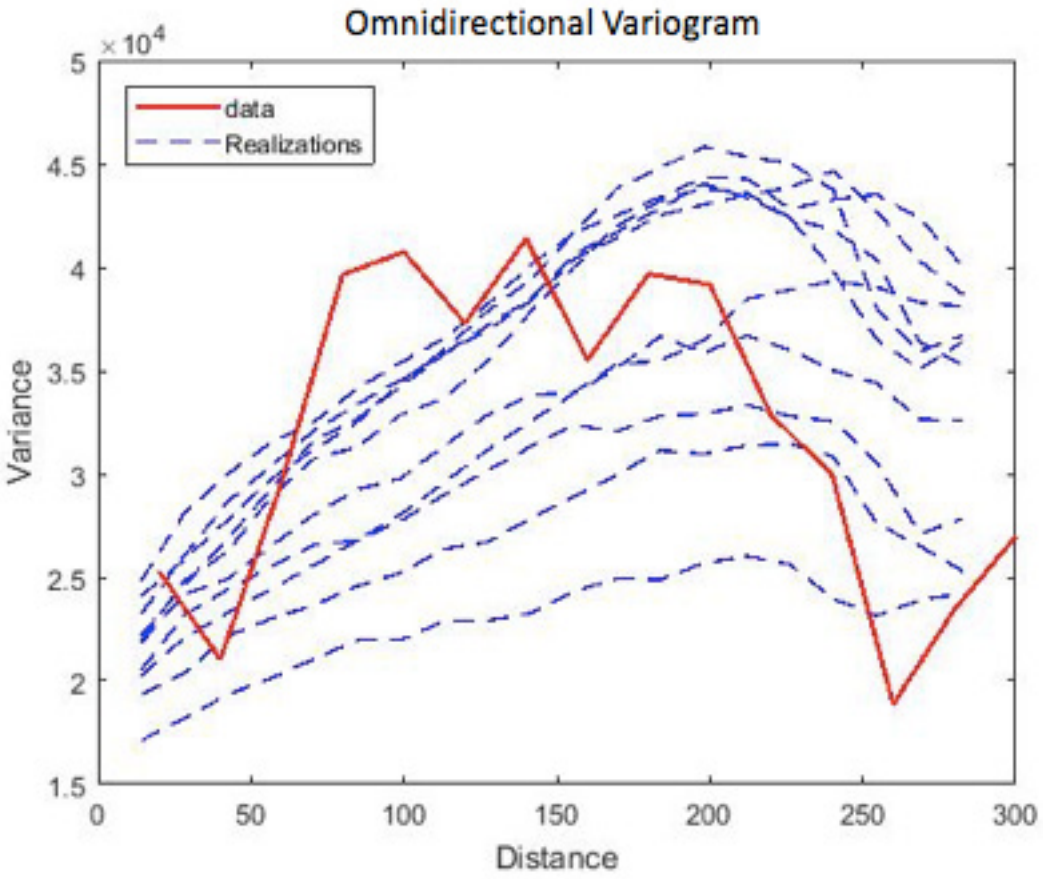

Figure 35. *Omnidirectional Variogram model validation for CO_2*

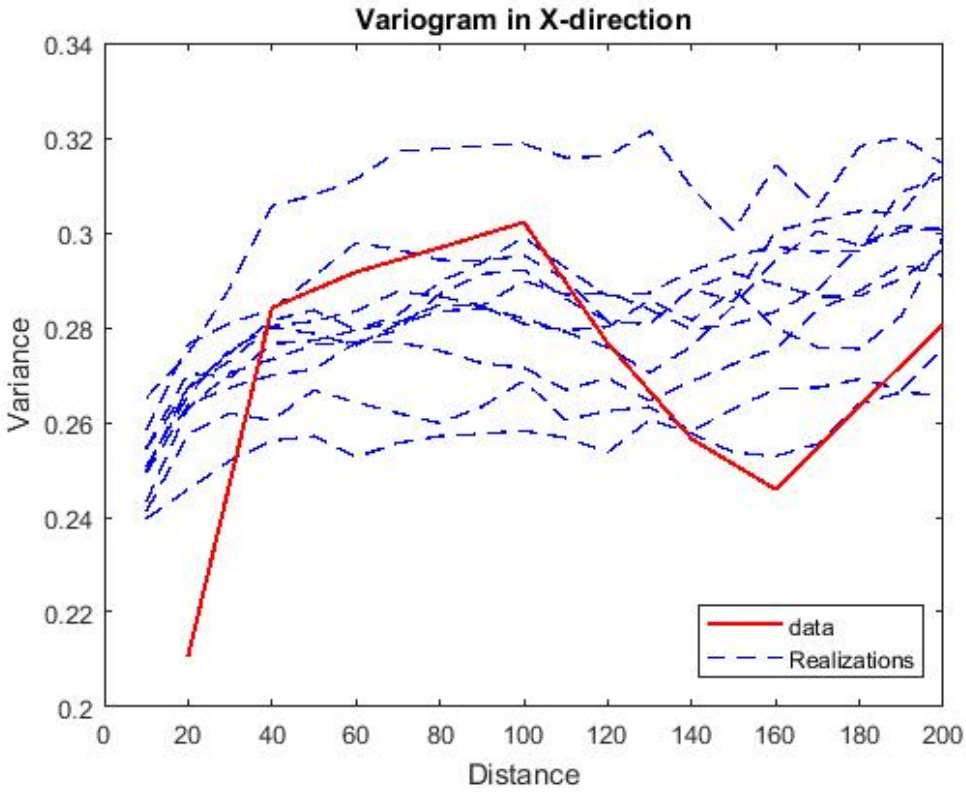

Figure 36. *Variogram model validation for H_2S in the X direction*

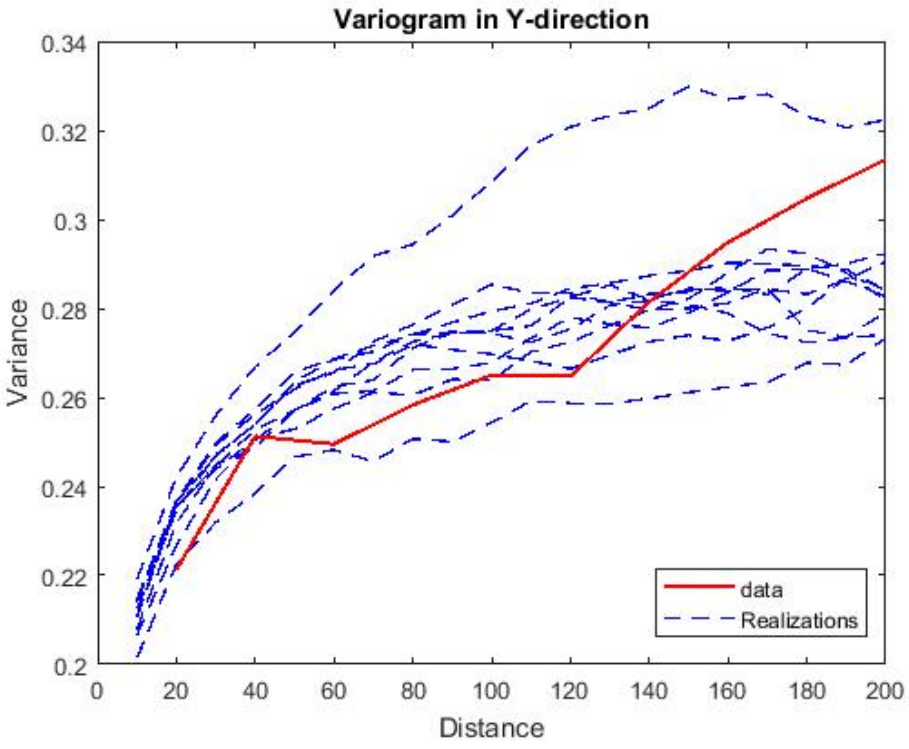

Figure 37. *Variogram model validation for H_2S in the Y direction*

Appendix III

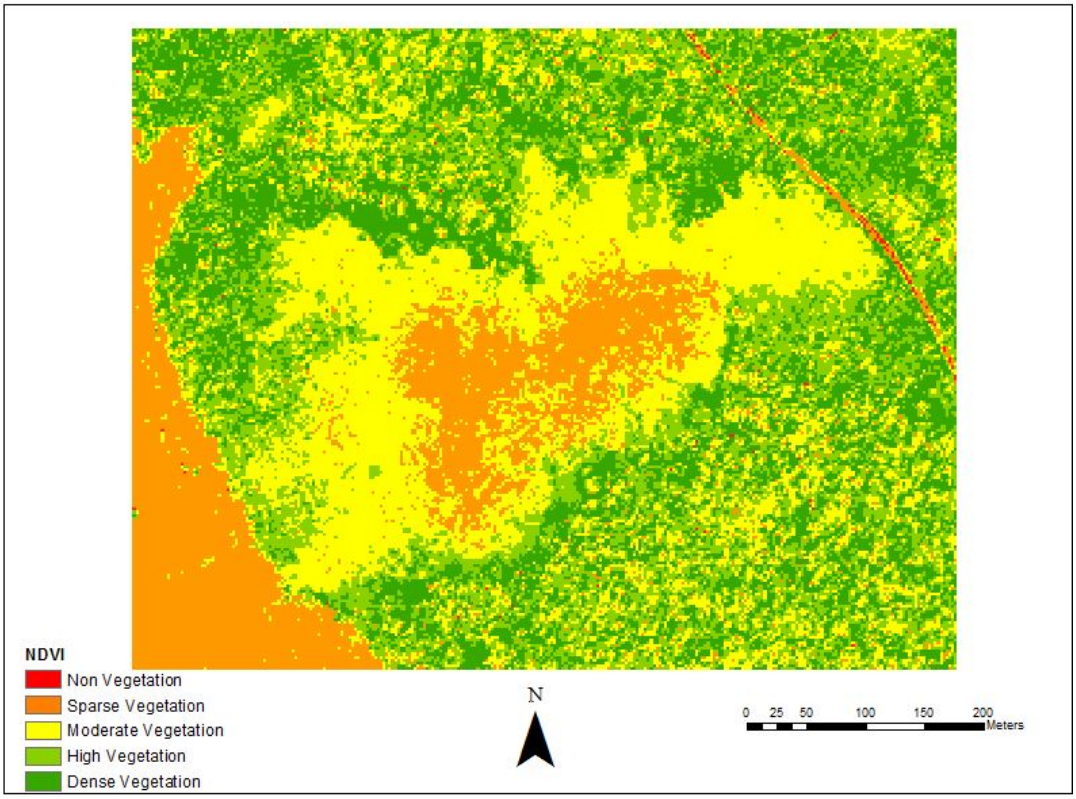

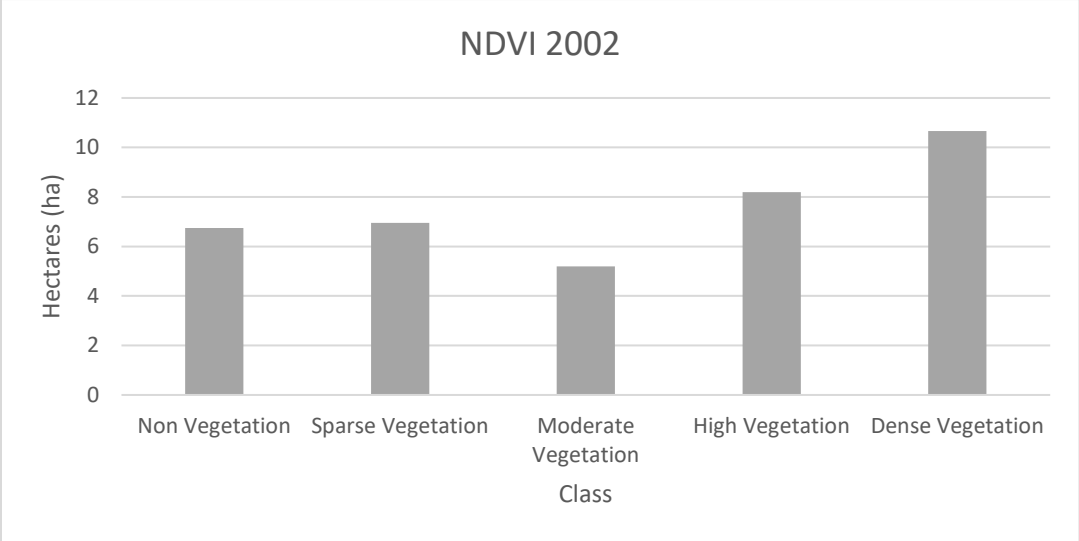

Figure 38. *2002 NDVI classification map and area of classes in hectares.*

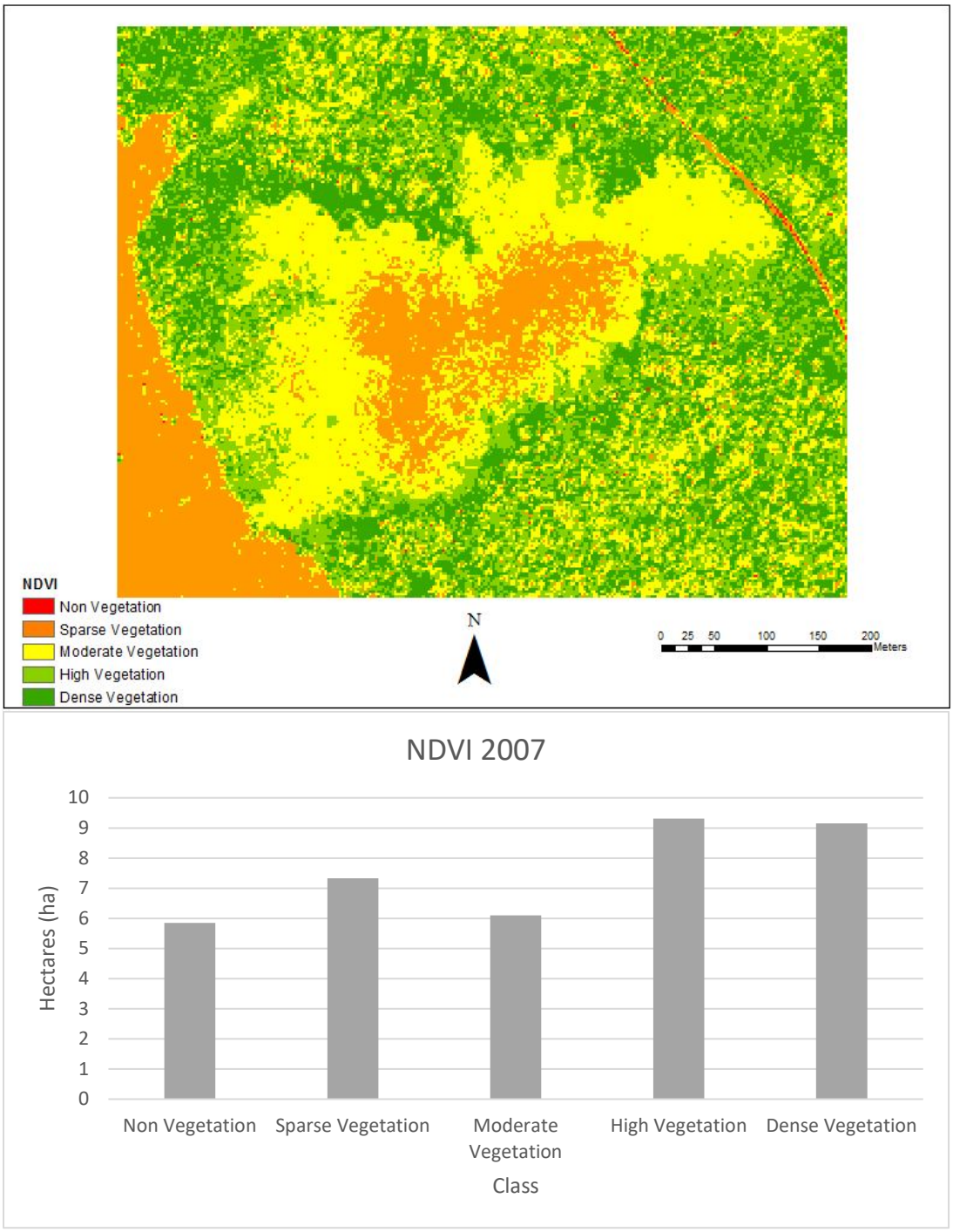

Figure 39. *2007 NDVI classification map and area of classes in hectares.*

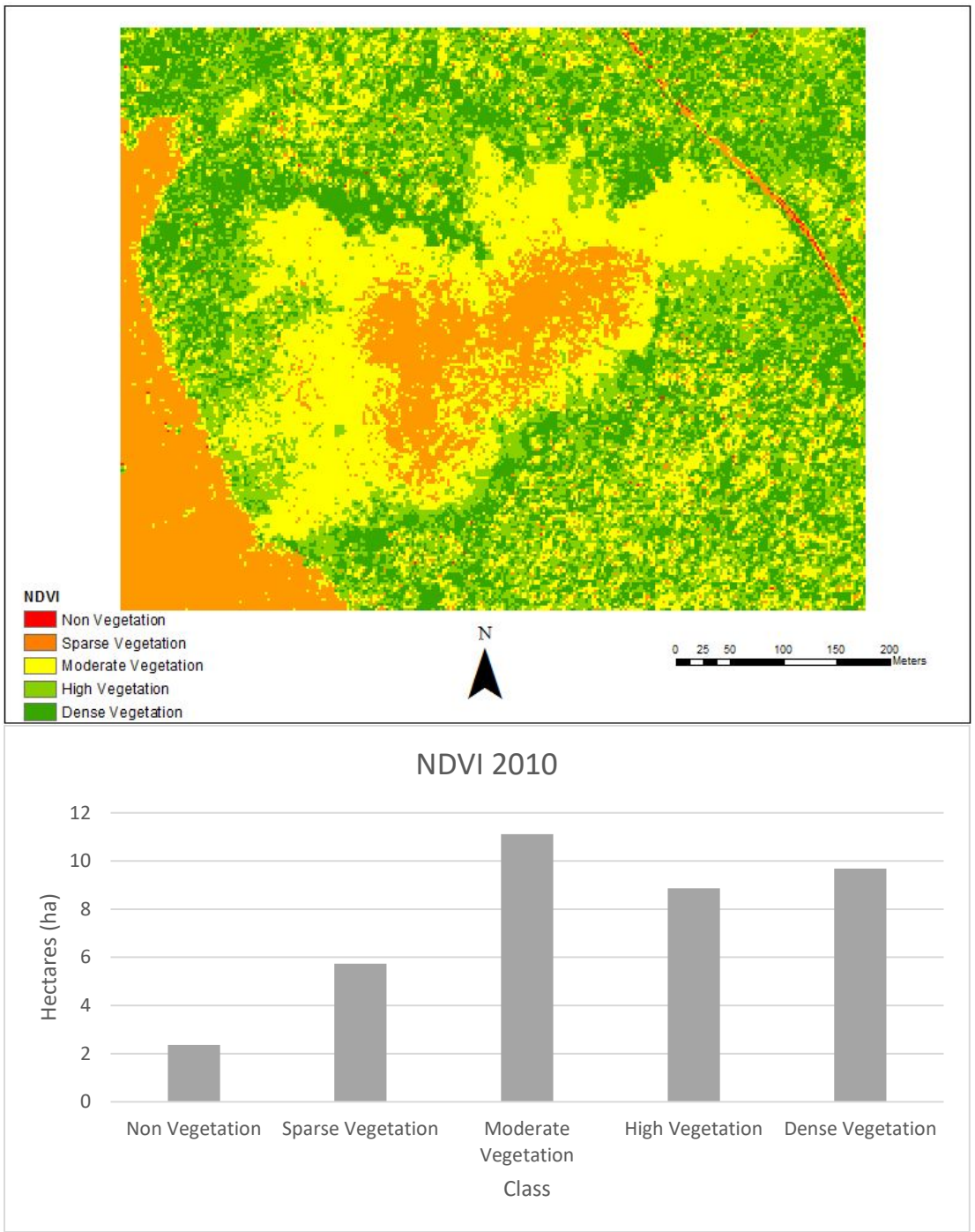

Figure 40. *2010 NDVI classification map and area of classes in hectares.*

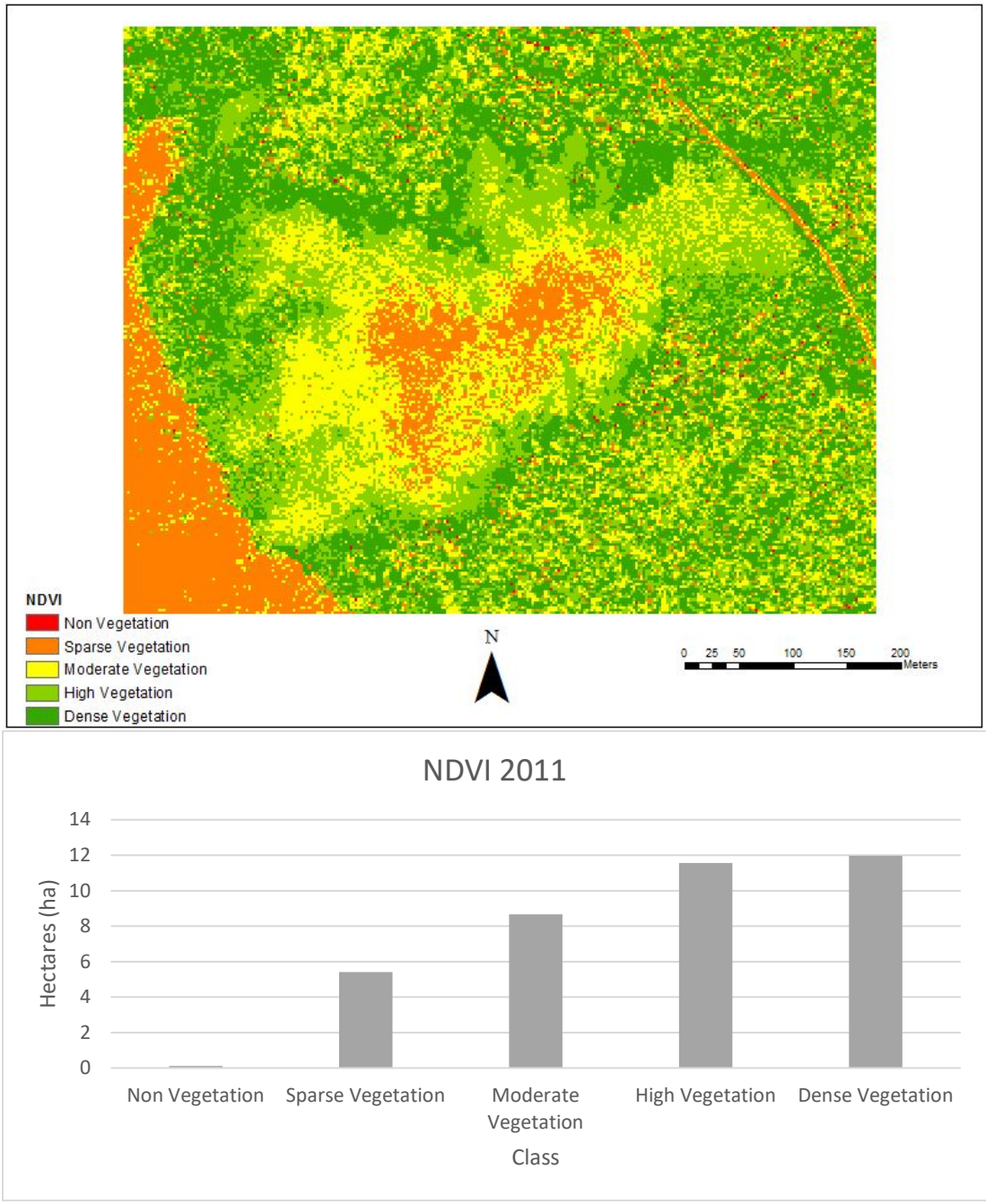

Figure 41. 2011 NDVI classification map and area of classes in hectares.

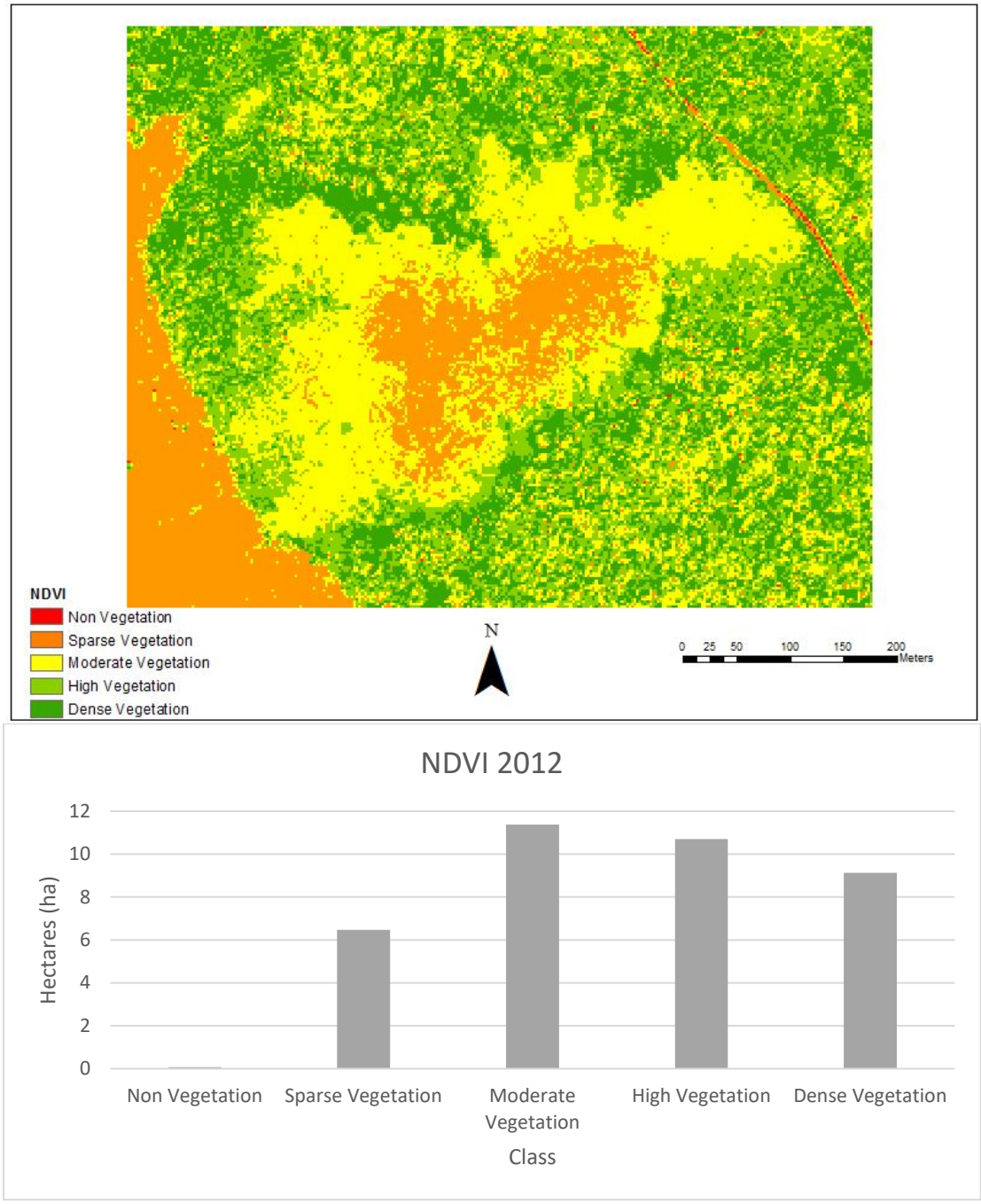

***Figure 42**. 2012 NDVI classification map and area of classes in hectares.*

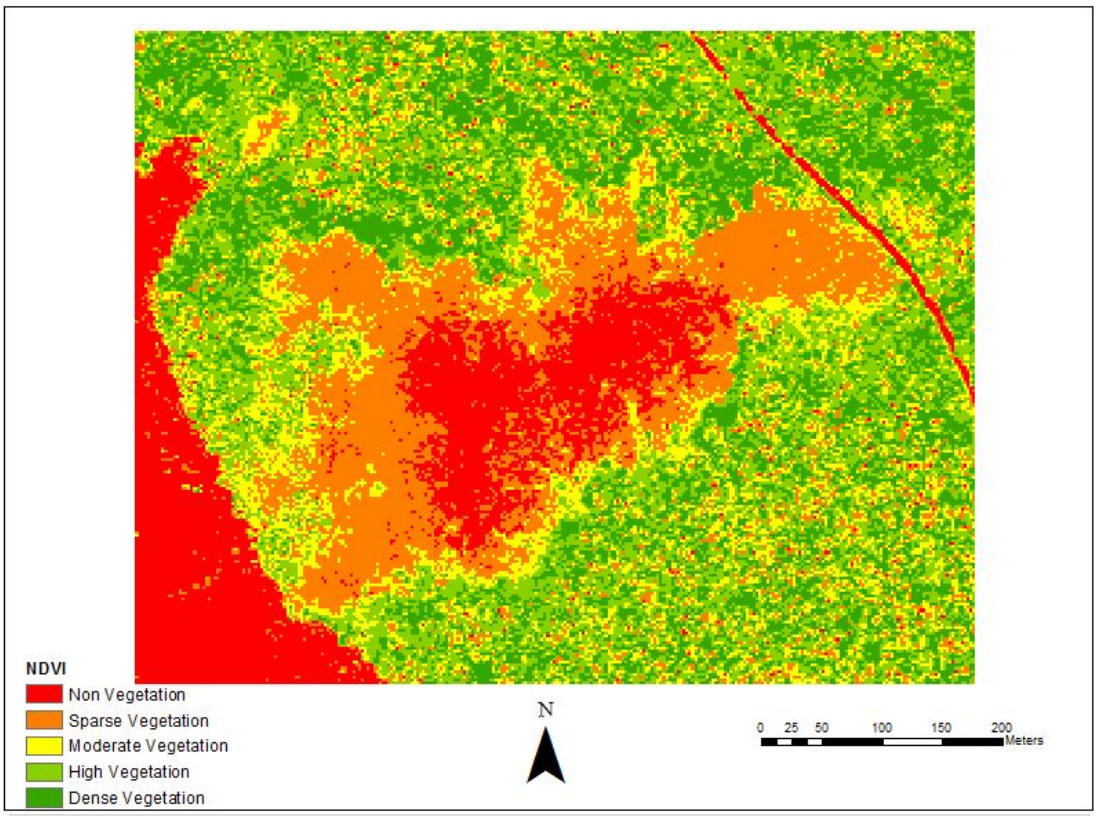

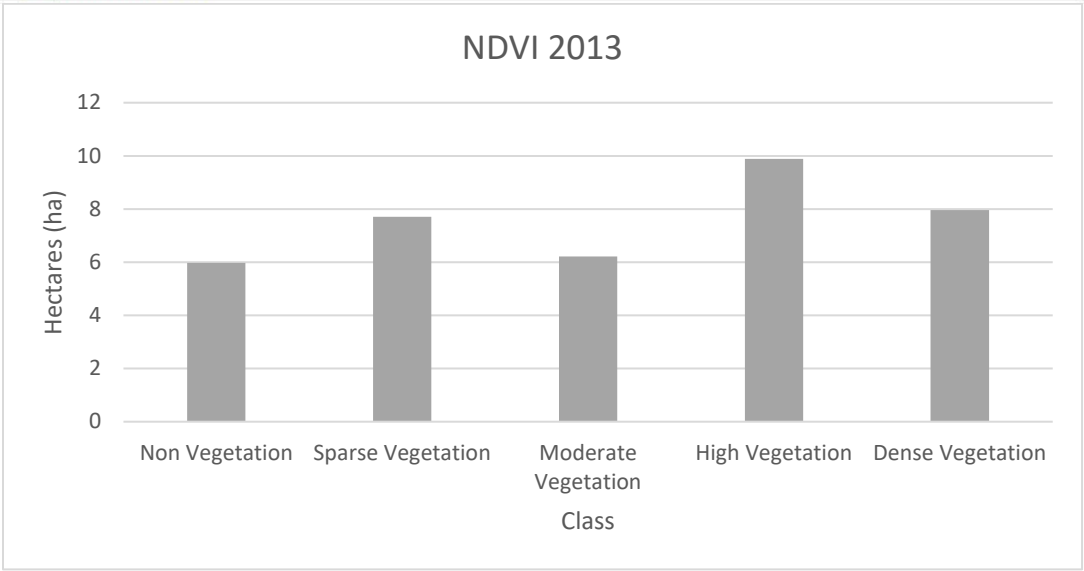

Figure 43. *2013 NDVI classification map and area of classes in hectares.*

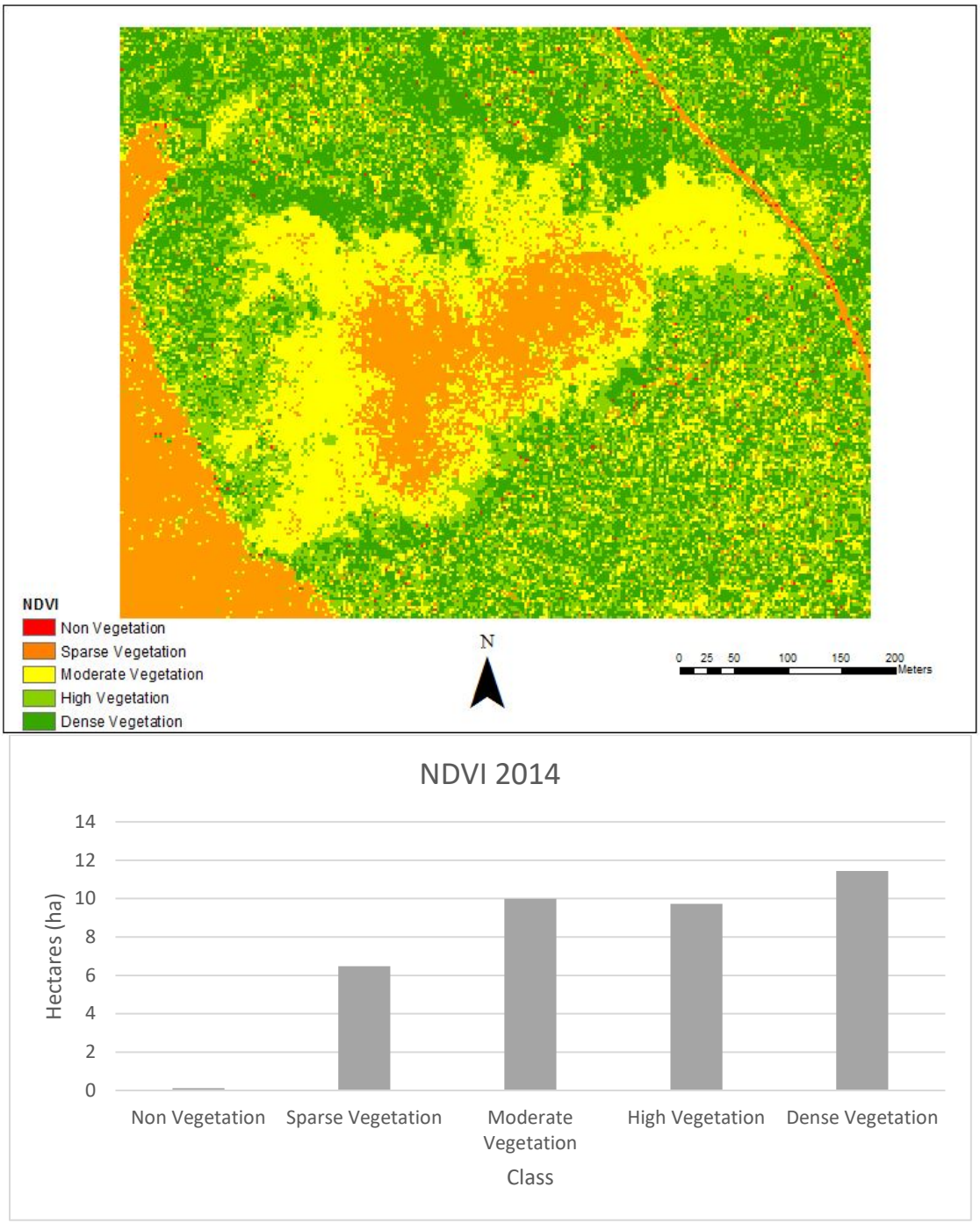

Figure 44. *2014 NDVI classification map and area of classes in hectares.*

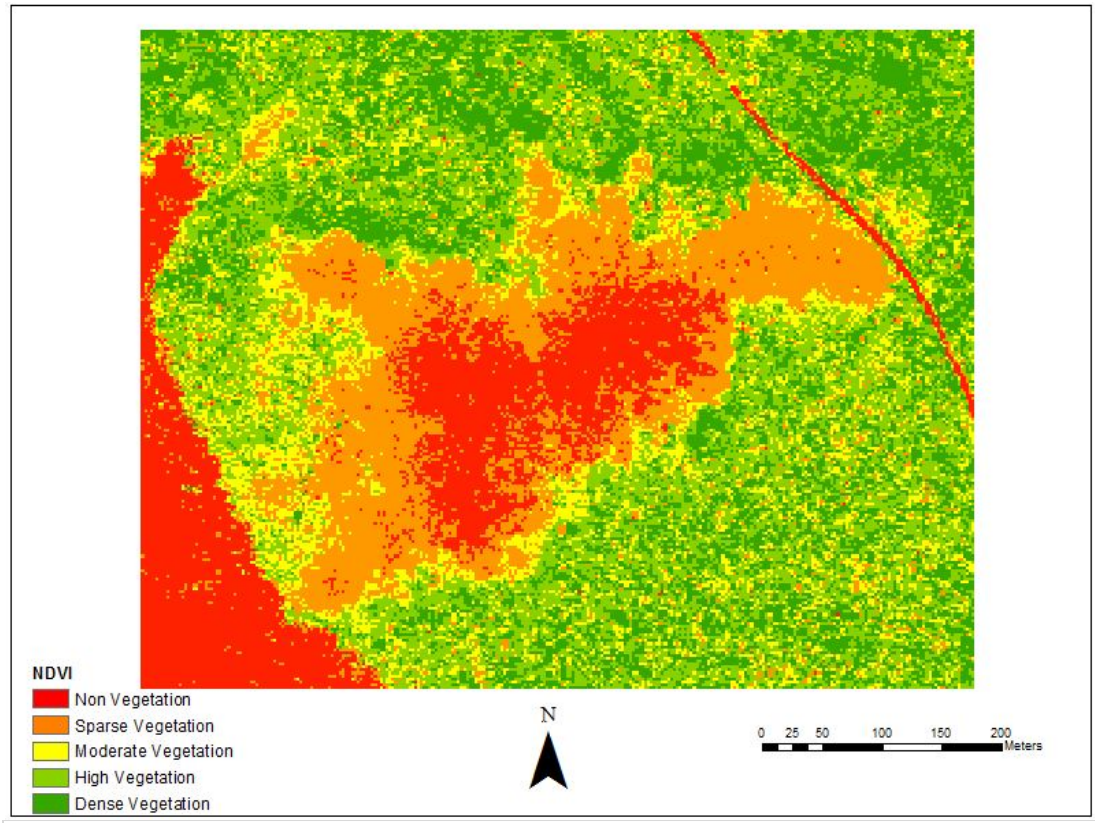

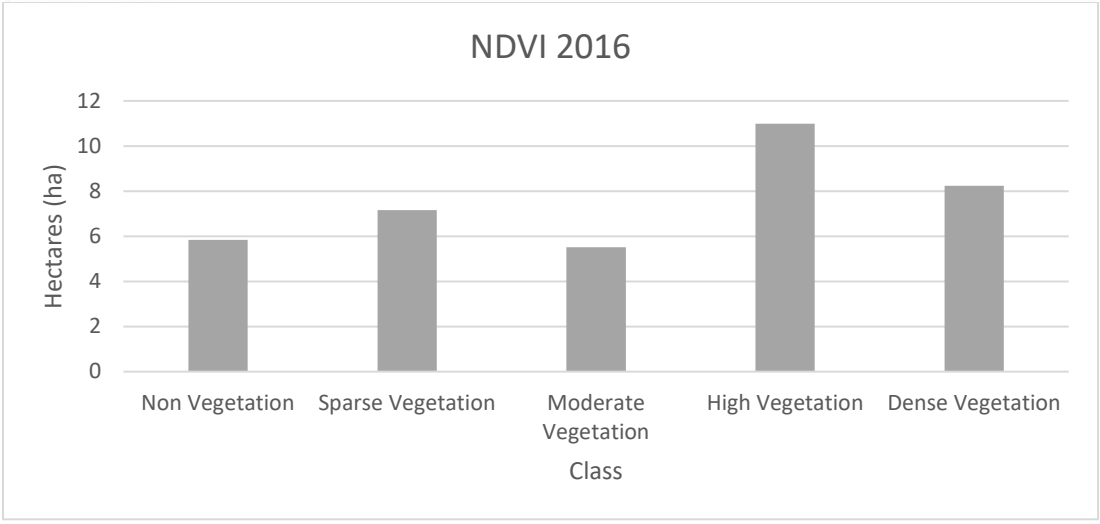

Figure 45. *2016 NDVI classification map and area of classes in hectares.*

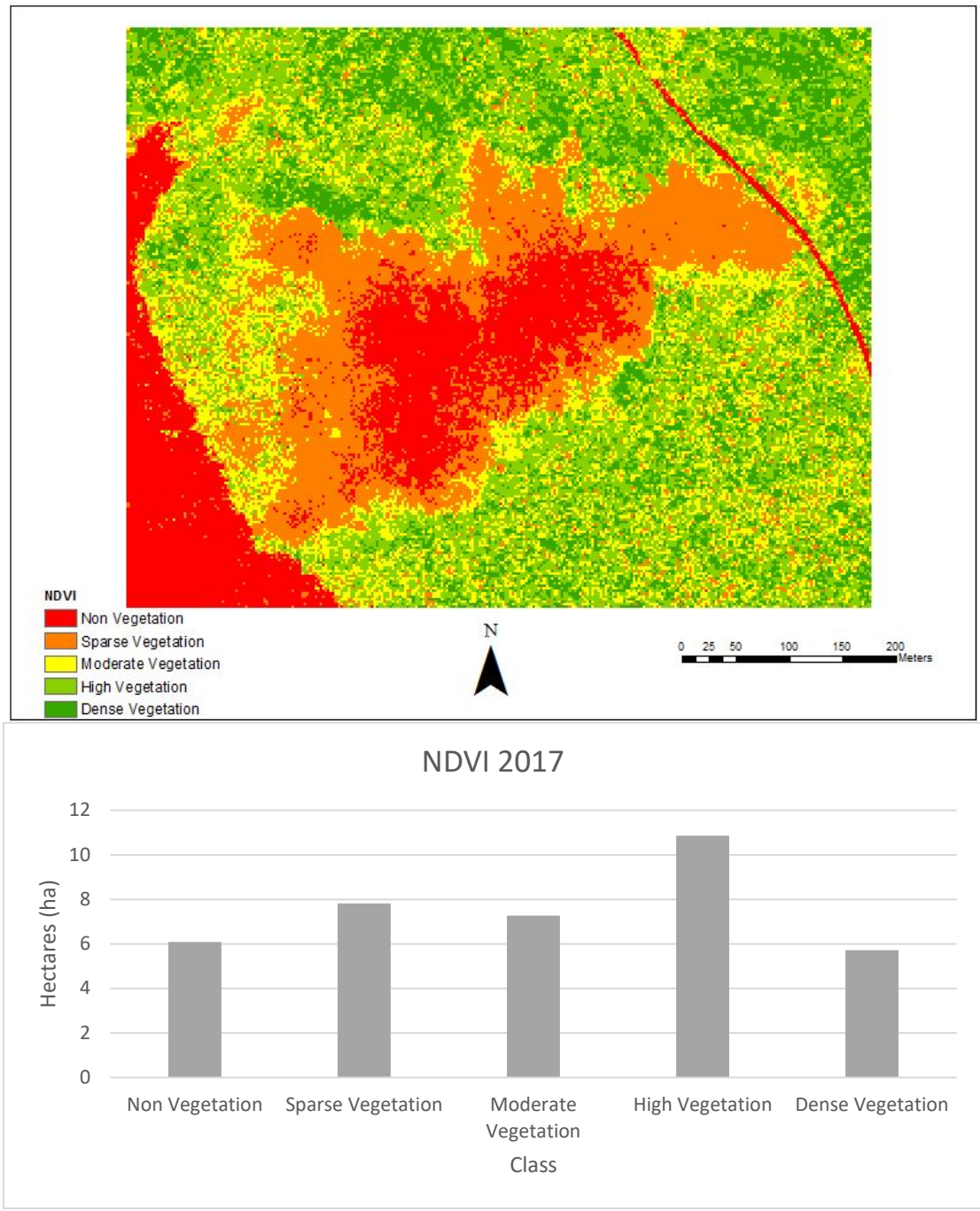

Figure 46. *2017 NDVI classification map and area of classes in hectares.*

Appendix IV

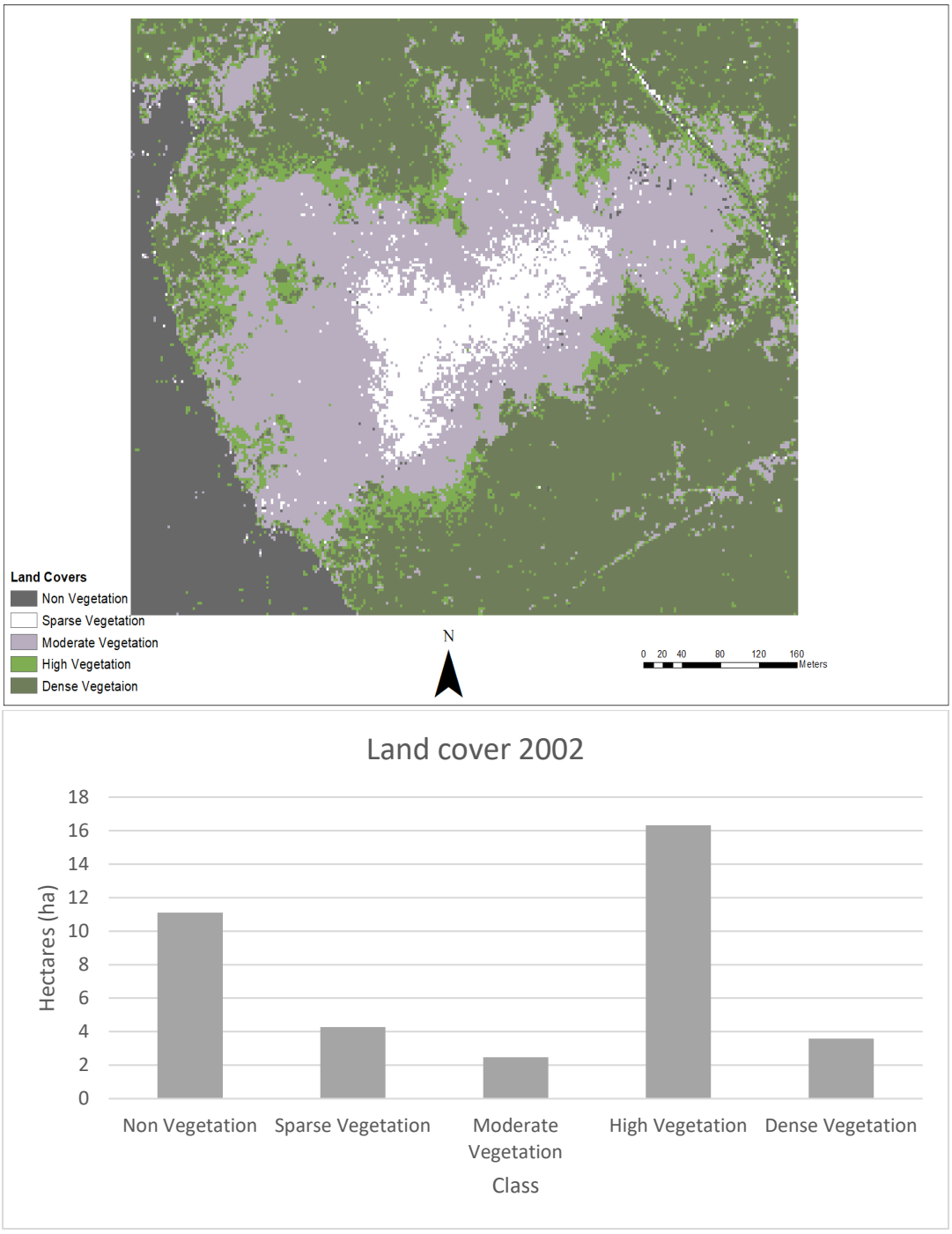

Figure 47. *2002 supervised classification map and area of classes in hectares.*

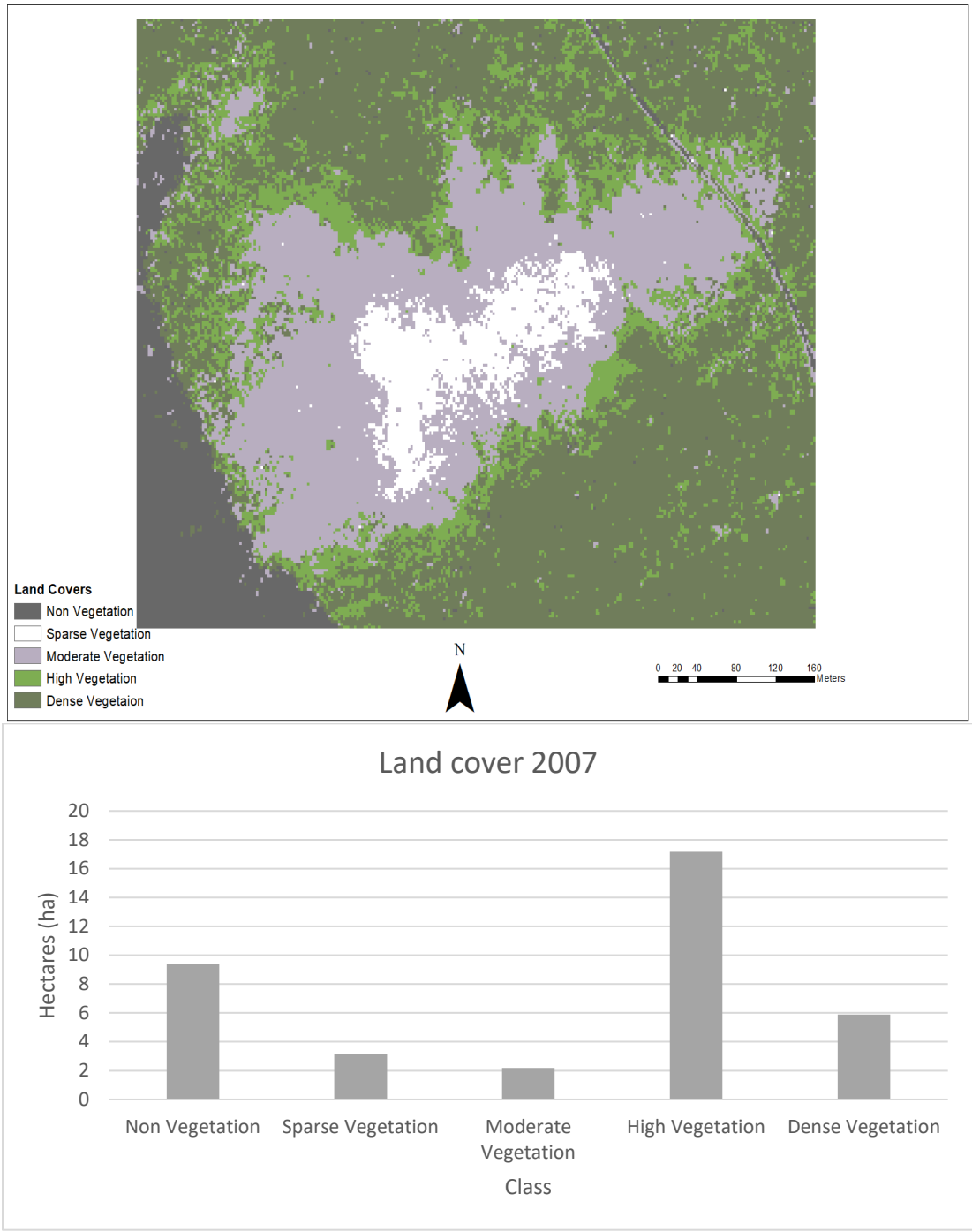

Figure 48. 2007 supervised classification map and area of classes in hectares.

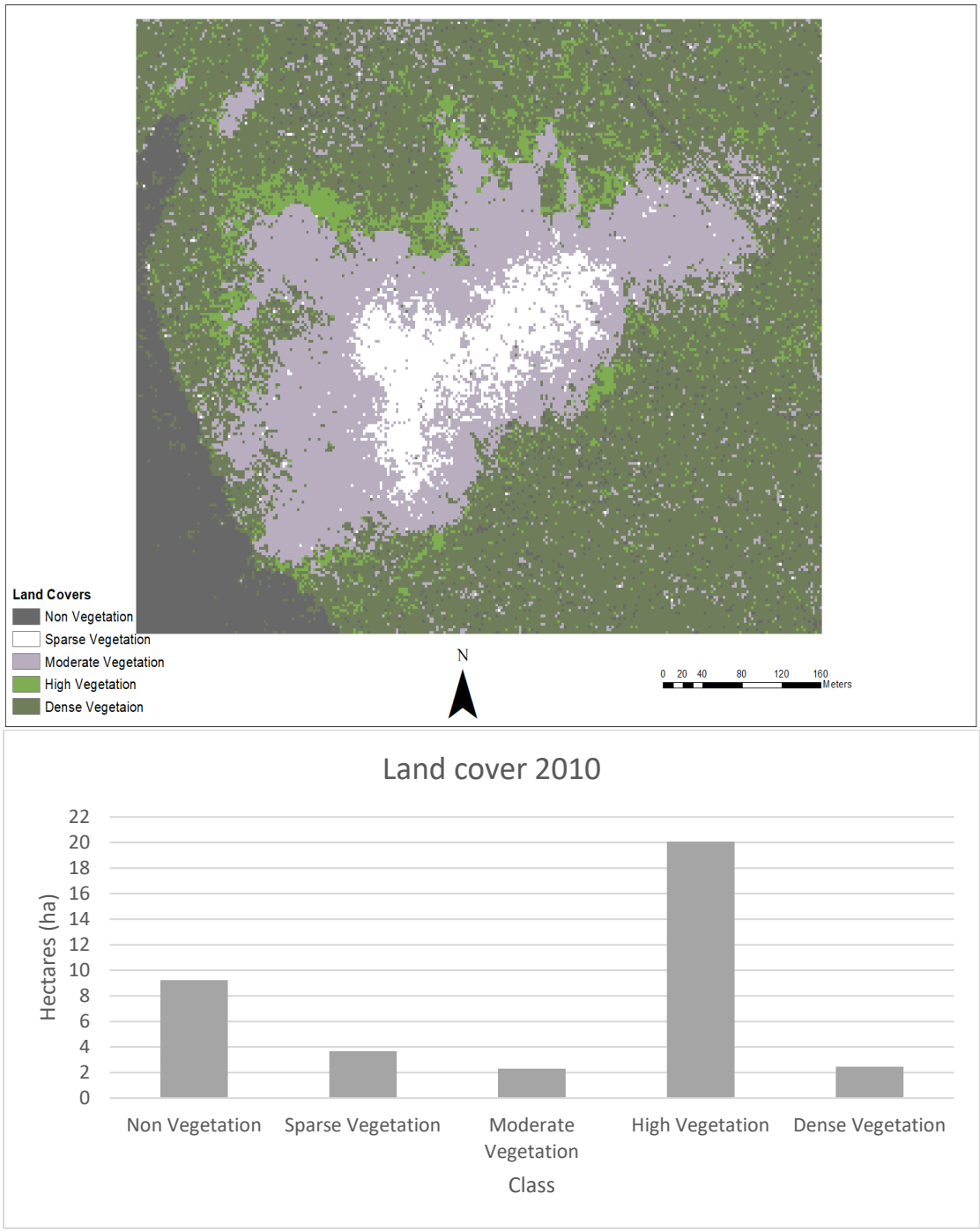

***Figure 49**. 2010 supervised classification map and area of classes in hectares.*

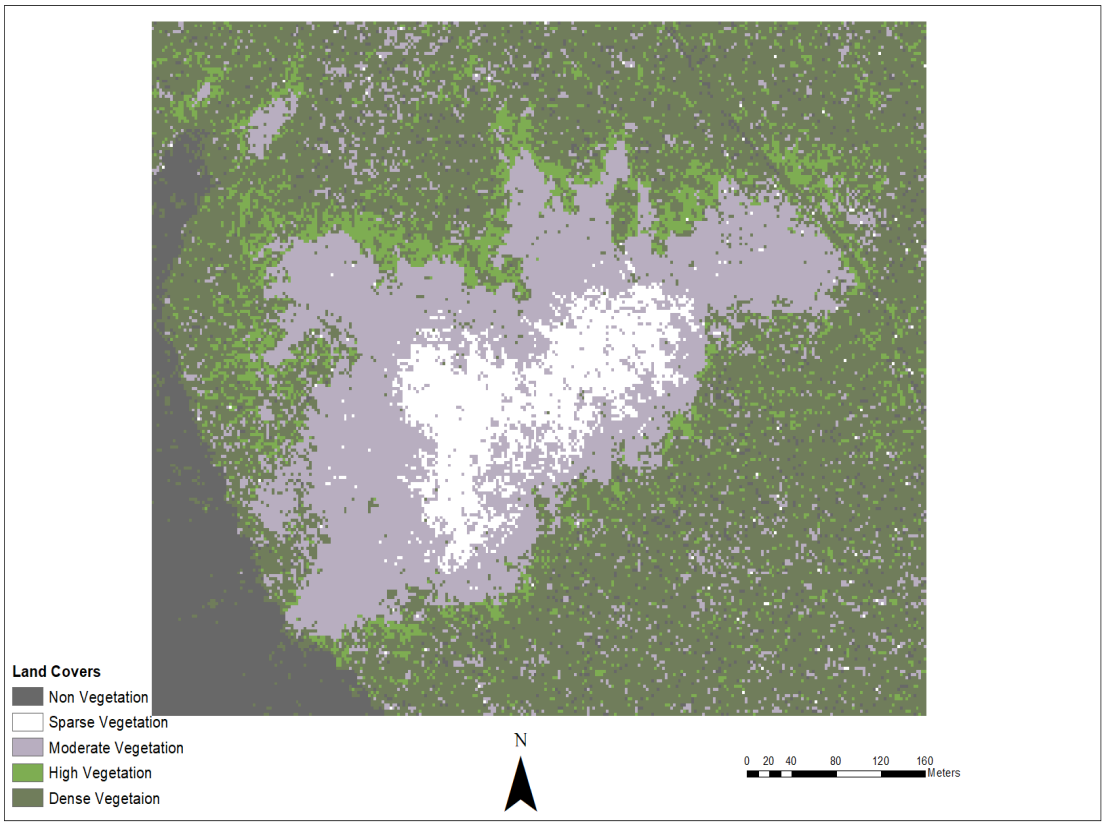

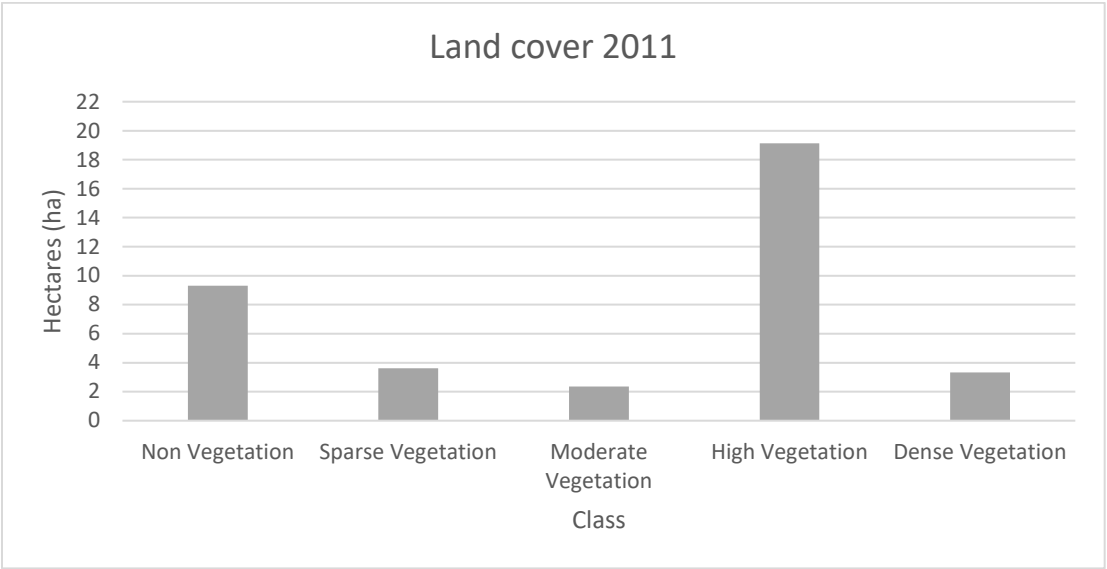

Figure 50. *2011 supervised classification map and area of classes in hectares.*

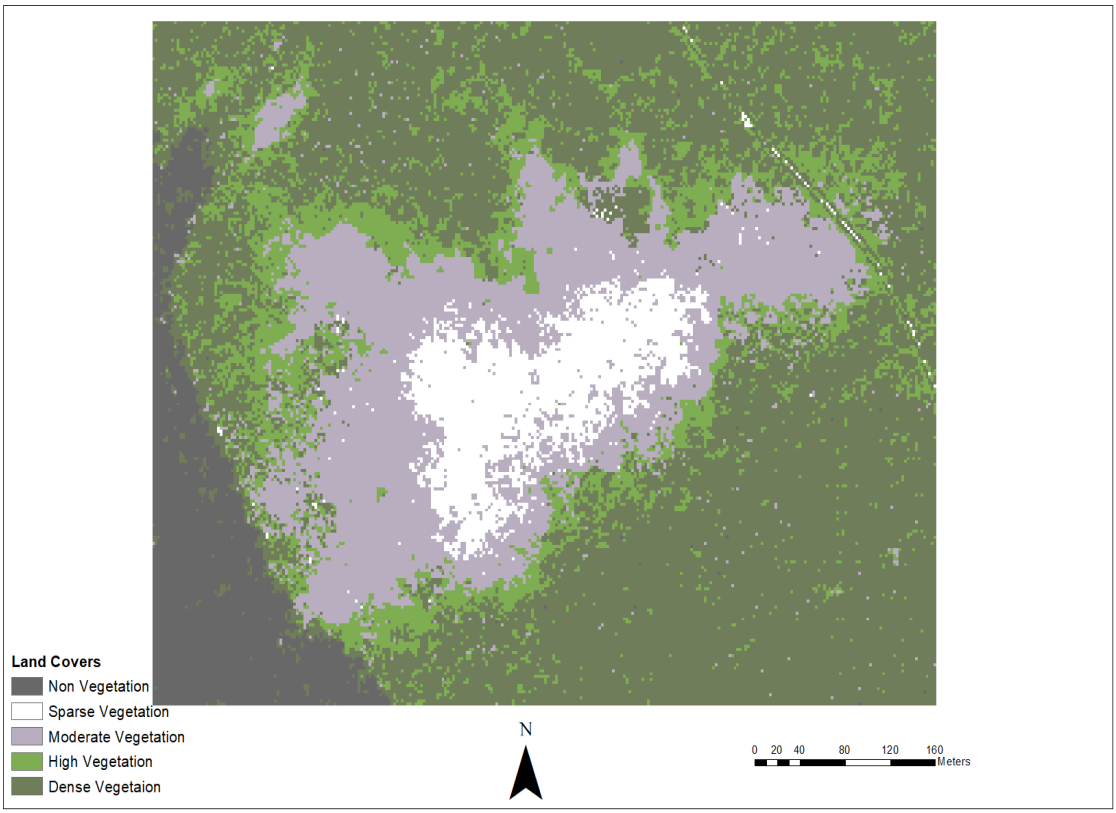

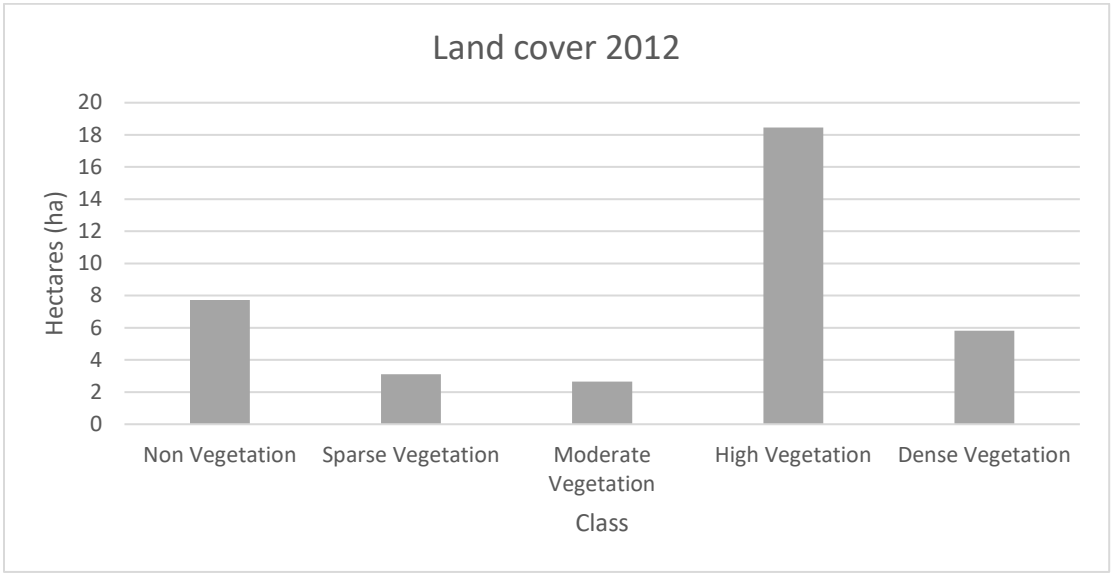

Figure 51. *2012 supervised classification map and area of classes in hectares.*

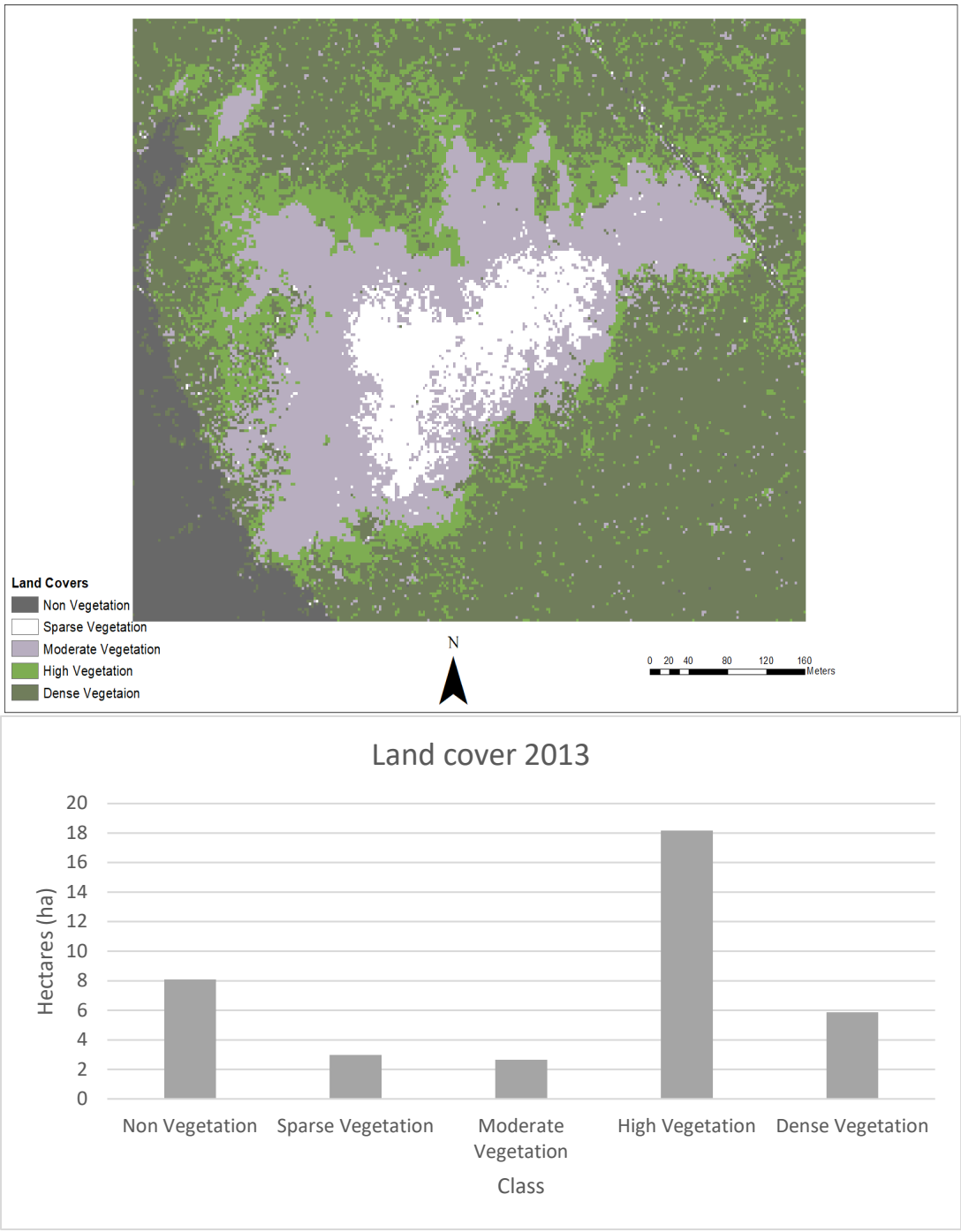

Figure 52. *2013 supervised classification map and area of classes in hectares.*

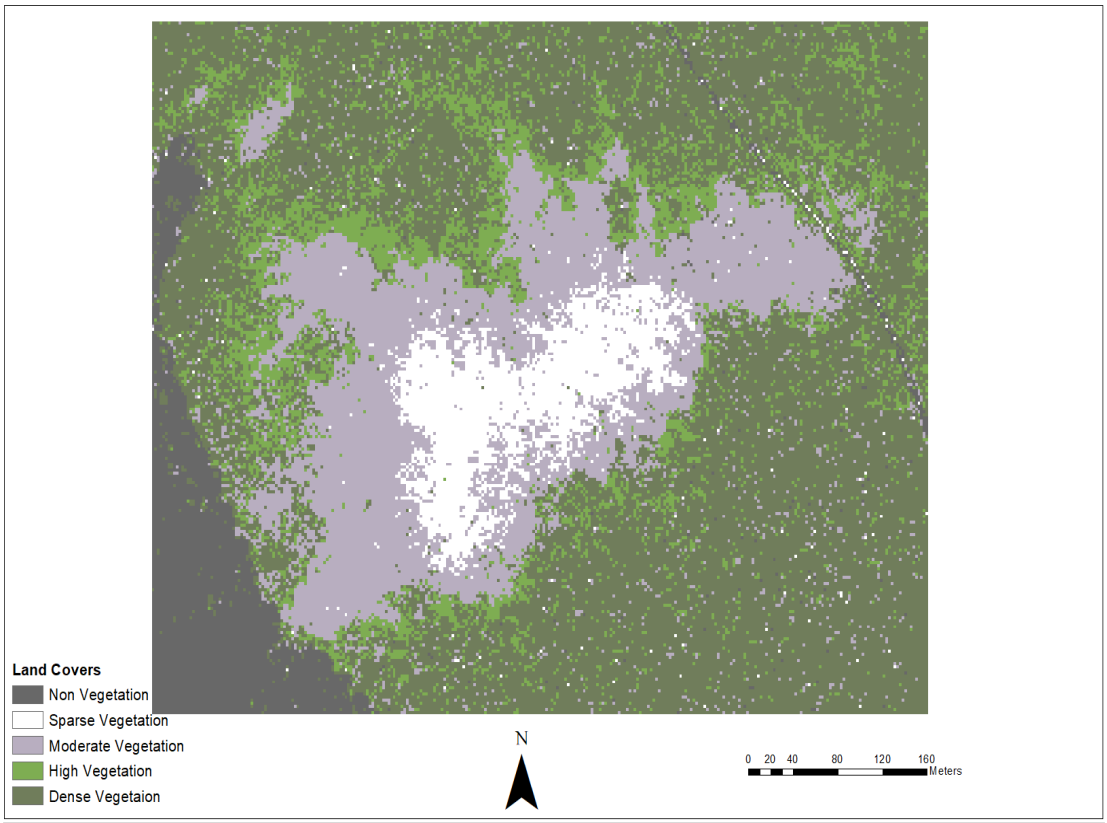

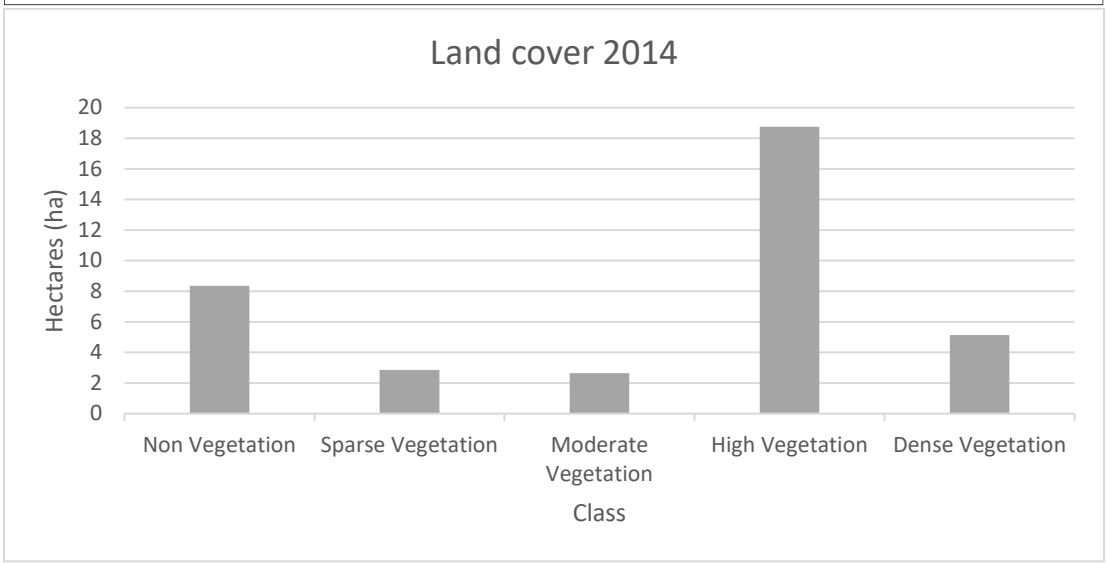

Figure 53. *2014 supervised classification map and area of classes in hectares.*

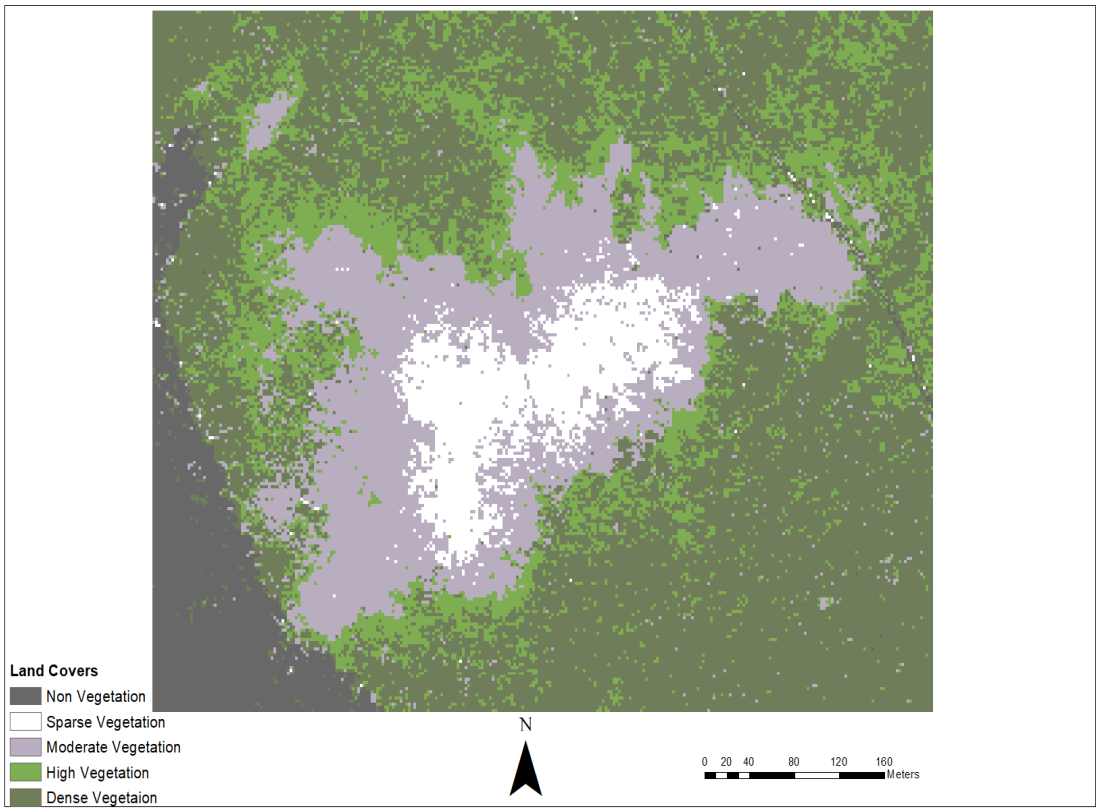

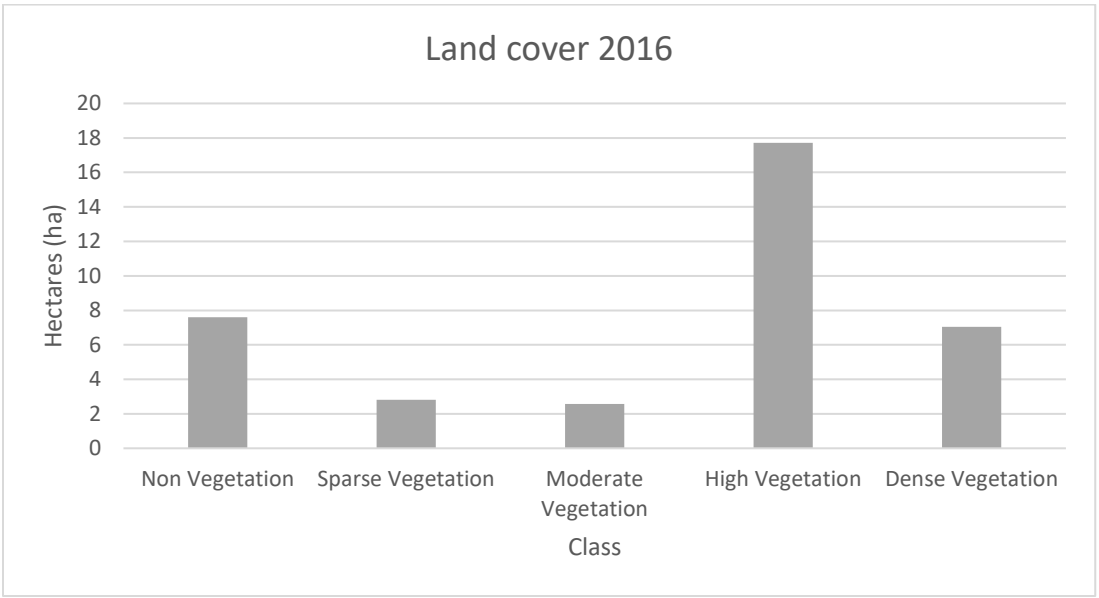

Figure 54. *2016 supervised classification map and area of classes in hectares.*

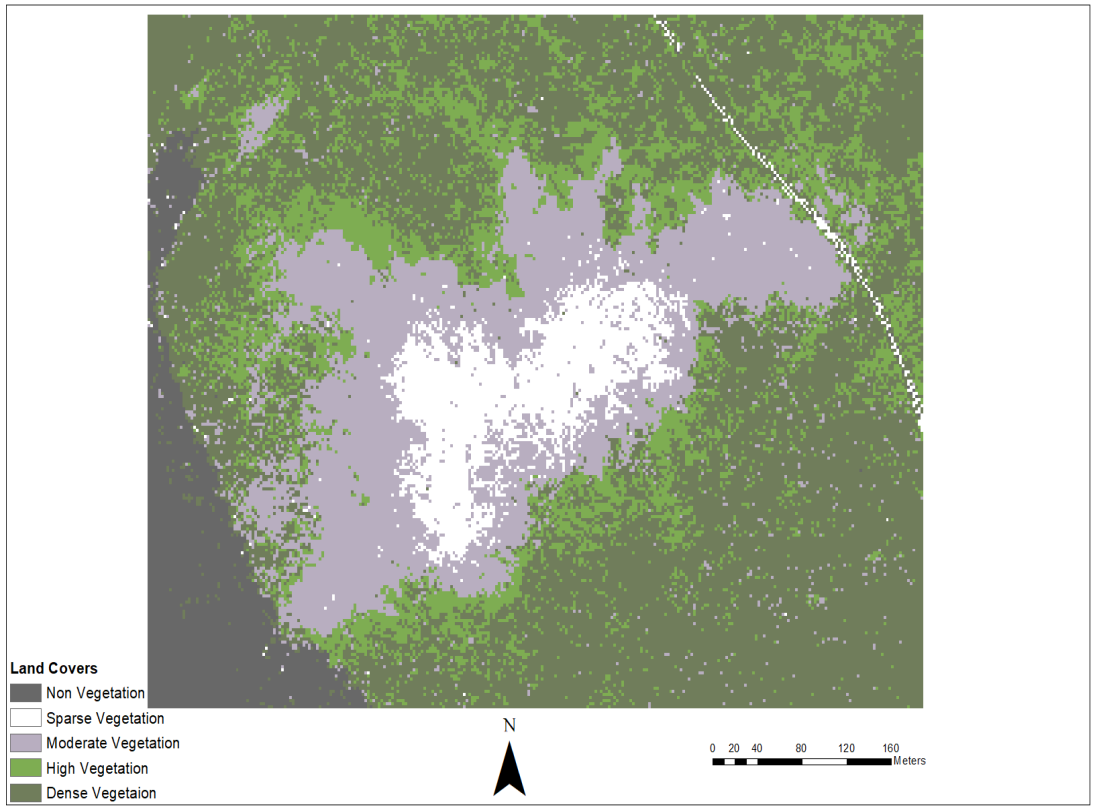

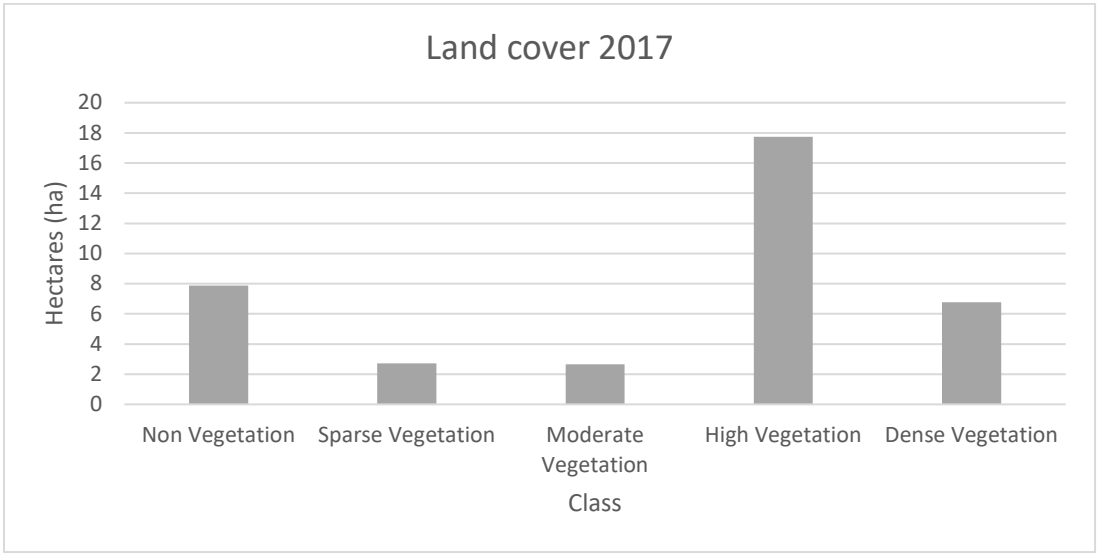

***Figure 55**. 2017 supervised classification map and area of classes in hectares.*